# Simulation Methods for Vehicle Disc Brake

# Noise, Vibration & Harshness

By

# **Mohammad Esgandari**



A thesis submitted to the University of Birmingham for the degree of

Doctor of Philosophy

School of Mechanical Engineering

The University of Birmingham

August 2014

# UNIVERSITYOF
# BIRMINGHAM

## University of Birmingham Research Archive

### e-theses repository

# Abstract

After decades of investigating brake noise using advanced tools and methods, brake squeal remains a major problem of the automotive industry. The Finite Element Analysis (FEA) method has long been used as a means of reliable simulation of brake noise, mainly using the Complex Eigenvalue Analysis (CEA) to predict the occurrence of instabilities resulting in brake noise. However it has been shown that CEA often over-predicts instabilities.

A major improvement for CEA proposed in this study is tuning the model with an accurate level of damping. Different sources of damping are investigated and the system components are tuned using Rayleigh damping method. Also, an effective representative model for the brake insulator is proposed. The FEA model of the brake system tuned with the damping characteristics highlights the actual unstable frequencies by eliminating the over-predictions.

This study also investigates effectiveness of a hybrid Implicit-Explicit FEA method which combines frequency domain and time domain solution schemes. The time/frequency domain co-simulation analysis presents time-domain analysis results more efficiently.

Frictional forces are known as a major contributing factor in brake noise generation. A new brake pad design is proposed, addressing the frictional forces at the disc-pad contact interface. This concept is based on the hypothesis that variation of frictional coefficient over the radius of the brake pad is effective in reducing the susceptibility of brake squeal.

*To my beloved Marzieh ...*

# Acknowledgements

# Contents

# Glossary

Subscripts:

$i$: Iteration

$\alpha$: Mode

Roman / Greek Letters:

$M$ or $m$: Mass

$C$ or $c$: Damping

$K$: Stiffness

$\lambda$: Eigenvalue

$\varphi$: Eigenvector

$f$: Frequency (Hz)

$\omega$: Frequency (rad)

$q$: Modal amplitude

$\mu$: Coefficient of friction

$\zeta_\alpha$: Critical damping

$\alpha$: Coefficient of mass proportional damping

$\beta$: Coefficients of stiffness proportional damping

$\xi$: Damping ratio

$S$: Structural damping coefficient

$t$: Time

$G$: Non-linear equation of nodal displacement

$u$: Nodal displacement

$B$: Strain-displacement matrix

$\sigma$: Stress

$dV$: Integral over volume

$dS$: Integral over surface

$N$: Element shape matrix

$F$: Force

$I$: Internal element forces

Abbreviations:

FEA: Finite Element Analysis

CAE: Computer Aided Engineering

CEA: Complex Eigenvalue Analysis

CAD: Computer Aided Design

NVH: Noise, Vibration and Harshness

PBP: Partitioned Brake Pad

COF: Coefficient of Friction

DOE: Design of Experiment

SAE: Society of Automobile Engineers

FFT: Fast Fourier Transform

FRF: Frequency Response Function

SDOF: Single-Degree of Freedom

MDOF: Multi-Degree of Freedom

AMS: Automatic Multi-level Sub-structuring

MAC: Modal Assurance Criterion

RFD: Relative Frequency Difference

# List of Figures

# List of Tables

# Chapter 1: Introduction

## 1.1.    Introduction

The aims of the research presented in this thesis were to develop simulation methods for more accurately predicting the brake noise using Finite Element Analysis (FEA) simulation tools. Developing methodologies and Computer Aided Engineering (CAE) techniques using the FEA tools to predict the likelihood of occurrence of brake noise at the virtual design stage was the major aim of the study. As a significant prerequisite for that, obtaining a thorough understanding of the fundamental initiation and radiation mechanisms of brake noise was among the major aims.

A further aim was to identify the key factors controlling brake noise radiation and hence the potential control measures for limiting the noise generation mechanism in order to be able to design potentially noise-free brake systems. Furthermore, by identifying the influential control measures, a potential method for limiting the noise generation mechanism was also desired.

## 1.2.    Research Objectives

To achieve the aims of the research, the following objectives were set:

- Identification of the fundamental mechanisms of initiation and radiation of high frequency brake noise (squeal).

- Identification of possible control measures potentially capable of limiting the brake noise.

- Development of FEA solution schemes, incorporating application of damping from various sources, mainly material damping, contact damping and the damping from the brake shims. Investigation of simple but representative design criteria for a model of the brake shim.

- Development of a comprehensive understanding of significance of various key factors in performing the instability analysis using the on the brake system FEA model.

- Development of time-domain and/or frequency-domain analysis solution scheme addressing the computing time/cost associated with the time domain analysis and the limitations associated with the frequency domain analysis.

## 1.3.    Overview of the Thesis

Studies undertaken to meet the objectives of the research are presented in the following six chapters.

Chapter 2 presents an in-depth review of the literature published in the field. An extensive literature survey starts with the invention of disc brakes in 1902 and covers publications as early as 1930s to the present date. Various methods of investigating the subject of brake noise as well as formerly proposed solutions are reviewed, which prepares the basis for selection of the best approach and most relevant theories describing the brake noise phenomenon and squeal in particular.

Chapter 3, the methodology chapter, continues by further elaboration of the methods utilised for the current study. The experimental methodology including complete brake system dynamometer and vehicle test procedures are explained. In continuation, methodologies for performing the modal experiments are reviewed, which are undertaken to correlate the FEA model with the modal characteristics of the system components. The FEA model set up as

well as the theoretical background is reviewed and the analysis procedure is presented. The methodology chapter finishes with a review of the significance of damping in the simulation.

Chapter 4 presents the study of system damping characteristics. This includes application of different damping tuning solutions for more accurate prediction of instabilities indicating likelihood of brake noise, including but not limited to application of brake shims. Different sources of damping are investigated; material damping, contact damping and the damping from brake shims. Finally a complete CEA is performed on the model tuned with the best damping tuning techniques and correlated with the experimental test results.

Chapter 5 presents the new brake pad invented by the author, the Partitioned Brake Pad (PBP). This is a potential fundamental solution for limiting the noise initiation mechanisms, rather than a secondary fix for it. The PBP is analysed for instabilities related to brake noise, and has shown very low strength of instabilities, indicating a brake system with low potential noise. The concept is also examined for braking torque, and the analyses results suggest the PBP has more than 30% higher braking torque, compared with the same brake unit with the original friction material.

Chapter 6 includes the study of a hybrid time-frequency domain analysis methodology for brake noise investigation. The co-simulation technique is applied to the brake system model based on hypotheses concluded from the brake noise initiation and radiation mechanisms. The simulation completes and returns time domain results using less computing time/power compared to the frequency-domain analysis (i.e. CEA).

Finally, in chapter 7, conclusions from the research are presented, as well as the potential areas for future research. Also, highlights of the academic contributions of this research to the field are presented.

# Chapter 2: Literature Review

## 2.1.    Introduction

Frederick William Lanchester (1868-1946) invented the disc brake in 1902 [1-3]. Ever since the invention of brakes, research focused on improving braking power and reliability, but vehicle acoustics and relative comfort, despite their significance, were not taken seriously initially [4]. Numerous research have been conducted to understand, simulate and possibly eliminate brake noise since 1930 [5, 6], but only in the very recent investigations some effective results have been obtained in terms of reducing the brake noise.

Vehicle comfort, nowadays, is considered as a major factor in vehicle overall quality. This highlights the importance of vehicle Noise, Vibration and Harshness (NVH) performance which can directly affect vehicle comfort level. Also, customers assume the brake noise is a problem and may raise a warranty claim. This is costing millions of pounds every year to car manufacturers.

Brake noise studies in the early stages only attempted to eliminate or reduce noise, while later studies focused on understanding noise generation mechanisms. The majority of studies have been performed using experimental, analytical and computational methods. Brake noise is categorised into several sub-categories during the different stages of studying the topic. Classifications are usually based on the noise generation mechanism.

Ouyang *et al* [7] divided brake noise into three major categories of creep-groan, judder and squeal. Among the studies performed on brake noise, the majority of the research has focused

on squeal. This is due to the nature of the noise being more noticeable, irritating and more expensive for the automotive industry.

The content of this chapter is as follows; first, an overview of the theories defining brake squeal is presented. Next, an overview of major studies of brake noise and different approaches used to perform them are presented. Then, the significance of friction is reviewed. This is followed by brake noise prediction and elimination methods.

The intention of this literature review is to present a comprehensive understanding of the brake squeal problem. This includes brake squeal mechanisms, available techniques and tools, and refinements on the existing methodology and analysis. The literature review also addresses present issues and aspects of the problem that have not been investigated to a great extent, especially in the simulation of disc brake squeal noise using the FEA method.

## 2.2.    Theories of Squeal Definition & Mechanisms

Technically, squeal is a mono-harmonic high frequency noise emitted at low speeds, in the frequency range of 1-20 kHz, owing to many factors; mainly structural and material [8, 9]. It occurs more frequently under light braking applications with slow deceleration, mild pressure and relatively low temperatures of about 150-250 °C [10]. During a braking application, each disc brake dissipates heat at a rate of over 50 kW, in the form of heat generation, as well as noise of over 100 dB, measured at a reasonable distance [11].

Minor variations in operating temperature, brake pressure (both load magnitude, and how severe it is applied), disc velocity (car speed), and brake pad COF will result in different squeal frequencies [10, 12].

The most significant complication involved in all brake researches is the fugitive nature of the brake squeal problem, i.e., it is non-repeatable from one car to another or even the same brake at slightly different operating conditions. Also every component of the brake system individually has its own natural modes of vibration, and when they are all assembled together, they make unstable modes of squeal frequencies. This is referred to as component free and coupled vibration modes [12].

Different theories are suggested in the literature to explain brake squeal from different perspectives. A significant step forward in studying brake noise is to understand the mechanism of the unstable friction induced vibration in brake systems. There is no unique mathematical model and theory which explains the dynamics of the friction.

In different studies conducted by Oden and Martins [13], Crolla and Lang [14] and Ibrahim [15, 16], they have identified four major mechanisms for the initiation of friction-induced system instabilities, resulting in the friction-induced vibrations in the brake systems: variation in the COF, stick-slip, sprag-slip and modal coupling.

### 2.2.1. Variation in the Friction Coefficient

An early experimental study by Mills [6] introduced the idea that the brake squeal is associated with the decrease of the coefficient of dynamic friction ($\mu_k$) compared to the sliding velocity. This mechanism is still considered to be valid for explaining low frequency brake vibration problems such as judder and groan. However, it was later found that it is insufficient to explain some friction-induced vibrations.

Sinclair [17] developed a mathematical model to show that the relative decrease of the dynamic frictional coefficient results in unstable oscillations,  causing self-excited vibrations in the model. This idea can also be found in some more recent studies.

Shin *et al* [18] also suggestd that the onset of self-excited vibrations was by a falling friction characteristic and can produce self-excited vibrations even in the case of one degree of freedom.

Hochlenert [19] found that brake squeal noise was initiated by an instability due to the frictional forces, leading to self-excited vibrations. Vonwagner [20] also agrees with this and summarises similar theories in the literature as: change of the friction characteristic or the relative orientation of the frictional forces relative to the speed at the contact interface [18, 21-23]. The greater the coefficient of friction, the more the likelihood of squeal [24].

### 2.2.2. Stick-Slip and Negative Damping

Stick-slip is a low sliding speed phenomenon which happens when the static coefficient of friction is higher than the dynamic coefficient. Also, negative damping is when the coefficient of dynamic friction decreases while the speed at the contact interface increases. The mass sliding on a moving belt is a simple representation of the stick-slip phenomena. There is no change in the friction force as the mass is sliding on the belt. However, the sliding force increases until it exceeds the static friction force maximum and consequently, the mass starts to slide. This continues until the force causing the sliding drops to the sliding friction value. This is when sliding and sticking occurs in succession.

Fosberry and Holubecki [25, 26] suggested that squeal happens as a result of stick-slip and negative damping. The stick-slip theory is mainly employed to explain low frequency brake

vibration problems. An example of this is given in Behrendt *et al* [27] who uses this theory to explain creep-groan. However, the negative damping theory still has been shown to effect brake squeal [28].

### 2.2.3. Sprag-Slip

Spurr [29] was the first researcher who suggested a new theory for defining brake squeal. He proposed the sprag-slip theory. The sprag-slip phenomenon occurs due to a locking action of a body sliding on a surface such that motion becomes impossible. In his theory, the unstable oscillations would also occur in a system with a constant coefficient of friction.
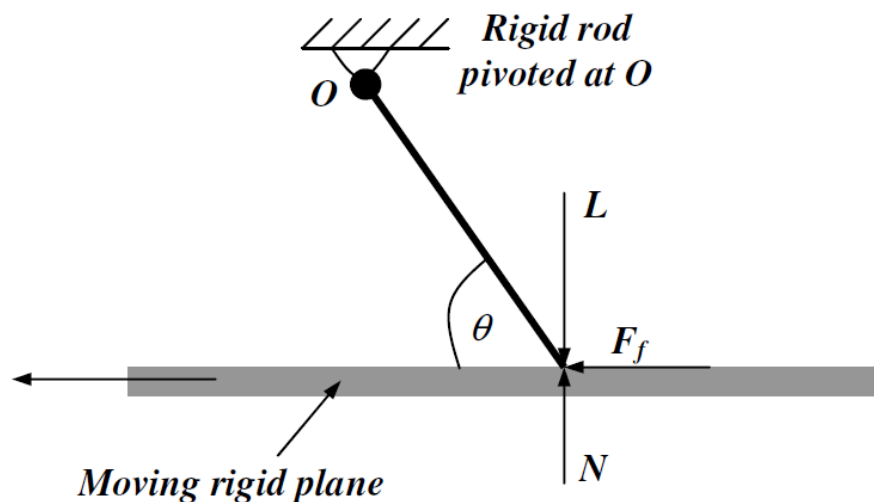


Figure 1, Schematic diagram of sprag-slip theory [30]

In 1971 he experimentally confirmed the sprag-slip mechanism. His experiments showed that squeal was associated with the local position of the contact interface, as well as the level of braking pressure. Later, Earles and Soar [31] investigated the sprag-slip theory using experimental and analytical approaches. An experimental study based on the pin-on-disc and a 1-DOF analytical model was developed to highlight the importance of the non-linear characteristics of the contact interface of the assembled brake system. They concluded that

self-induced vibrations are associated with a specific range of angles of orientation of the pin, which was due to the non-linearities in the system.

In recent years, Sinou *et al* [32] and Fieldhouse *et al* ([33, 34]) have also used Spurr's sprag-slip model as the main mechanism of brake noise.

### 2.2.4. Modal Coupling

After Spurr proposed the sprag-slip theory, researchers further developed and generalised his theory to describe the mechanism as a geometrically induced or kinematic constraint instability. By application of this theory, Jarvis and Mills [35] showed that the variation of the COF relative to the sliding speed was insufficient to cause the friction-induced vibrations. This could indicate that the instability was due to coupling even if the coefficient of friction was constant.

North proposed a new theory and developed a binary flutter model which could replicate the disc brake assembly more realistically. An 8-DOF [36] and then a 2-DOF [37] model considered the geometrical characteristics of the brake components, as well as taking into account the stiffness of the interactive components. The distinguishing aspect of this theory was that two different modes of the disc were considered, and also the frictional forces produced by pressure of brake pads were present as follower forces. The model accurately reproduced the squeal frequencies, mode shapes and range of brake-line pressure.

Millner [38] extended North's model, developing a 6-DOF lumped parameter model that was coupled by a kinematic constraint. By correlating the predictions of the model with the experimental data, he concluded that initiation of squeal was dependent on the COF of the

pad, the mass and stiffness parameters of the disc brake assembly, and the characteristics of the piston-pad contact .

Dweib and D'Souza [39] also showed that frictional instability can occur due to the coupling between the normal, tangential and torsional degrees of freedom.

There are also various opinions expressing a coincidence between the squeal frequencies and the natural frequencies of a system. Modal coupling has been among the most accepted theories of the brake squeal in recent years. Kung *et al* [40] explained squeal was caused by modal coupling. Akay *et al* and Flint [41] investigated the modal coupling of friction interface. Giannini [42, 43] investigated the brake noise using beam and disc experimental set-up and looked at the modal coupling between the disc and beam. Khan *et al* [44] investigated brake noise of motorcycle and proposed the application of brake shims to counteract the brake noise. Park *et al* [45] proposed modal decoupling based on geometrical variations which can shift frequencies of resonance.

## 2.3.    Major Research on Brake Noise

Numerous research studying the brake squeal problem have used experimental, analytical or numerical investigation methods. Quite often, some studies have also used a combination of two of the mentioned approaches. Each of these methods has their own limitations, and offers its own unique advantages.

Experimental methods are usually very useful in order to confirm results from other studies, as they demonstrate a complete presentation of the NVH performance of brakes. Experimental methods are also essential to provide results for confirmation of other approaches, as well as releasing the final design of the brake system into market.

Analytical methods are useful in presenting a relatively simplified image of the system instabilities. However, their main disadvantage is that they are not fully capable of taking component deformation into account. Also, analytical approaches are limited in terms of a number of parameters. Analytical methods were the most common approach of brake noise studies before FEA became available to the researchers and boosted use of numerical methods. Analytical approaches not only seemed to be inadequate to provide a comprehensive understanding of the phenomenon but also in providing a tool to predict squeal.

Drawbacks of analytical approaches can be overcame with the application of numerical approaches. The FEA method allows the creation of MDOF models. Unlike analytical approaches, numerical approaches also could take component deformability into account. One major advantage of numerical methods is that FEA packages using these methods can provide a design tool which can predict squeal.

The following section is a brief review of investigations conducted by researchers and scientists using each of the mentioned methods.

### 2.3.1. Experimental Approaches

Experimental approaches were the very first method of investigating brake noise. Early examples of this are Lamarque [46] and Mills [6].

Fosberry and Holubecki [25, 26] performed brake dynamometer experiments to measure disc vibrations and temperatures, as well as the brake torque. Their initial assumption was that squeal is associated with the negative $\mu - n$ slope characteristics but in 1961 [25, 26] they hypothesized that squeal can happen if the coefficient of static friction is higher than the coefficient of kinetic friction.

In an experimental study of squeal mechanism, Dunlap *et al* [40] investigated different types of brake noise and concluded that any noise at frequencies below 1 kHz was due to excitations in the contact interface caused by the frictional forces, which results in modal coupling. He also concluded that high frequency (above 5 kHz) noise is related to the in-plane vibration of the disc.

In order to capture sound pressure level ($dB$) and vibrational behaviours, it was common to use a microphone and an accelerometer. Tarter [47] used these tools and investigated effects of modifications to the disc, friction material and pad contact geometry on brake squeal. The study found modifications to the disc geometry effective in elimination of the noise, where frictional properties and contact geometry were only effective in reducing the noise.

In a new approach, Ichiba and Nagasawa [48] installed small accelerometers on the back plate, the disc, and the friction material in order to measure their vibrational characteristics. They suggested there is a coincidence between the squeal generation and the variations of frictional force.

James [49] used non-contact displacement transducers to study the brake squeal. He measured the perpendicular vibrations of the squealing disc in frequencies up to 8 kHz. His experiment showed that the modal behaviour of the disc at the squeal frequency can produce stationary or travelling waves (backward or forward), the first being more common.

In an experimental study Kumamoto *et al* [50] used the same method to analyse brake pad behaviour, with a focus on the pad restraint conditions. They attached a piezoelectric accelerometer on the caliper to measure vibration waveform. They also located pressure distribution measurement sensors in the caliper housing and measured the contact load. They found that the initiation of the noise was caused by vibrations at the surfaces of the pad

abutments and the caliper, enabling the pad to vibrate at the corners. They built a FEA model of the disc brake and the analysis results confirmed the experimental results. They also concluded that the initiation of noise can be limited by increasing the rigidity of the pad and a more stable fixture in the pad abutment areas.

Another experimental method practiced by researchers is using double-pulsed laser holography, which enables more accurately capturing of vibrations of the brake system components. Nishiwaki *et al* [51] used this laser imaging tool to visualise the vibration of the disc and pads during brake squeal generation. They found that in the event of squeal, the disc and pad vibrate in bending and torsional modes, respectively. They also found the modal behaviour of the disc being the driving factor for the modes of the pad.

Using the same technique, Fieldhouse and Newcomb [52, 53] visualised vibrations of a squealing disc brake. Confirming the finding of Nishiwaki regarding the vibration modes of the noisy brake, they found that an out-of-plane mode of the disc was more potential to initiate brake noise, compared to in-plane modes. They also reported that the pad end flutter significantly contributed to this. There was also a correlation between the noise frequencies and the natural frequencies of the disc and the pad.

A decade later, Steel *et al* [54] investigated the significance of in-plane and out-of-plane modes using double-pulsed laser holography. They found in-plane modes to be more dominant compared to the out-of-plane modes.

Matsuzaki and Izumihara [55] used sound intensity analysis method to study the in-plane vibration of the disc. They identified the noise sources and the vibration modes of the components during squeal. They confirmed that the in-plane modes of the disc were the main cause of noise generation.

McDaniel *et al* [56] studied squeal using acoustic radiation. They measured acceleration and velocity as the response to a time-harmonic shaker excitation. Velocity measurements for each mode were used to compute radiation efficiency and intensities at the natural frequencies of the brake system. They found the forces from the disc in-plane modes to be much greater than the transverse forces, which was facilitating modal coupling between the system components.

Vadari *et al* [57] discussed the future of experimental approaches. They focused on the vehicle on-board data acquisition, integrated brake noise measurement system, and dynamometer testing. They highlighted the necessity of continued development for establishing standardized methods to quantify noise occurrences and characteristics. This can eliminate subjective measurements of the brake noise propensity. They suggested using more robust on-board data acquisition tools and methodologies for vehicle tests, more reliable brake dynamometers with standardised test procedures, and a correct tool to visualise noise and vibration behaviour during squeal.

Experimental methods are still practiced by some researchers. In a recent study, Nishiwaki *et al* [58] developed an experimental set-up development for brake squeal basic research to study low frequency brake noise. They investigated the effects of kinetic energy change in dynamic instability.

### 2.3.2. Analytical Approaches

The experimental methods described in the previous section are mainly focused on attempts to identify mechanisms underlying brake noise and vibration. This section focuses on the analytical approaches of studies of brake systems.

Nishiwaki [59] attempted to model brake instability mechanisms. He derived a generalised theory of brake noise by combining more than one squeal mechanism and developed mathematical models for both drum and disc brakes. He investigated disc brake squeal as well as groan. He concluded that brake squeal is generated by the dynamic instability of the brake system caused by variations of the frictional forces.

Ouyang *et al* [22] studied the parametric resonance phenomenon in discs. They investigated application of two forms of the load system. Firstly, a discrete transverse mass-spring damping set and secondly a distributed mass-spring system. In a later investigation (Ouyang *et al* [60]) they added spring-dashpot element on the pillars of the vented disc. This investigation showed that with in the case of resonances at constant friction level, the dashpot elements can result in a modification to the strength and frequency of the resonances. However, dashpot elements, due to addition of damping, can also initiate additional resonances. They concluded that the damping in the disc is significant in modifying the resonances.

Ouyang and Mottershead [61] used a simple rotating mass-spring-damper system with friction to investigate unstable travelling waves in the friction-induced vibrations of the discs. They observed that friction, in the format of a follower force, is the most significant destabilising factor in the system, which could destabilise travelling waves in both modes of combination resonances.

Chowdhary *et al* [62] confirmed the modal coupling theory by modelling the disc as a thin plate and the backing plates as thin annular sector plates. The study investigated the flutter-typed instabilities in the components with close natural frequencies where the coupled modes were forming.

Hoffmann *et al* [63] investigated the modal coupling mechanism through a 2-DOF model. This investigation also revealed that simultaneous transverse oscillation and in-plane displacement of the frictional forces might lead to the generation of vibrational energy.

Flint and Hulten [41] created a mathematical model to study high frequency squeal.

They created a model based on the sliding beam experimental set-up. Then they further developed their model to include pistons and the caliper. They confirmed that the disc has a dominant role in the occurrence of brake squeal, and also revealed that the deformation-induced couplings from the friction material are significant in onset of the instability.

Yang *et al* [64] investigated the role of both in-plane and out-of-plane modes of the disc in generation of brake squeal. They performed analytical investigations and then confirmed the results using the FEA method. They also performed investigation using dynamometers, and concluded that the circumferential in-plane modes were influential in activating the mechanism for high frequency squeal. They observed modal coupling between bending and in-plane modes in close frequencies could couple, and they found geometry asymmetry or non-linearity enabling that.

Component and parameter sensitivity investigations are quite common in analytical approaches. This can result in identification of the key component or parameter and be used to suppress the brake noise. As an example, Brooks *et al* [65] developed a 12-DOF model of a brake with a fixed caliper with two pistons, and used CEA to conduct sensitivity investigations. Among the factors they investigated is the piston positions, and they found that the system is more stable when the piston is closer to the leading edge. They also confirmed the modal coupling theory to be valid, particularly at high values of pad stiffness.

Sherif [66] used analytical methods to investigate the effect of contact stiffness on the instability of the system. The analyses results confirmed that instabilities resulting in brake squeal occur mainly as a result of the tangential forces in the contact interface, which is related to the brake's friction material.

Nossier *et al* [67] studied the effect of the pad geometry on squeal. They found the brake disc to be the key component on the generation of brake noise, as they observed a correlation between the dynamic properties of the disc and the occurrence of squeal.

Watany *et al* [68] developed a 3-DOF model based on the experimental material properties. They calculated natural frequencies of the brake components based on the component's masses, modal stiffness and coupling stiffness. They observed a correlation in the noise frequencies and the natural frequencies of the disc.

El-Butch and Ibrahim [69] developed a 7-DOF mathematical model and investigated the effect of geometrical characteristics and contact interface parameters on instability. They used time domain response to show vibrational behaviour of the system. They concluded that the contact stiffness of the caliper is effective in the vibrations causing noise. In addition, they found that higher friction levels between the piston and pad back plate can excite some modes.

In a recent study by Ibrahim [70] he has developed a 10-DOF system to study Young's modulus of ventilated disc and friction materials in the format of a parametric sensitivity study.

### 2.3.3. Numerical / Computer Aided Engineering Approaches

Recent advances in computer technology have enabled researchers to build more complicated and comprehensive numerical models to study the brake squeal. These models often also provide relatively quick results, compared to experimental and analytical models as well as older numerical techniques. Improvements in the algorithms and formulation of loads and boundary conditions have enabled researchers to obtain a more accurate representation of the phenomenon.

There are three major numerical analysis methods for investigating the brake noise, namely Complex Eigenvalue Analysis (CEA), transient analysis and normal mode analysis. In recent years, the research community has preferred the CEA over the transient analysis for performing brake squeal analysis. A comparison between these three methods was made by Mahajan *et al* [71] while Ouyang *et al* [7] made the comparison with omission of the normal mode analysis.

The most important part of the modelling performed is the interface between the pads and the disc. By application of the brakes, due to the high level of pressure in the compressed contact interface, a very thin layer of mixed material is formed which consists of the friction material and the disc material [72].

Crolla & Lang [14] believed that despite all sophistications in numerical methods, the FEA results had not reached suitable principles for design of large degree of freedom FEA models leading to noise-free brakes. However, there have been great developments in FEA since then. They believed FEA will be the most powerful design tool for the issue in the near future by expanding computational capabilities of FEA packages, once the difficulty in modelling frictional interactions therein are removed. Yang and Gibson [73], agreeing with Crolla &

Lang, emphasizes on experiments as the most successful approach, being the "sole means for verifying any solution to brake squeal". Papinniem also elaborates on the topic, in agreement with the work done by Yang and Gibson [12].

Nagy *et al* [74] used dynamic transient analysis in a FEA model to study the brake squeal. They used two different software packages (MSC/NASTRAN and MSC/DYNA) to model the brake system. They assigned non-linear contact properties to the disc-pad contact interface and found that the frictional properties are significantly important in controlling the stability of the brake system. They also reported that the instability is not sensitive to the speed of the disc.

Chargin *et al* [75] developed a FEA model to analyse disc brake squeal using transient analysis. Their model was an early replication of the CEA. They used Implicit integration algorithm with tangent matrices of the steady-state solution. Then they transferred the matrices to the CEA and identified the unstable modes.

Hu and Nagy [76] developed an Explicit dynamic code to conduct a DOE for brake squeal. Later, Hu *et al* [71] automated the selection of the design combinations using a programme. This programme did so according to the DOE matrix, performed the simulation, conducted Fast Fourier Transform (FFT) (to convert time-domain to frequency-domain) and computed an intensity factor. Their FEA model included the disc, caliper, pad assemblies, and the brake hydraulic fluid. They utilised the generalised Coulomb friction model where the COF was determined by contact pressure and sliding velocity. They concluded that friction material, rotor thickness, the pad chamfer and the pad slot were the factors associated with the brake squeal.

Hamzeh *et al* [77] performed stability analysis of the dynamic characteristics of friction induced vibrations. They modified Oden-Martins model [13] and added velocity-dependent friction to simulate the contact interface between the pad and disc. This investigation showed that mechanism initiating the instability could be either $\mu - n$ characteristics or the modal coupling.

Auweraer *et al* [78] developed a MBS model consisting of the disc and the pads. They considered complex surface contacts and dynamics characteristics of the deformable components in their model. They performed transient analysis using DADS FEA software package. They correlated the results with their experiments. They found that in the event of squeal, the disc and pad had similar patterns of vibration. They concluded that the disc has the dominant influence on the squeal generation.

Massi [79] defined characteristics of an optimum and accurate nonlinear model. He suggested that such a nonlinear model, beyond the material nonlinearity, should take into account the disc rotation, real-time contact stiffness, and local stick phenomena. He concluded that linear CEA are useful to predict the squeal onset in a wide range of driving parameters while dynamic transient analysis are able to reproduce the squeal phenomena in the time domain.

Among various analysis procedures which can be performed to obtain frequency results, CEA is highly efficient as it shows up all the instabilities in one run for the model. One downside of CEA is that not all the instabilities obtained are observed in the real test, and this reason has caused many engineers in the industry to avoid using it as this over-prediction is confusing if not correlated or validated with other data.

Liles [80] was among the first to incorporate the CEA with the FEA method. He built a detailed model and validated each of the components by performing modal experiments. He

used linear spring elements for component interconnections, and assumed full contact in the disc-pad contact interface. Apart from the minor geometrical factors, he highlighted that higher COF and wear of the friction material were enablers of squeal.

Ghesquiere and Castel [81] attempted to obtain a realistic contact pressure distribution. They found that the disc and pad are not in full contact all the time. They also confirmed that the modal coupling of disc and pad is the reason for the generation of squeal, and they explained squeal caused by modal proximity. In a recent study, Spelsberg-Korspeter *et al* [82] reviewed the shortcomings of Complex Eigenvalue Analysis. There are also other researchers mentioning the fact that despite all the recent progress, CEA is yet to be further developed in order to be used as a predictive tool for the brake squeal.

In order to analyse the stability of the disc brake system, CEA results are represented either in terms of the eigenvalue real part or the negative damping ratio.

There has been a debate as to whether the real part or the damping ratio is a better measure of squeal propensity or the strength of instability. Ouyang *et al* [7, 83] have used real part as an indication of instabilities, while damping ratio is used by Nouby *et al* [84] and correlated with the real part. AbuBakar [30] has briefly explained how the damping ratio can be recognized as a measure of the strength of instability, relating it to the terms standing for the damping in Coulomb friction. Wallner [85] showed there is a proportionality between them. It is therefore reasonable to assume that the propensity for brake instability can be expressed in terms of either the complex eigenvalue real part or the damping ratio.

Massi *et al* [79] suggested combining two methods to confirm the prediction of squeal. They believed that the CEA is prone to over-predict unstable modes, which they confirmed by correlating the CEA results with the experimental results. They suggested using the stability

analysis to predict system instabilities in the frequency domain and then use non-linear analysis to reproduce squeal phenomena in the time domain.

CEA is highly affected by the model setup. Wallner [85] mentions that the results of a CEA do not only depend on the element types; there are other significant factors such as rotation speed, brake pressure, friction coefficient, material property, etc. which can affect results. The real and imaginary parts of the eigenvalues refer to strength of instability and the frequency of the corresponding unstable modes.

Numerical approaches investigating brake squeal have matured in the early years of the 21st century by significant advances in the computing power which also resulted in more complex modelling and analysis software packages. The majority of numerical investigations of post-2000 are focused on refinements on methodologies for analysis. In other words, recent researches using numerical approaches are attempting to improve the correlation level of the CAE simulations by applying the most appropriate loading functions, material properties, contact definitions, and boundary conditions.

Dom *et al* [86] developed a design of experiment study to correlate and update the FEA model in order to more accurately capture squeal behaviour. They did so by modifying the geometry of the components or their material properties, and modifying the contact elements in the assemblies. They performed Operating Deflection Shape (ODS) measurements to obtain mode shapes of the brake components. They also used the Modal Assurance Criterion (MAC) matrix and correlated their FEA and experimental results.

Goto *et al* [87] also proposed another design of experiment study to improve the level of the correlation of modal behaviour. They assigned spring elements as design variables that represent contact stiffness. This method is called Response Surface Method (RSM). This was

in the continuation of the work done by Nack [88] , attempting to capture the nonlinear contact condition of the disc/pads interface using one-way spring elements. Both researchers believed that the optimum design solution should take modal coupling into account, which requires a correct estimation of modal behaviours of the components and assembly.

Kung *et al* [89] and Bajer *et al* [90] performed CEA using the eigensolver of Abaqus (v 6.4). Their analysis included nonlinear static analysis of application of brake and rotation of the disc, modal analysis to extract the natural frequencies and CEA to obtain unstable frequencies and mode shapes. They used direct contact coupling proposed by Yuan [91] and Blaschke *et al* [92].

Chung *et al* [93] used modal analysis and the symbolic programme of Matlab matrix eigenvalue solution to decrease the computational times for CEA. Modal domain analysis used natural frequencies of components to predict unstable modes, and only perform CEA on the critical frequencies. This could reduce computational time.

Guan and Huang [94]  analysed the squeal problem from an energy viewpoint and used total energy transfer as an indication of the propensity of the system to squeal. They concluded that the proposed method allows identifying the influence of the geometrical parameters on the squeal propensity, and would be able to predict squeal propensity similar to positive real parts of the CEA.

Sinou *et al* [95] attempted to incorporate the nonlinear behaviour of the system into the CEA. They proposed a method called Complex Nonlinear Modal Analysis (CNLMA). A high level of correlation was achieved between the obtained results and the solution of the nonlinear system. This simple method required less computing power and took less time to execute compared to transient analysis.

In a recent attempt, Horing *et al* [96] improved the reliability of CEA by more accurately modelling friction material properties.

The good agreement with experimental experiences [8, 42, 43, 97, 98] proves the fact that squeal instability occurs in linear conditions. However, once the noise is generated, there are nonlinearities introduced to the system, especially in the contact interface. As Massi [79] presents the squeal instability, at its onset, occurs in the linear field. He believes that probably the most reliable, accurate and comprehensive solution could be performing two different numerical approaches to identify squeal mechanism, one being the FEA modal analysis of the disc brake system and define its eigenvalues, and relate them to the squeal occurrence. Another one being a nonlinear analysis in the time domain, with a focus on the contact problem with the friction between deformable bodies, namely disc and friction materials (pads). Then the two approaches (probably different models) are compared, and the onset of squeal is predicted both in the frequency domain by the linear model and in the time domain by the nonlinear one [79].

## 2.4. Friction and Frictional Forces

The most critical part of the knowledge required for the brake noise modelling is to understand the friction between pad and disc surfaces and the frictional forces present there. Temperature and wear are two of the main difficulties in modelling this extremely complex situation [11]. Friction is assumed to be the main parameter involved in formation of the brake squeal. There have been numerous investigations in order to obtain a clearer understanding of frictional forces.

Berger [99] attempted simulating the dynamics of the system by proposing various models for friction. Most of his models rely on the relatively simple Amonton's Law [100]. Also a number of studies use the Oden-Martin friction model [13] which enables incorporation of non-linearities of the system providing a more realistic representation of the frictional behaviour.

The other aspect of modelling frictional forces is to incorporate material removal which is defined as a wear coefficient, depending on different operational conditions. Most models incorporating frictional behaviours have little focus on the actual frictional forces and wear simulation and are usually aimed at instability prediction.

D'souza and Dweib [101] conducted the pin-on-disc testing in order to study frictional behaviours. They concluded that four different friction regimes exist in the contact interface namely linear, non-linear, transient and self-excited vibration regions. In a later study, they observed that modal coupling of normal and torsional resonances is the major reason for self-excited vibrations.

Tworzydlo *et al* [102] investigated the frictional behaviour of a pin-on-disc system including self-excited oscillation and stick-slip motion using CEA and transient analysis. Their experiments agreed with the four frictional behaviours introduced by D'souza and Dweib [101]. Their investigations also show that modal coupling was the mechanism of self-excited vibration. Tworzydlo *et al* [103] also adopted this approach in their studies.

Ibrahim *et al* [104] develop an analytical model to simulate the dynamics of the friction element. They concluded that the normal force sourced from friction can cause parametric instabilities in the form of squeal.

Eriksson and Jacobson [105] performed a sensitivity study to assess the influence of friction in formation of squeal. They observed that higher coefficient of friction has more potential to generate squeal. Also, they did not find any correlation between the negative slope of $\mu - n$ feature and squeal behaviour. They concluded that squeal is generated by friction and depends on operating conditions such as pressure, temperature, speed, humidity and other variables. A recent extensive study on the effect of humidity on friction materials by Kim *et al* [106] is a proof of this.

Hohmann *et al* [107] and Bajer *et al* [108] attempted simulating pad wear using 2 dimensional and 3 dimensional models respectively. Even though they used FEA, they used a wear function which ignored temperature effects to obtain wear displacement or material removal.

Kim *et al* [109] studied wear using a metal/metal wear in block-on-ring system. Based on the experimental data, they calculated the wear depth and then performed an FEA to simulate the material removal on the friction surface, using wear formulation. They could achieve a good correlation in wear depth.

Yuhas *et al* [110] utilised ultrasonic methods to characterize the non-linear elastic properties of friction materials. They concluded that the loading history can influence the dynamics of friction materials.

In different attempts to simulate wear effects in disc brakes; many studies only simulate wear depth, not changes in the surface finish. The majority of the work done make lots of assumptions to simplify the system, hence are unrealistic. The best way to investigate wear is experimental methods which take into account all operating conditions.

## 2.5.     Brake Noise Prediction and Reduction Methods

Numerous techniques or methods have been presented in the literature to reduce or at least limit the brake squeal. Chen *et al* [111] present recommendations to suppress and eliminate squeal occurrence. The major part of these guidelines includes optimisation of the damping, minimising the impulsive excitation and reducing the modal coupling. These three guidelines seem to be essential for squeal reduction methods.

The brake squeal is caused by a system instability related to the interaction of structural components of the brake system [23, 31], also called modal coupling. Frequency of the squeal also depends on the natural frequencies of the brake system components, and more specifically on that of the rotor [12]. In fact, the friction coefficient of the disc-pad interface is responsible for coupling the normal and tangential stresses at the contact surface [79].

Ouyang & Cao [8] believe that the compressibility of the brake fluid influences the brake performance, and varies with temperature and humidity. In addition to material properties, there are other parameters that are not readily available, including: stiffness of the brake fluid, the stiffness linking the caliper and the mounting pins, the circumferential stiffness of the piston head. These are factors associated with the fugitive nature of the brake squeal problem.

In 1961 Fosberry and Holubecki [26] proposed potential changes that could limit the squeal occurrence: offsetting the pad towards the leading edge (also called chamfer), supporting the pad abutment, using a split disc with an annular ring attached to the top-hat section, and addition of extra set of pads.

Ishihara *et al* [112] addressed the low-frequency brake squeal. They observed that COF and pressure variations simultaneous with vibrations in the normal direction of the contact

interface had a great influence in squeal. Changing the COF, the contact interface position, the vibration characteristics of the disc and caliper, and variation of the stiffness of the pad material could reduce squeal. They also proved by experiments that changing the rotor geometry and material can reduce brake noise.

Dunlap *et al* [113] provided a set of guidelines for each type of disc brake noise. They relate low frequency noise to lining material properties. They believed low frequency noise can be supressed by modal decoupling of caliper and disc. While for squeal, they suggest increasing the brake disc stiffness. They also observed that the geometry of the brake pad and the level of braking pressure were significant factors on generation of brake squeal. They also found brake insulators to be significantly effective in limiting the squeal level.

Nakajima and Okada [114] suggested that moving the piston position towards the leading or trailing edges was effective to reduce squeal.

Dessouki *et al* [115] identified three major categories of brake noise: caliper bracket induced squeal, pad induced squeal and disc induced squeal. For the caliper related noise they recommended stiffening the bracket. For the pad-induced squeal, they prescribed addition of chamfers, shorter length of pads and brake shims. For disc-induced squeal, they used slice cuts in the radial direction, increase cheek thickness and disc damping.

Kido *et al* [116] combined analytical and numerical approaches using a 3-DOF model. They aimed to set guidelines for squeal suppression and use FEA methods for design stage predictions.

Nishiwaki *et al* [51] believed that brake squeal is mainly driven by the modal behaviour of the disc. They altered the disc geometry by removing a number of vanes and fins, which was in

fact shifting the modes of the disc. Matsuzaki and Izumihara [55] also proposed a similar approach.

Fieldhouse *et al* [54] proposed disc asymmetry to reduce disc brake squeal, believing it can decouple bending modes. They made radial holes in the disc rim to do so. Kung *et al* [40] investigated the modal contribution factor of the disc in formation of squeal and reported the rate of 23 per cent. They concluded that disc geometry can be influential in modal decoupling. Modifications to geometry of the system components, and mainly the brake disc, has been investigated by other researchers too, Baba *et al* [117], Bergman *et al* [118], Pfeifer [119] and Shi *et al* [18]. If not all, the majority of these studies admit that modal coupling is the major cause of brake noise and recommend geometrical changes to different components (mainly disc) to perform modal decoupling.

In summary, potential solutions for the brake noise seems to be as follows, although most of these solutions are simply different techniques of modal decoupling:

- Reducing coefficient of friction [29, 80, 118], although it reduces braking performance

- Use of visco-elastic damping material on the back of back-plate (shims) [120, 121]

- Modifying geometry of major parts (pads [67, 122], disc [51, 123] and caliper [124, 125])

- Modifying material stiffness and damping [126, 127]

- Pad attachment method (clips geometry and installation) [128]

## 2.6.    Summary and Conclusion

Considering various perspectives of major researchers of the field, and also taking advantage of the recent developments in numerical analysis software, the best investigation approach

seems to be use of the FEA and more specifically CEA. This is the methodology practiced by Professor Ouyang and Dr Abu Bakar, whose work has influenced this research significantly.

The numerical analysis results should be compared and validated by some specific experiments which simultaneously assess reactions of the same brake system to the imposed conditions. Also, once adequate reliable data is obtained from the above mentioned steps, possibility of using the new numerical tools such as Artificial Intelligence becomes an option.

Friction seems to be the major destabilising factor, initialising instabilities causing brake noise. The instability is due to energy transfer from similar modes or coinciding resonant frequencies of brake system components. Onset of instability is related to the frictional forces, and the modal coupling is the mechanism of generation of noise, driven by this force.

Frictional forces as the major source of instability require an in-depth study, and modal coupling as the representation of the system instability needs to be investigated. Modal decoupling techniques need to be applied to develop a design procedure. In doing so, ability to simulate the modal coupling has a major significance. This needs to be addressed by improving the level of realism in the simulations of the system. There are certain aspects of the FEA models and more specifically the CEA method which has been ignored in the past. This includes but is not limited to the material properties and more specifically material stiffness and damping, mesh quality and element types, definition of the boundary conditions of the system components including loadings and contact definitions,

Also, selection of the most suitable procedures incorporated in the software package is significantly important, such as selection of the correct solver, the correct means of application of material properties (mainly system damping) and element types based on their behaviours.

These become even more significant as the current studies usually compromise on the level of complexity of the FEA model, due to various factors mentioned above. This could be the reason why majority of the studies mention that numerical approaches are not yet mature enough to simulate the phenomenon, while they have only used a small part of what is available in the software packages.

There seems to be a significant need for an in-depth investigation which goes beyond the available knowledge by employing a powerful software package and the required computing power. Also, performing the different known techniques on one single brake unit as the reference can be beneficial. Therefore this study sets out to identify potential areas where the simulation of the brake system can be significantly improved.

Simulation of the system damping is a significant potential in limiting over-prediction of instabilities by CEA. Hence simulation of damping is investigated from two perspectives of simulation of material damping of the system components and the secondary damping added to the system by application of brake shims.

Another major investigation aimed at improving the efficiency of the brake system simulation is developing a new simulation technique which addresses a critical debate in the field. The effectiveness and efficiency of time domain and frequency domain analyses have been discussed at length in the literature. There are various factors involved in the selection of each method by different researchers which have changed over time. The advantages and disadvantages of each method are investigated with a view to developing a new combined method.

The new method should combine the time domain and frequency domain solvers in an efficient way based on hypotheses concluded from the mechanism of generation and radiation

of brake noise. The aim is for the co-simulation analysis to return time domain results using less computing time/power compared to the frequency domain analysis performed using CEA.

Beyond the improved simulation of the brake system to more accurately replicate (and refine) the brake noise on an existing brake unit, there is also a significant potential on the brake noise refinements. The major potential aspect for such an improvement is the friction material as the frictional forces are influential factors in noise generation mechanisms. Therefore, a potential solution in controlling the frictional forces at the disc-pad contact interface is another aim of this research.

# Chapter 3: Methodology

## 3.1.    Introduction

Numerical methods have shown their capability in providing a more comprehensive simulation of the brake noise phenomenon. More significantly, FEA has become the preferred tool for investigating the topic by the brake NVH research community. FEA method is a cost effective and fast solution for simulating the system in the early stages of build. This enables prediction of the instabilities which can cause brake noise in the early design and development stages. FEA is also capable of providing a realistic representation of the brake system by taking system nonlinearities into account and presenting component deflections precisely. These advantages of FEA provide a promising potential for this method being the enabler for reaching a design and analysis tool for a quiet brake.

As reviewed in the previous chapter, there have been significant improvements to the numerical approaches of brake noise investigation. The recent advancements in the FEA method mostly address CEA and its limitations. The most significant limitations of CEA are in providing an accurate prediction of the unstable frequencies of the system, or the relative strength of instabilities. These two aspects of the CEA results, if improved, can enable prediction of the occurrence of brake noise more accurately. In other words, majority of the improvements on the CEA method will contribute to improving these two aspects of the analysis results.

There are different solution schemes and numerous software packages available to perform FEA. The numerical analysis approach of the study, and more specifically the software package employed to perform the analysis should be selected carefully. Each of the available

software packages offers different advantages. However, the major limiting factor of the majority of them is the required computing power and the time they require for delivering an analysis. Once the available computing power is defined, the software package can be selected based on the expectations from the analysis results.

The FEA model needs to be validated before performing the study, in order to ensure that the model is correctly representing the actual structure and behaviour of the brake system. The validated model can be expected to correctly predict system instabilities. Common methods of model validation mainly come from the experimental approaches of brake noise investigation. A common method of validating the numerical model in general is to correlate the fundamental aspects of the system with experimental results. The common practice for this step is correlation of the modal behaviours of the individual components of the system with experimental results. Other types of experimental methods are obviously brake dynamometer or vehicle on-board noise search tests which can confirm findings of the numerical investigations.

This chapter presents the methodology of performing the study in general. This starts with a review of the experimental methods employed, as well as the detailed steps for building up the numerical model and performing the analysis.

## 3.2. Brake Dynamometer and Vehicle Noise Search Experiments

In order to be able to assess the NVH characteristics of the brake unit chosen for the study, a comprehensive brake dynamometer noise search test was performed. For this purpose, the

brake corner unit was mounted to the vehicle corner structure which simulates the suspension links holding the brake unit to the chassis. This can be seen in Figure 2.



**Figure 2, Brake corner unit mounted on the dynamometer**

The brake unit underwent the SAE J2521 standard brake noise investigation test. This test includes different braking manoeuvres including drag, reverse braking, deceleration and normal forward direction braking. These manoeuvres are described Table 1:

**Table 1, SAE J2521 test manoeuvres**

| Module | Repetition | Velocity (km/h) | Pressure (bar) | IBT (°C) |
|---|---|---|---|---|
| Drag | 266 drags | 3 & 10 | 5-30 | 50-300-50 |
| Deceleration | 108 stops | 50 | 5-30 | 50-250-50 |
| Forward & Reverse | 50 drags | 3 & -3 | 0-20 | 150-50 |

Figure 3 represents results of the test.
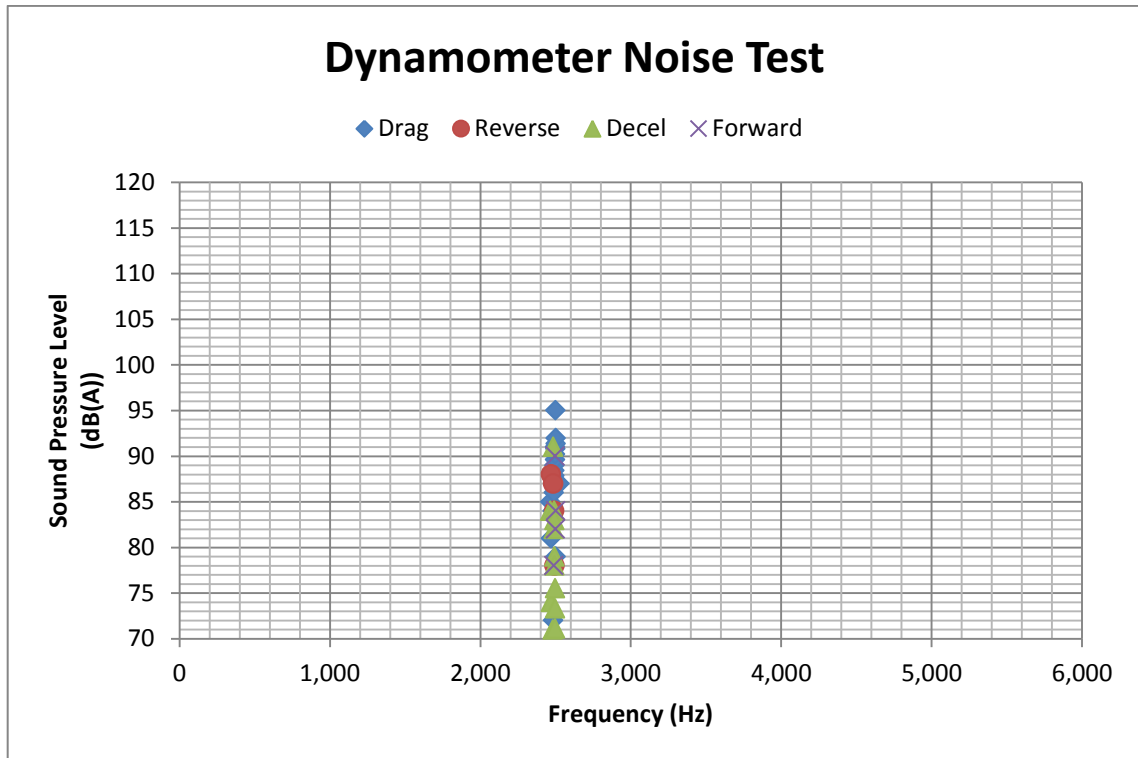
**Figure 3, Maximum sound pressure level vs. frequency (SAE J2521) (JLR)**

The dynamometer test shows a major noise recorded at the frequency range of about 2.5 kHz. Since this noise is repeated on different braking scenarios like reverse direction, deceleration and drag, it is counted as a major noise with very high likelihood of happening on the production vehicle too.

In order to fully assess the NVH performance of the brake unit, a vehicle brake noise search experiment has also been performed. This will be the basis to correlate the results of the numerical investigation with. The vehicle test is performed by installing various sensors to different parts of the vehicle, to record the required data. The instrumented vehicle carried thermal sensors on the brake disc to record the approximate temperature of the frictional interface. This data can also be referred to for selection of the correct shim, since the damping in the rubber material is a variable of the temperature. Also, in order to record the brake noise, microphones were installed on different parts of the car. The most common location for

recording the noise is inside the car, near the driver or passenger's ear. This depends on the brake corner being evaluated, in front or rear and on left or right.

Although the vehicle test is the most accurate representation of the NVH performance of the brake in real life (i.e. installed on the car driven by the customer), it is known that the vehicle test might demonstrate some NVH behaviour that is not consistent among the tests. This is due to the numerous variables involved in the vehicle brake noise test, majority of them in the category of noise initiation mechanisms. Some brake noise initiation mechanisms only exist on the car and are dependent on the actual manoeuvre performed. An example of this is when the car steers to one side while brakes are applied, and consequently a tension is introduced on the suspension links. This load can slightly shift the resonant frequencies of the components, making some modes easier to transfer energy and couple as an unstable mode causing vibrations. These types of noise are not commonly associated with the brake system directly. However, they are assumed to be a result of the interaction of the brake unit with the chassis through the suspension, i.e. suspension links and the method of installation of the brake corner unit to the suspension through knuckle and by the joint bushes mainly. In order to obtain a robust and reliable result from the vehicle noise search tests, the set of different manoeuvres should be repeated to identify the recurrent noises. Figure 4 previews the vehicle test results, based on the most frequent noise occurrences obtained from a set of tests.
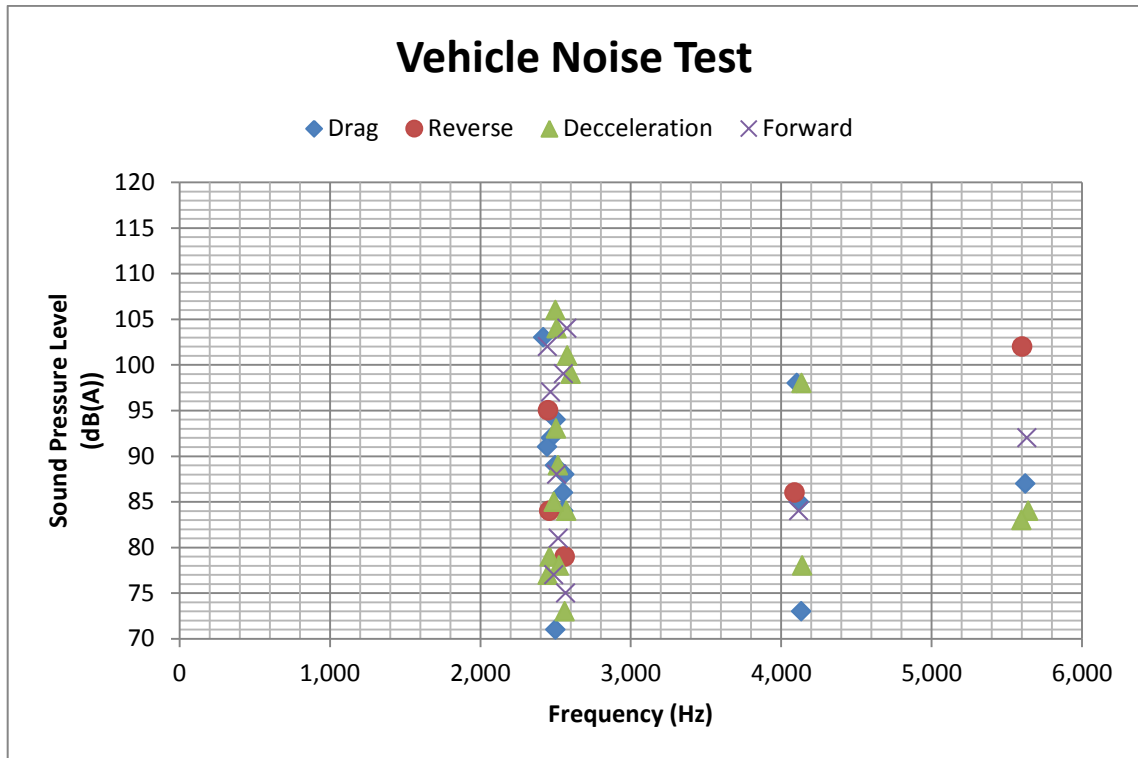
**Figure 4, Vehicle brake noise test result (JLR)**

The 2.5 kHz noise is recorded on all braking scenarios both on the dynamometer and the vehicle. There are also noise recorded at 4.1 kHz and 5.6 kHz which has only occurred in limited deceleration scenarios on the vehicle tests. Considering the few occurrences of noise and the fact that the vehicle noise tests were performed using an engineering prototype rather than a production vehicle, the 4.1 kHz and 5.6 kHz noises could have been caused by a different variable and should be looked at differently. Therefore, the CAE analysis is aimed at correlating with the most probable noise from the corner unit, commonly being observed on the dynamometer and vehicle. It is also important to remember that the brake noise simulation does not take the whole vehicle into account and the analysis results are expected to mainly correlate with the brake dynamometer noise search results.

## 3.3. Modal Experiments of Brake System Components

As mentioned in the introduction, a principal method for verifying the model employed for the numerical investigation is performing modal experiments. This can ensure the FEA model is exhibiting the same major characteristics. Correlation of the modal behaviour can ensure both material properties and geometrical specifications of the component have been simulated accurately. Modal studies, experimental or analytical, investigate dynamics of a mechanical system or structure. In the experimental modal study which is in the frequency domain, the system response is presented in the format of Frequency Response Function (FRF). Two major methods of performing modal experiments are impact hammer and shaker test.

FRF method consists of measuring the input (excitation) and output (response) simultaneously. In order to derive the transfer function, the laplace transform of the response is divided by the Laplace transform of the excitation function. There are different types of Fourier transform-based instruments which can implement different types of excitation sources and return the FRF. This is where a data acquisition software is employed to receive the data from the sensors and return the FRF data.

### 3.3.1. Test Rig Design for Modal Experiments

In order to perform the modal experiments, a test rig was designed and built. The structure has been designed based on the components' size and mass to accommodate both hammer test and shaker test. Figure 5 shows the CAD model of the final structure.
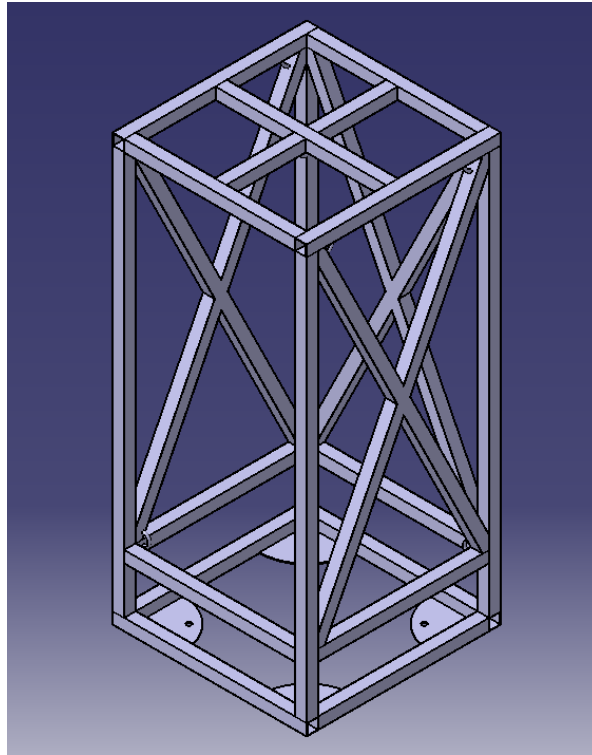
**Figure 5, CAD design of the test rig structure using Catia v5**

### 3.3.2. Design of Experiments

The modal study consists of determining the behaviour of the brake system components, as well as estimation of the level of damping in each component. The aim of this design of experiment is to validate the modal experiments based on the CAE FRF prediction. The modal experiments will provide the level of material and contact damping, which will be used to perform the damping tuning study later.

Initially the hammer test and shaker test are performed on every component of the brake system. The test results are compared and correlated with the CAE results. A Frequency Response Function (FRF) is obtained from the measure of the impact force input and the acceleration output. The Labview [129] software is employed to record the vibration input force and the output acceleration.

For the hammer test the FRF is calculated using the Fast Fourier Transform (FFT) and for the shaker tests, the FRF was measured directly since the force and acceleration were measured at individual frequencies (swept sine).

Light weight components have been tested using the impact hammer, since the mass added to the structure due to the mechanism used to mount the load cell (shaker shaft) could significantly alter the dynamics of the structure. This causes the force measured by the load cell to be more important than the force that is actually applied to the structure. Likewise the shaker is isolated from the structure by mounting it to a solid bedding in order to prevent any reactions from the shaker base back to the structure.

In order to obtain the most accurate results, the boundary conditions of the experiment need to represent the free-free CAE analysis conditions as much as possible. Therefore, the components are suspended from the test rig using rubber strings. Moreover, in these test conditions the six rigid body motions would not interfere with the flexible body modes. The frequency of the rigid body modes in that case would not be higher than 0.01 kHz. By accurately windowing the hammer test responses, it is assured that the noise potentially generated by the rigid body modes is not recorded. Figure 6 presents the design of experiment for this study. In this DOE initially the CAE modal extraction is performed. Then hammer test and shaker test are performed on components and assemblies. In order to ensure both test methods are returning consistent results, one component is chosen to undergo both tests. Based on the individual component tests, material damping data was obtained and the assembly-level shaker test data provided estimation of contact damping level.
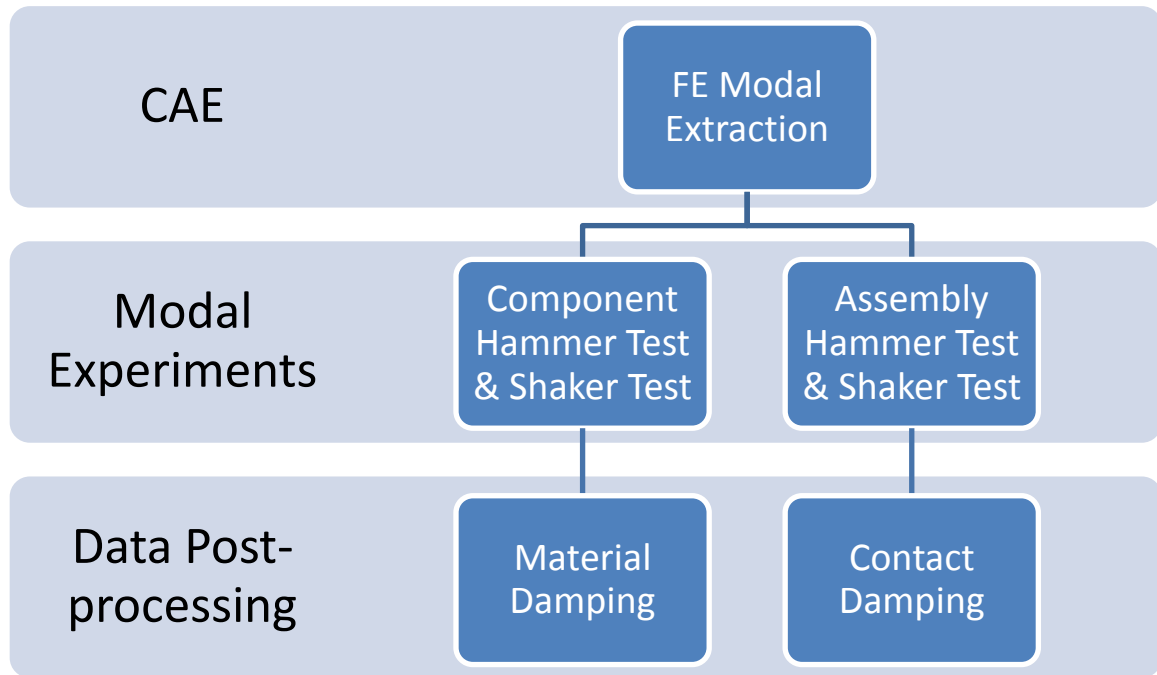
**Figure 6, Design of Experiment - modal studies**

Also, a Matlab-based script [130] has been utilised to visualize the modal behaviour of the components at their resonant frequencies from the experimental data.

The peaks of the FRF graph represent the actual resonant frequencies of the components. Once the resonant frequencies are determined, mode shapes are then plotted to confirm that the mode shape excited matches the CAE predictions. It is however considered that there are cases when the CAE modal prediction reports resonant frequencies (and mode shapes) which do not exist in the test. This is due to the sensitivity of the solver to the fluctuations of the FRF graph, assuming minor peaks as resonances.

Swept Sine is the test on the caliper + knuckle assembly that was performed with the shaker. The accuracy of the Swept Sine and the unequal mass distribution of this assembly accounts for the choice of this technique over the hammer test. The main advantage of such a technique is that it excites the structure precisely at each frequency within a given range. In those cases, the range of the frequency chosen is the same as the CAE tests, i.e. 0.01 - 6 kHz.

The transition from the component hammer test and shaker test to the assemblies is confirmed with the test on the knuckle since its weight is sufficiently great not to be disturbed by the mount of the cell load thus enabling it to be tested by those methods. The component is tested with the two techniques and the correlation with the CAE results in both cases is then evaluated.

### 3.3.3. Shaker Test

The most useful shakers are the hydraulic and electromagnetic types. The force produced by the electromagnetic shaker is generated by an alternating current, which is driving a magnetic coil. There are several types of shakers depending on the force they can produce. Commonly, electromagnetic shakers are able to generate a force from 0.5 Hz up to 20 kHz. Figure 7 illustrates the schematic of a shaker test set-up.
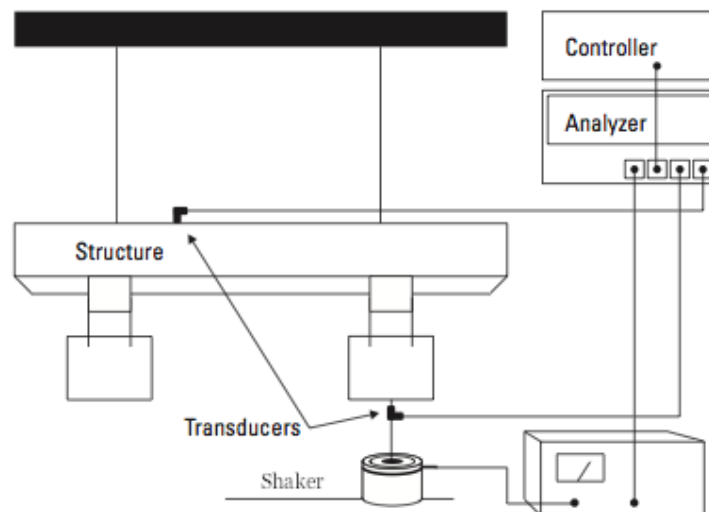


Figure 7, Shaker test settings

Many features have to be considered for performing the shaker test. The shaker is physically mounted to the structure in order to excite it thus creating possible alterations on the dynamics of the structure. This is more likely to occur on the relatively lighter structures. The mass added to the structure due to the mechanism used to mount the load cell may account for the

alterations. The FRF is a single input function which means only the excitation force should be transmitted through the main axis of the load cell. There might be relative movements of the shaker shaft from the based it is installed on, which can introduce inaccuracies. In order to minimise the displacements of the shaker, it is a common practice to fix the shaker body to the test bed. Also, to minimize the problem of lateral forces, the shaker should be connected to the load cell through a thin rod, called a "stinger", to allow the structure to move freely in the other directions. Otherwise reaction forces can be transmitted through the base of the shaker back to the structure. Also electromagnetic shakers can experience some impedance mismatch between the structure and the shaker coil. When the effective mass associated with a resonance is minor, a response can be obtained with minimal force. This can result in a drop in the force spectrum in the vicinity of the resonance, which can be misunderstood as noise. Figure 8 shows the brake knuckle being tested on the rig using a shaker.
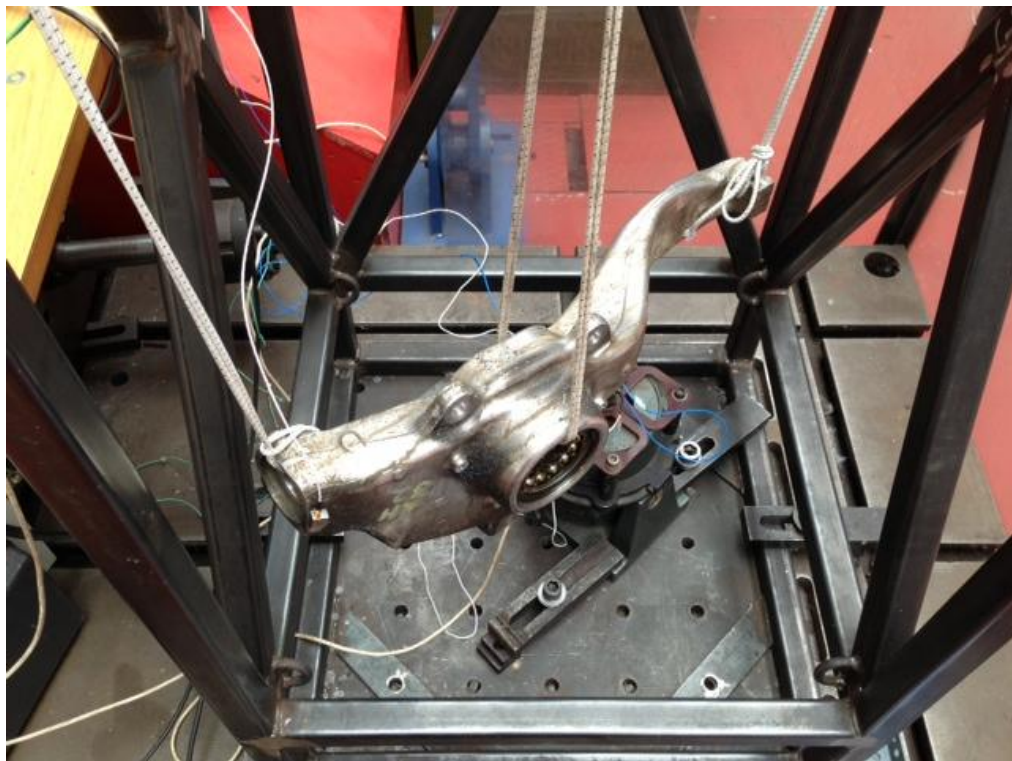


Figure 8, Brake knuckle being tested using a shaker on the test rig (UOB)

### 3.3.4. Hammer Test

A common excitation mechanism in modal testing is the use of impact device, also called impact hammer. It is a relatively simple technique to implement since this technique requires very little hardware and provides shorter measurement times. The method of applying the impulse includes an acoustic hammer, and a suspended mass. Figure 9 presents an outline of the hammer test procedure.
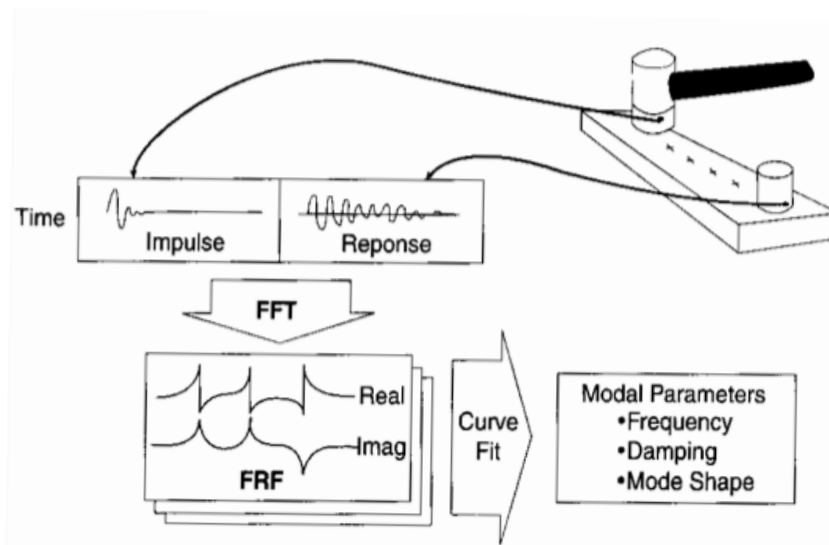


Figure 9, Hammer test settings

The impact force from the hammer is an input given by the user, and the amplitude of the energy applied to the structure is a function of the mass and the velocity of the hammer. This is due to the concept of linear momentum.

There are two major signal processing problems associated with impact testing. Firstly, the impact is sensitive to the time, and variation in the impact time can introduce noise. Secondly, if the response is recorded in a short time, leakage can be present in the response signal. Both these problems can be compensated by using windowing techniques. Since the force pulse is usually very short relative to the length of the time record, the portion of the signal after the

pulse is considered as noise and therefore can be eliminated without affecting the pulse itself. Figure 10 shows the brake hub suspended from the test rig, being tested using the impact hammer technique.



Figure 10, Brake hub hammer test (UOB)

### 3.3.5. Damping in Modal Testing

In order to determine the damping ratio using the FRF graph the half-power bandwidth method [131] is used. This method has been extensively used for both SDOF and MDOF structures. Application of this method for estimation of the component damping has limited meaning without modelling the structure using a SDOF system or by a series of decoupled SDOF systems. The application of the half-power bandwidth method is extended to MDOF structures assuming that each peak in the frequency response function is affected only by the mode under study. Also, the method is challenged in cases of MDOF structures with closely spaced modes, for being susceptible to possible mode coupling. The degree of this mode

coupling in a structure depends on the interplay among its damping distribution, its geometric characteristics (from which its natural frequencies can be found) and its type of excitation.
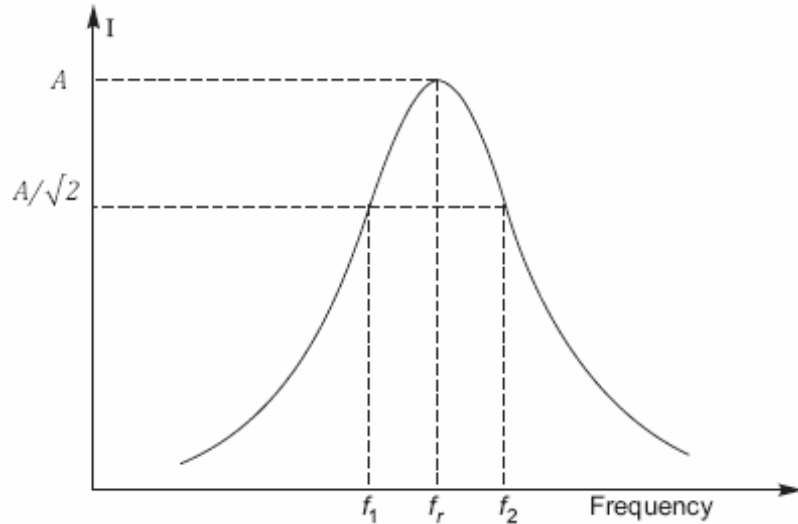


Figure 11, Half power bandwidth damping

It is assumed that the half of the power dissipation in the mode chosen occurs in the frequency band $[f_1, f_2]$, where $f_1$ and $f_2$ correspond to $A/\sqrt{2}$. It is shown that the damping ratio $\xi$ is approximately:

$$\xi = \frac{f_2 - f_1}{f_{res}}$$

Equation 1

These experimental methods have been performed widely in many research studies. This gives the confidence that the results obtained are meeting a sufficient level of accuracy. Also, the ease of implementation, versatility and accuracy of these tests account for their popularity.

## 3.4. FEA Model Built and Complex Eigenvalue Analysis (CEA)

In order to perform the numerical study, the FEA approach has been selected. The software package for performing the FEA simulation is Abaqus CAE, and the Lanczos solver performs

CEA in order to assess the stability of the system in the defined frequency domain. The analysis results provide unstable frequencies of the system, as well as an estimation of strength of corresponding instability.

For this reason, an FEA model has been developed based on the CAD data of the components. The model has been assessed in terms of sensitivity to mesh characteristics, and the optimum mesh size and type have been chosen. The analysis procedure has been defined and the results are presented in a consistent format in one single graph.

This section reviews different steps of FEA model build and analysis in the steps mentioned.

### 3.4.1. Model Set-up

The FEA model of the brake system consists of all components of the corner unit, including links and connections where it is mounted on the car. Figure 12 represents the isometric view of the FEA model.
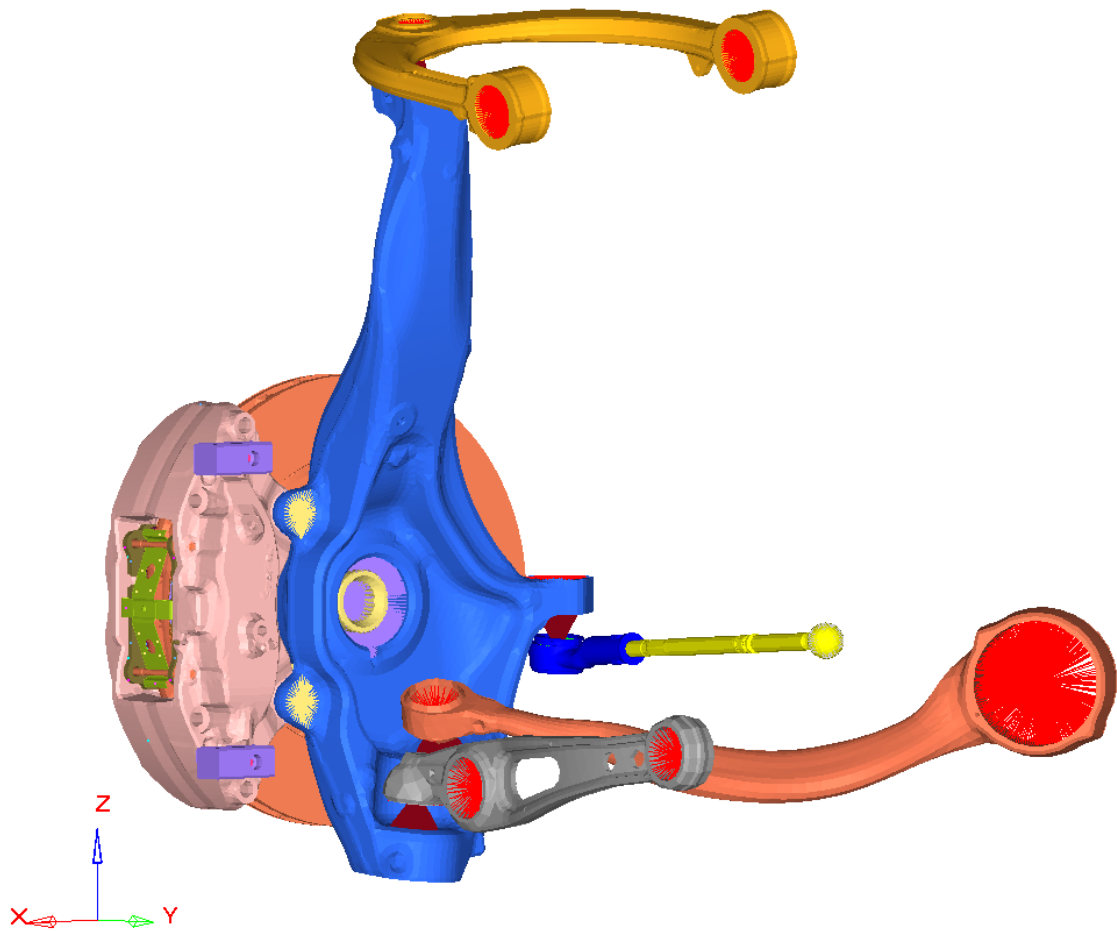
**Figure 12, Brake CAE model in HyperMesh software - isometric view**

Major components included in the model are as follows:

- Disc

- Hub

- Caliper assembly (housing, pistons and seals, central spring and lumped masses)

- Pad assembly (friction material, back-plates and shim)

- Knuckle

- Suspension links (upper, lateral and tension control arms)

- Bushes and bearings

The geometry is imported to the FEA software as a CAD model in either .IGES or .STEP format. Then surfaces are trimmed to be prepared for a fine mesh (this is technically called surface clean-up), in order to obtain more accurate results. This includes fillets, surface connection margins, parts edges etc., where automatic meshing might not be accurate enough which causes element distortion in the analysis step.

The next step is assigning the material properties. This is when the CAD model starts becoming a FEA model. Each component is assigned its corresponding material properties. Figure 13 presents a breakdown of the CAE model components:
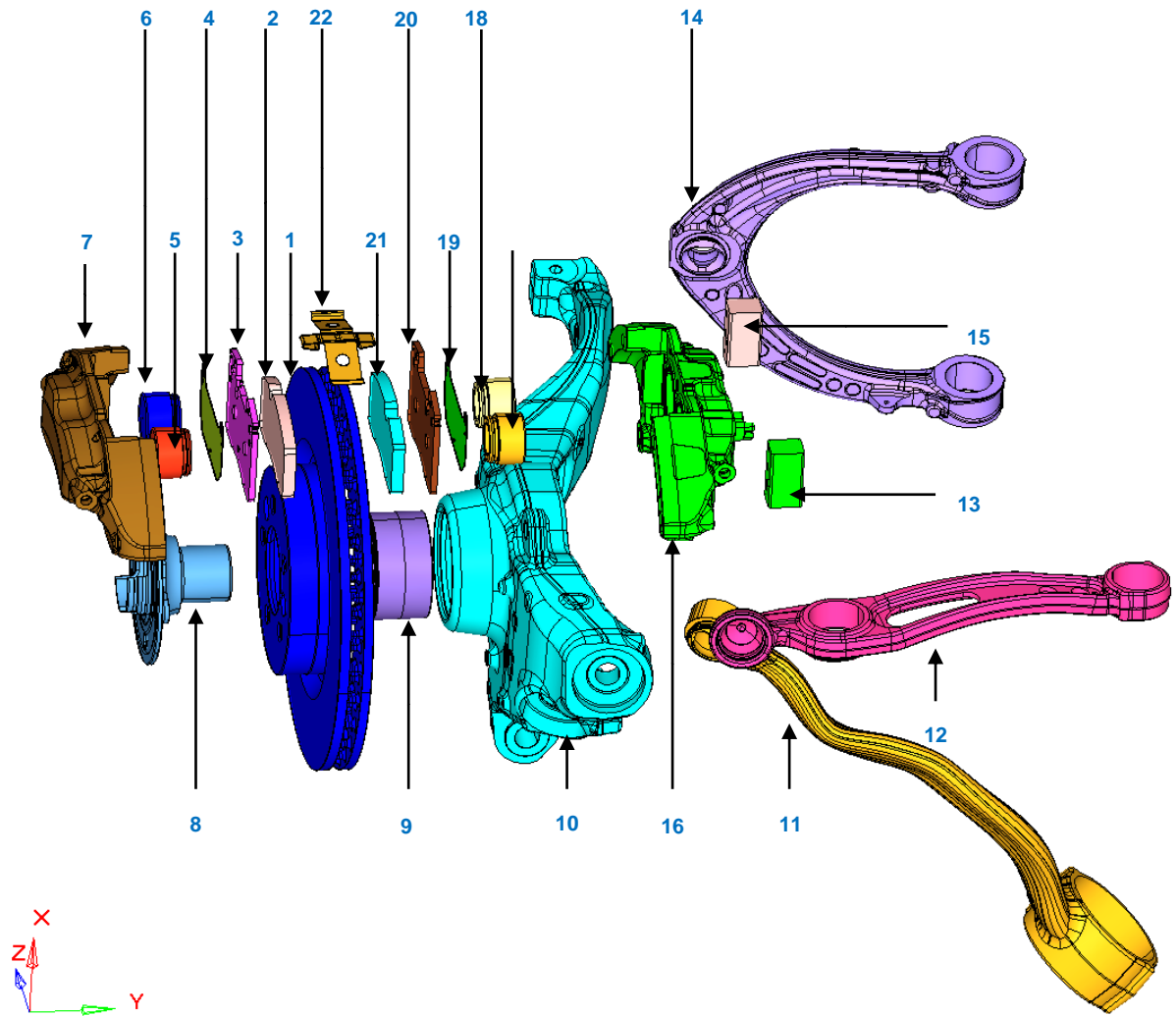
**Figure 13, Breakdown of CAE model components**

Table 2 presents the part names as mentioned in Figure 13, as well as their corresponding material:

**Table 2, Brake CAE model components and materials**

| Number | Part Name | Material |
|--------|-----------|----------|
| 1 | Disc | Grey Iron |
| 2 | Outer Pad | Friction Material |
| 3 | Outer Back-plate | Steel |
| 4 | Outer Shim | Steel |
| 5 | Outer Piston (Left) | Forged Steel |
| 6 | Outer Piston (Right) | Forged Steel |
| 7 | Caliper Outer Body | Aluminium |
| 8 | Hub | Forged Steel |
| 9 | Bearing | Steel |
| 10 | Knuckle | Aluminium |
| 11 | Tension Control Arm | Steel |
| 12 | Lateral Control Arm | Steel |
| 13 | Lumped Mass (Right) | Forged Steel |
| 14 | Upper Control Arm | Aluminium |
| 15 | Lumped Mass (Left) | Forged Steel |
| 16 | Caliper Inner Body | Aluminium |
| 17 | Inner Piston (Left) | Forged Steel |
| 18 | Inner Piston (Right) | Forged Steel |
| 19 | Inner Shim | Steel |
| 20 | Inner Back-plate | Steel |
| 21 | Inner Pad | Friction Material |
| 22 | Central Spring | Forged Steel |

The materials mentioned in Table 2 are assigned to the corresponding components using the material properties provided in Table 3.

Table 3, Material properties for the corresponding materials in the CAE model

| Material | Density [kg/m^3] | Young's Modulus [MPa] | Poisson's Ratio |
|---|---|---|---|
| Grey Iron | 7,100 | 109,000 | 0.26 |
| Aluminium | 2,720 | 71,000 | 0.33 |
| Steel | 7,850 | 207,000 | 0.30 |
| Forged Steel | 7,820 | 206,800 | 0.29 |

The next step is assigning contact properties for the bodies in interaction. The contact properties and boundary conditions are defined to assemble the components in the appropriate way. This enables the assembled system in the FEA model to behave as per the physical model. The disc-pad interface which is the main interaction is assigned a coefficient of friction (COF) and undergoes a pressure from the piston. Other interactions include the bolted joints and bushes.

### 3.4.2. Mesh Convergence Study

The last step in converting the CAD model into a FEA model is assigning the appropriate mesh density to each of the components of the model. Different components are assigned a different mesh based on their geometry and sensitivity. This is based on the optimum mesh size study (also called mesh convergence study). Components vary in the mesh characteristics not only from element size point of view, but also each component might require different type of mesh enabling application of specific loadings, boundary conditions or analyses.

In order to ensure the CAE model is meshed using the optimum element size, a mesh convergence study has been performed on the disc. This is a comparison of the reported frequency of the resonant frequencies of the part, once meshed with different element sizes. As seen in Figure 14, element size 6 mm (shown in orange) is the point where the mesh is fine enough to ensure the analysis results are accurate. However, where possible, components have been assigned even a finer mesh. This depends on the geometry of the component.
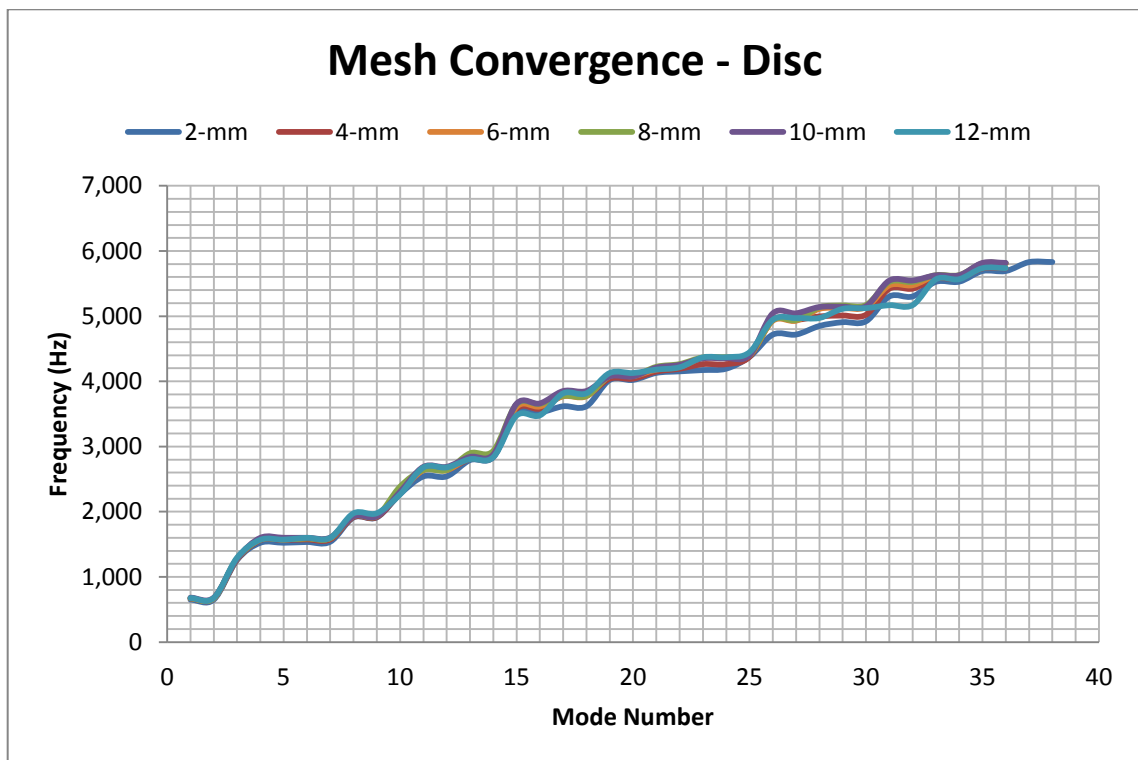


Figure 14, Mesh convergence study - Disc

Also, Table 4 is a detailed representation of variation in the reported frequency for all resonant frequencies of the disc meshed in different element sizes.

**Table 4, Variation in the reported frequency of the resonant frequencies vs. mesh size**

| Mode Number | Frequency (Hz) | | | | | |
|---|---|---|---|---|---|---|
| | 2 mm | 4 mm | 6 mm | 8 mm | 10 mm | 12 mm |
| 1 | 650.65 | 668.3 | 671.29 | 672.59 | 681.62 | 675.9 |
| 2 | 650.82 | 668.4 | 671.55 | 672.77 | 681.7 | 676.28 |
| 3 | 1259.4 | 1265.8 | 1280.9 | 1276.8 | 1277.2 | 1294.8 |
| 4 | 1523.5 | 1563.3 | 1572.1 | 1573.9 | 1599.3 | 1569.4 |
| 5 | 1523.8 | 1567.1 | 1572.6 | 1574.4 | 1599.8 | 1572 |
| 6 | 1535.1 | 1574.6 | 1593.3 | 1590 | 1600.1 | 1599.7 |
| 7 | 1538.9 | 1574.8 | 1596.4 | 1593 | 1603.6 | 1599.9 |
| 8 | 1911.7 | 1916.5 | 1937.2 | 1932.9 | 1929.5 | 1975.8 |
| 9 | 1912.7 | 1917.4 | 1938.1 | 1933.7 | 1930.4 | 1976.6 |
| 10 | 2272 | 2286.5 | 2301.5 | 2385.2 | 2306.3 | 2266.5 |
| 11 | 2541.4 | 2643.8 | 2637 | 2640.6 | 2688.8 | 2679.2 |
| 12 | 2542 | 2644.2 | 2637.8 | 2641.1 | 2689 | 2679.8 |
| 13 | 2791.4 | 2807.8 | 2829.8 | 2896.7 | 2841.1 | 2806.1 |
| 14 | 2836.6 | 2850.8 | 2870 | 2933.9 | 2878.1 | 2837.7 |
| 15 | 3516.6 | 3577.4 | 3608.8 | 3649.4 | 3657.2 | 3474.8 |
| 16 | 3522.5 | 3582.4 | 3614.3 | 3653.8 | 3661.6 | 3478.1 |
| 17 | 3617.2 | 3780.3 | 3769.9 | 3776.4 | 3851.6 | 3816.4 |
| 18 | 3618 | 3780.7 | 3771.3 | 3778.2 | 3852.1 | 3816.8 |
| 19 | 4021.1 | 4040.7 | 4080.6 | 4082.2 | 4076 | 4128.1 |
| 20 | 4021.6 | 4041.1 | 4081 | 4082.5 | 4076.2 | 4128.2 |
| 21 | 4129.7 | 4150.3 | 4180.1 | 4223.1 | 4210.2 | 4180.7 |
| 22 | 4153.1 | 4192.8 | 4224.3 | 4264.8 | 4252.7 | 4215.7 |

| 23 | 4173.1 | 4264 | 4360.4 | 4367.3 | 4352.4 | 4368.2 |
| 24 | 4194.5 | 4264.3 | 4363.7 | 4370.6 | 4354.8 | 4370.9 |
| 25 | 4376.3 | 4376.2 | 4400.2 | 4404.2 | 4401.5 | 4447 |
| 26 | 4717.2 | 4943.2 | 4929.2 | 4940.8 | 5043.2 | 4945.1 |
| 27 | 4718.1 | 4943.4 | 4930.4 | 4941.2 | 5044.3 | 4971.1 |
| 28 | 4849.4 | 4996.6 | 5112.5 | 5135 | 5140.8 | 4972.4 |
| 29 | 4907.7 | 5009.7 | 5123.7 | 5163.6 | 5145.8 | 5112.8 |
| 30 | 4921.1 | 5021.8 | 5138.9 | 5170.5 | 5152.3 | 5123.2 |
| 31 | 5301.8 | 5421.6 | 5472.7 | 5524.2 | 5545.9 | 5168.7 |
| 32 | 5302.5 | 5422.1 | 5474.8 | 5525.4 | 5547 | 5169.4 |
| 33 | 5527.2 | 5576.5 | 5618.4 | 5629.4 | 5626.7 | 5565.7 |
| 34 | 5529 | 5577.5 | 5619 | 5630 | 5627.1 | 5568.1 |
| 35 | 5692.5 | 5732.6 | 5807.8 | 5808.7 | 5816.6 | 5736.3 |
| 36 | 5692.9 | 5733.2 | 5808.9 | 5809.3 | 5817.1 | 5736.6 |
| 37 | 5829.6 | -- | -- | -- | -- | -- |
| 38 | 5830.8 | -- | -- | -- | -- | -- |

Once the maximum element size was defined, components were meshed with the specific element sizes as tabulated in Table 5.

**Table 5, Brake model parts - Element size and type**

| Part Name | Element Size (mm) | Element Type |
|---|---|---|
| Disc | 6 | C3D10 |
| Friction Material | 2 | C3D10 |
| Back-plate | 2 | C3D10 |
| Shim (Steel) | 2 | C3D15 |
| Piston | 3.5 | C3D10 |
| Caliper Body | 4 | C3D10 |
| Hub | 6 | C3D10 |
| Bearing | 4 | C3D10 |
| Knuckle | 6 | C3D10M |
| Tension Control Arm | 6 | C3D10 |
| Lateral Control Arm | 6 | C3D10 |
| Upper Control Arm | 6 | C3D10 |
| Lumped Mass | 4 | C3D10 |
| Central Spring | 1 | C3D10 |

The model of the rotor, as shown in Figure 15, is constructed using second order tetrahedral elements (C3D10).
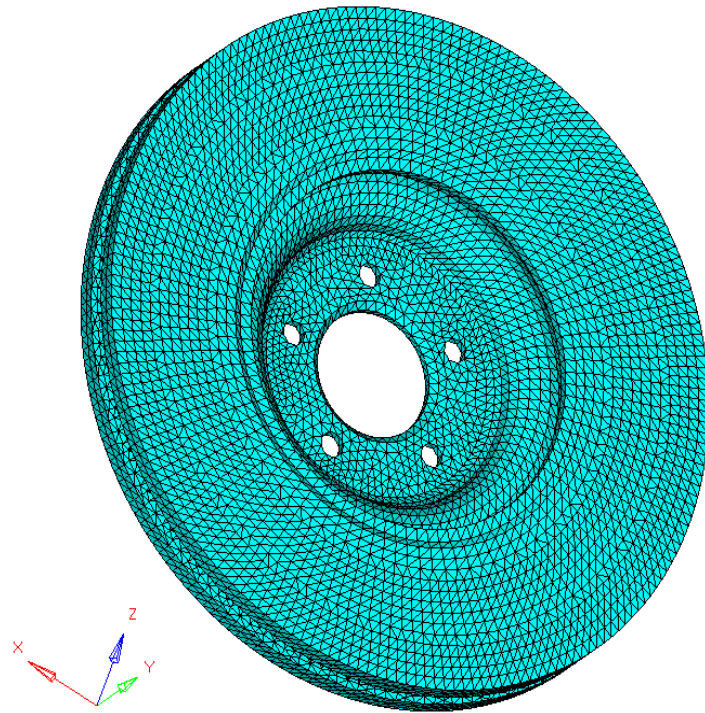
**Figure 15, CAE model - brake disc**

The pad assembly consists of the friction materials (also referred as pad), back-plate and the shims. The back-plates and the shims are made of steel and the pads are made of anisotropic friction material. The coefficient of friction used for the pad material ranges from 0.3 to 0.7. There will be no relative motion between the pad, back-plate and the shim as the interfaces between them are merged. The pad assemblies are shown in Figure 16.
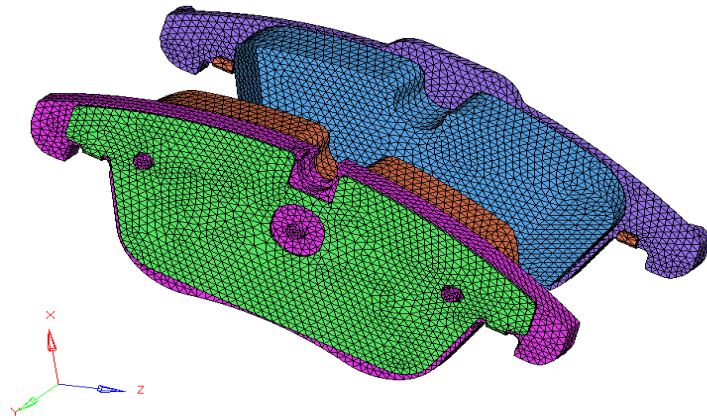
**Figure 16, CAE model - pad assembly**

Pistons operate in the bore of the caliper body and are the parts that convert the hydraulic pressure to mechanical force on the brake pad. The outer mesh of the piston is in contact with the inner surface of the bore of the caliper while there is a common mesh between the inner piston surface and the fluid elements. A set of pistons on one side of the caliper is presented in Figure 17.
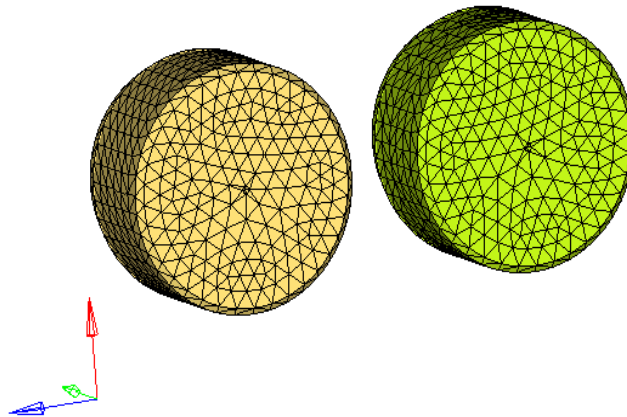


**Figure 17, CAE model - caliper piston**

The central spring is an independent component in the caliper assembly, which is meshed using C3D10 elements. The central spring is presented in Figure 18.
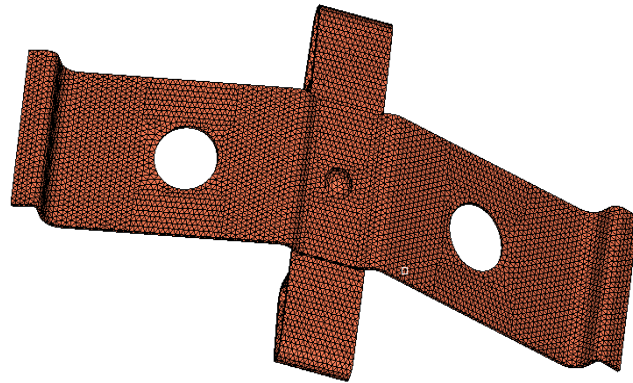
**Figure 18, CAE model - central spring**

The hub spins along with the rotor and is meshed using tetrahedral elements as seen in Figure 19.
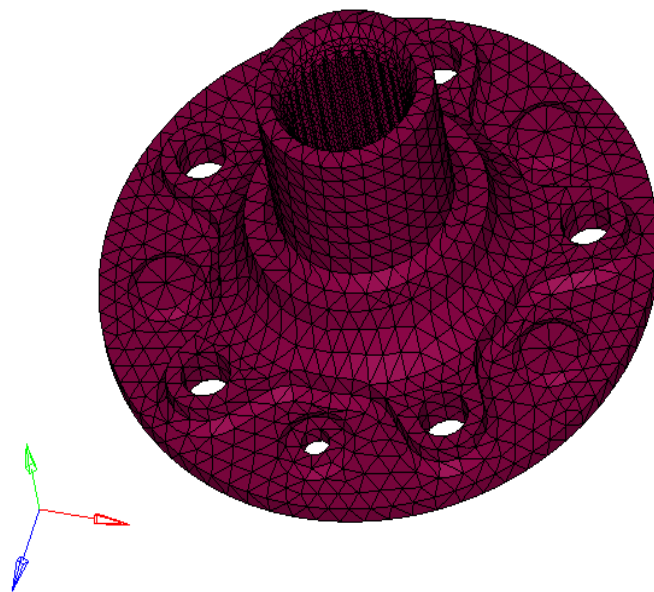


**Figure 19, CAE model - brake hub**

The knuckle is connected to the rest of the assembly components through the caliper, bearing housing and knuckle bolts. Initially the central part was meshed using 2D face elements of the bearing housing in order to maintain node to node connectivity and then the rest of the component was meshed. This is shown in Figure 20.

Figure 20, CAE model - brake knuckle

The front tension arm is an independent component from the assembly connecting the corner unit to the chassis. It is meshed as a circular part at both ends using tetrahedral elements. Figure 21 presents this model.



Figure 21, CAE model - front tension arm

The upper control arm is also another link between the corner unit and the chassis, which is meshed using tetrahedral elements as seen in Figure 22.

**Figure 22, CAE model - upper control arm**

Same as the upper control arm, the lateral tension arm is meshed using tetrahedral elements.

The element size used is 6 mm and the part is shown in Figure 23.



**Figure 23, CAE model - lateral control arm**

Other major parts are the bushes, which are modelled using spring elements (JOINTC). Figure

24 highlights the bushes in red and illustrates the local coordinate system for each.
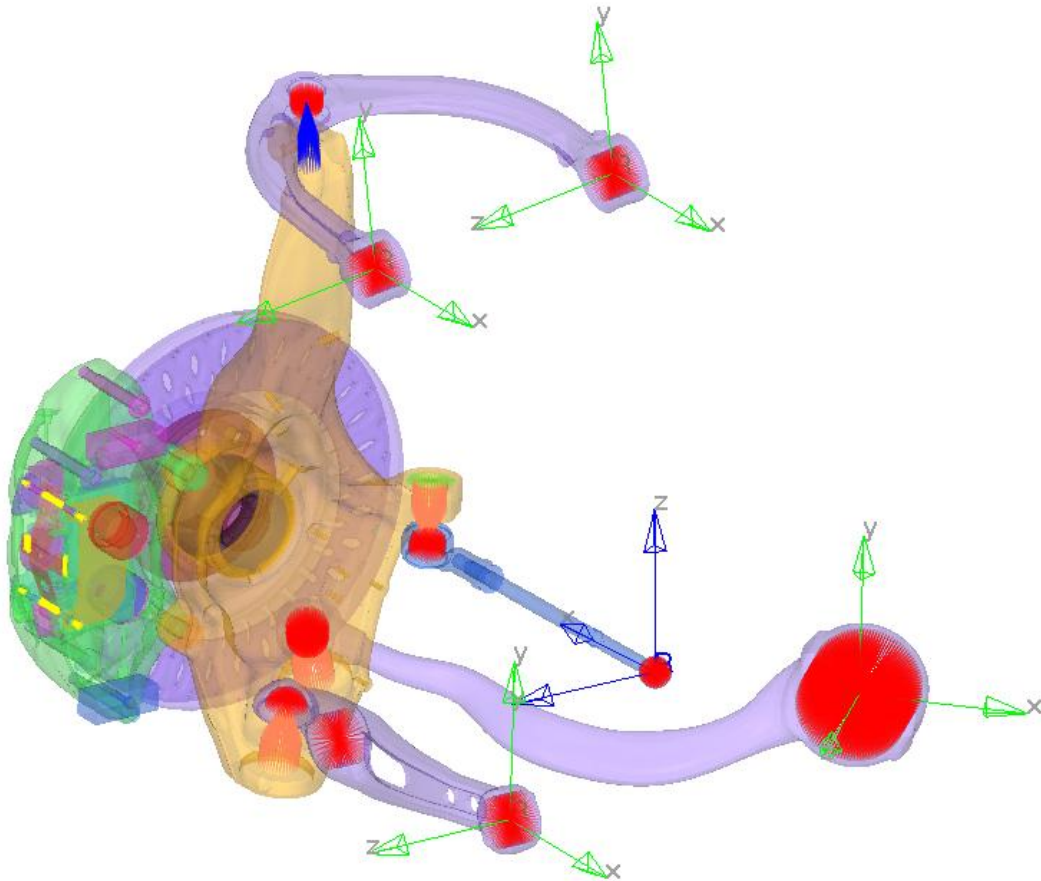
**Figure 24, CAE model - full model highlighting the bushes**

Once the model is meshed, the FEA analysis procedure can start. The next section describes this.

### 3.4.3. Analysis Procedure

Once the model is built up and meshed, the CEA solver is employed to predict the unstable frequencies of the system, in the defined range. Different iterations of CEA form a set of squeal analysis. Variables in the different iterations are the level of disc-pad contact interface COF, brake pressure and direction of wheel movement. The piston pressure variations simulate different levels of application of the brake. The analysis procedure is repeated for different levels of friction, pressure and in both forward and reverse directions. The set of

results obtained from all different iterations of the three variables mentioned forms the squeal analysis results.

After assigning the appropriate mesh to each of the system components, the FE model is ready to be assigned the required series of analyses steps. There are nine different steps as described below.

*Step 1:*

In this step the central spring undergoes a tension, and this is performed to give a more realistic contact behaviour between the central spring and the back-plate. Another imprecise method of modelling it is connecting the central spring directly to the back-plate using a rigid contact, but this will affect the stiffness of the spring by holding it from two sides.
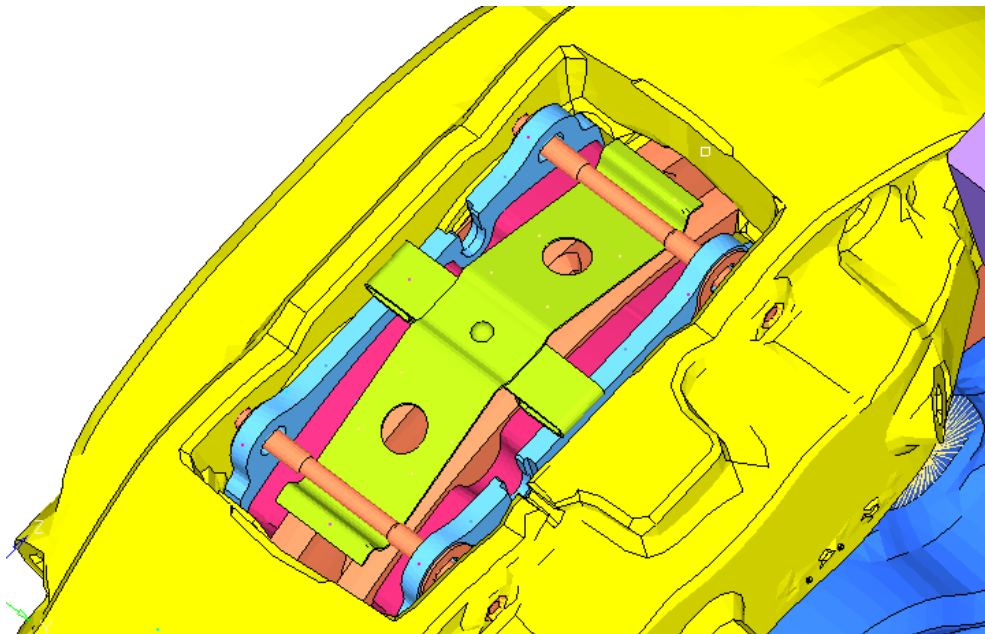


**Figure 25, Central spring in the caliper assembly**

*Step 2:*

In this step the initial volume of various components is calculated, and there is no loading involved. This is performed using *STEP, PERTURBATION.

*Step 3:*

In this step, an initial displacement of 0.1 mm is applied to all the bolt pretention reference nodes to eliminate any rigid body motion in the system and also establish the required contacts. This step definition will eliminate any convergence issues which may arise in preload of bolts in the next step.

*Step 4:*

Step 4 is a bolt clamp-up definition. This is where rotor-hub and caliper-knuckle pretension nodes are preloaded. There is a 42KN load on each bolt connecting the disc to the hub, and this value is 32KN for caliper-knuckle bolts. These values replicate the same loads applied on the corresponding bolts on the vehicle.



**Figure 26, Disc-Hub and Knuckle-Caliper Pretension Nodes (Yellow)**

*Step 5:*

Step five is the pretension free nodes fixation. In this step, all pretention nodes in the node set "preten" will be constrained to avoid any rigid body motion or instability in the runs in the subsequent steps.

*Step 6:*

This is when the brake fluid pistons are pressurised to push shims and consequently the pad assembly. This pressure can vary for different stages of the analysis. Typical pressure ranges from 2 bars to 20 bars.
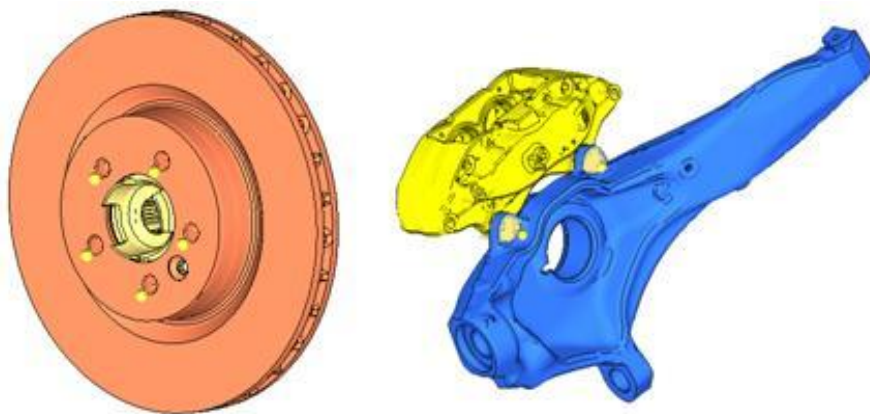
*Step 7:*

Step six is when the disc is rotated. The required rotational velocity is given to all the nodes of rotor and hub assembly to simulate the rotating wheel using *MOTION step. Also friction between the rotor and pads is specified by *CHANGEFRICTION step. The rotational velocity assumed for the disc in this analysis is 3.68 rad/sec, which has been used as an assumption to run all the analysis with a uniform velocity.

*Step 8:*

Modal analysis is performed in the eighth step. This includes extraction of natural frequencies using *FREQUENCY step as a requisite to perform mode-based complex eigenvalue analysis in the next step.

*Step 9:*

Step nine is finally when the complex eigenvalue analysis is carried out. Squeal modes are identified in this step**.** Low frequency squeal may generally be associated with frictional excitation coupled mode locking of brake corner components. The unstable mode can be identified during complex eigenvalue extraction. The eigenvectors represent the mode shape. The imaginary part represents the frequency of the instability and the real part is the strength of the instability, or in other words the growth rate of the amplitude of the mode. So the real part of the eigenvalue corresponding to an unstable mode is positive. The step is performed by *COMPLEXFREQUENCY.

### 3.4.4. Analytical Methodology of the CEA

The equation of motion of a vibrating system is repeatedly reviewed in the literature [7, 40, 83, 84, 132]. Also, the concept and formulation of the complex eigenvalue problem is an established topic in various publications [133-138]. Furthermore, the application of the complex eigenvalue problem to the modal analysis of a damped model (CEA) is integrated in most FEA packages. This section is a theoretical review of the CEA based on the mentioned references. The eigenvalue problem for natural modes of small vibration of a FEA model is:

$$(\lambda^2[M] + \lambda[C] + [K])(\varphi) = 0$$

<div align="right">Equation 2</div>

Where $[M]$: Mass matrix, symmetric and positive; $[C]$: Damping matrix; $[K]$: Stiffness matrix; $\mu$: Eigenvalue and $(\varphi)$: Eigenvector (mode of vibration). Also, the equation of motion for a basic system of single degree of freedom (one of the eigenmodes of the system of equations being solved by the solver) is:

$$m\ddot{q} + c\dot{q} + kq = 0$$

<div align="right">Equation 3</div>

Where $m$: mass, $c$: damping, $k$: stiffness, and $q$: modal amplitude. The solution will be in the format of $q = A \exp \lambda t$, assuming $A$ is a constant and

$$\lambda = -\frac{c}{2m} \pm \sqrt{\frac{c^2}{4m^2} - \frac{k}{m}}$$

<div align="right">Equation 4</div>

The solution may have real and imaginary parts, and that is because the terms under the square root can become negative. When $c$, damping, is negative, the real part of the solution $(-\frac{c}{2M})$ is positive. A negative damping causes system oscillation to grow rather than decaying

them which is normally expected from damping phenomena. Hence a positive real part is just another way of indicating potentiality of observing an instability [30]. However, what will be more important is choosing one which can be used as a measure of strength of instability too.

The basic equation of motion for a simple system is discussed above. However, what really happens when a FEA solver deals with an eigenvalue problem is different, mainly because of more complex system (degrees of freedom).

Abaqus/Standard, in general, uses the set of eigenmodes extracted in a previous eigenfrequency step to calculate the steady-state solution as a function of the frequency of the applied excitation. However, there is a direct steady-state linear dynamic analysis procedure, in which the equations of steady harmonic motion of the system are solved directly without using the eigenmodes, using "subspace" steady-state linear dynamic analysis procedure, in which the equations are projected onto a subspace of selected eigenmodes of the un-damped system.

Focusing on the linear steady-state response procedure based on the eigenmodes, the equation of motion can be viewed based on the mode index [30, 139]:

$$\ddot{q}_\alpha + C_\alpha \dot{q}_\alpha + \omega_\alpha^2 q_\alpha = \frac{1}{m_\alpha}(f_{1\alpha} + if_{2\alpha})\exp(i\Omega t)$$

<div align="right">**Equation 5**</div>

In this equation, $q_\alpha$: Amplitude of the mode $\alpha$; $C_\alpha$: Damping associated with the mode $\alpha$; $\omega_\alpha$: Undamped frequency of the mode $\alpha$; $m_\alpha$: Generalized mass associated with the mode $\alpha$; $(f_{1\alpha} + if_{2\alpha})\exp(i\Omega t)$: Forcing associated with the mode $\alpha$.

### 3.4.5. Analysis Results

The unstable mode can be identified during complex eigenvalue extraction as the real part of the eigenvalue corresponding to an unstable mode is positive. This data can be identified in Abaqus .DAT file. Although the software reports this information in the format of negative damping ratio, it is common practice to consider the absolute value of the negative damping ratio and report it in percentage. Figure 27 illustrates squeal analysis results for pressure variations of 2, 5 and 10 bars and coefficient of friction ($\mu$) of 0.3, 0.4, 0.5, 0.6 and 0.7. Squeal analysis results show that instabilities occur potentially in the frequency ranges of 1.4, 2.5-2.7, 3-3.2 and 5.2-5.6 KHz regions. However, these are only provisional results, and not all instabilities predicted by CEA may occur in reality. CEA results then should be investigated and correlated with dynamometer and car test results to locate real instabilities leading to noise, since the CEA always overestimates the instabilities as mentioned before.
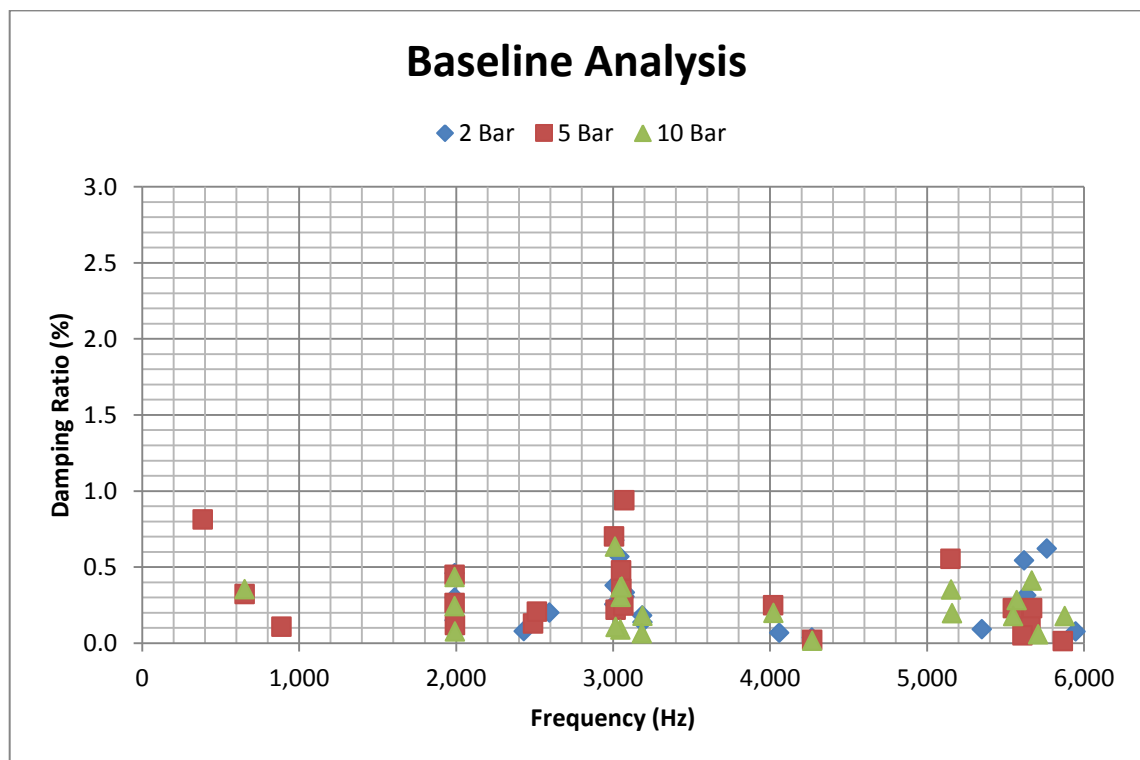


**Figure 27, CEA squeal analysis results - baseline model**

Figure 27 presents the analysis results using Abaqus software. CEA results from this model are assumed as a reference for comparing and evaluating the effectiveness of the developed techniques. Analysis results of the baseline model can slightly vary based on the solver version, which is relatively insignificant. However, for more accuracy, in each case of comparison, analysis results of the same version are compared.

In order to choose the most optimum solver, this study also compares the performance of different eigen-solver combinations available in Abaqus software.

- Lanczos

- Lanczos with SIM

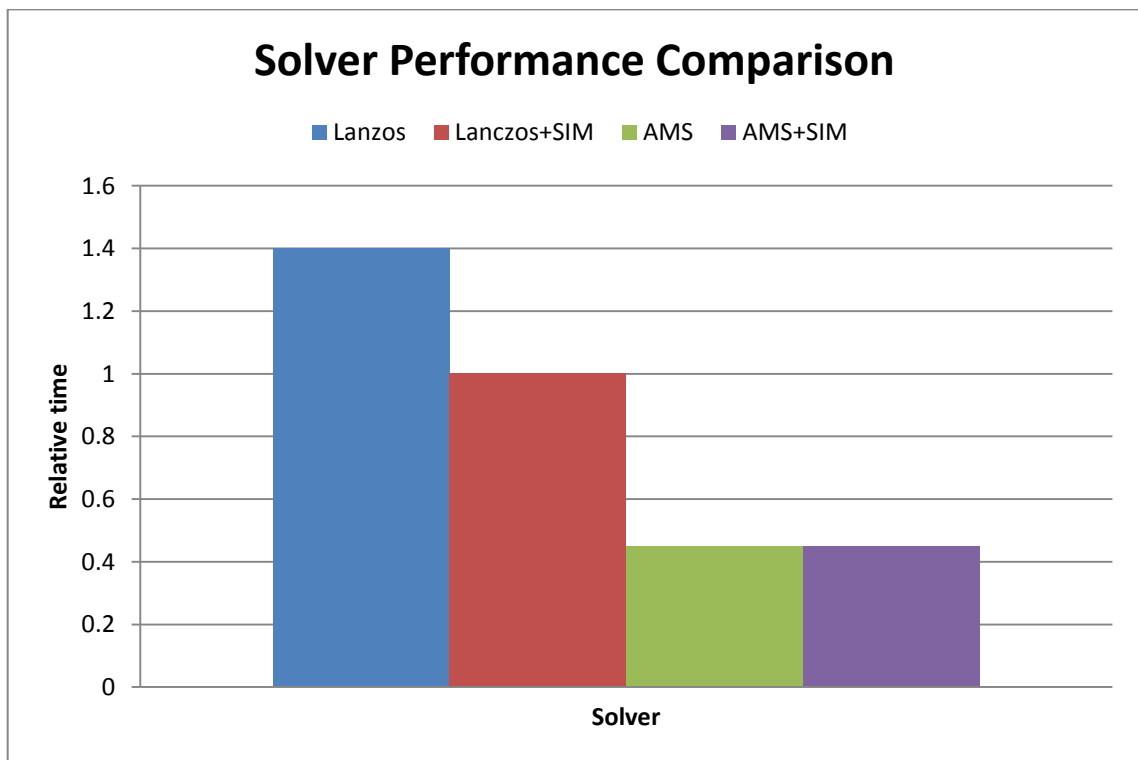- AMS (Automatic Multi-level Substructuring)

- AMS with SIM



**Figure 28, Abaqus 6.11 solvers and SIM structure analysis time**

Using the SIM structure along with Lanczos eigen-solver does not change the number of modes obtained by the solver, or even their frequencies. However, the solver time is lower using the SIM structure. Also, different instabilities were observed between the two solvers of Lanczos and AMS, with the Lanczos providing a better prediction of the system behaviours in terms of unstable frequencies. Consequently, the conventional solver set-up will be used for the study, which is Lanczos without SIM structure.

## 3.5.     FEA Model Damping Tuning

The FEA model is expected to replicate the actual behaviour of the system components. Therefore, material properties of the components in the model also should replicate the mechanical characteristics of the physical parts. One significant contributor to this is the damping characteristics of the materials applied to the component models.

Once the CEA problem is set up, in order to achieve more realistic behaviour from the system, various types of damping can be introduced into the system mainly based on the capabilities of the solver. There are different solutions for application of a certain level of damping to the model. However, they vary in the actual analytical solution of the CEA problem. Also, since the damping tuning is being performed using a software, the capability of the solver to incorporate the damping characteristics is significant. Different types of damping tuning available in Abaqus software package are:

- Modal damping
- Material (structural) damping
- Rayleigh damping

From the analytical viewpoint, application of each of these types of damping to the system adds specific terms to the equation of motion.

*Modal damping:*

$$C_\alpha = 2\xi_\alpha \omega_\alpha$$

Where $\xi_\alpha$ is a fraction of the critical damping in the mode ($\alpha$).

*Material (structural) damping:*

$$C_\alpha = \frac{S_\alpha \omega_\alpha^2 q_\alpha}{\dot{q}_\alpha}$$

Where $S_\alpha$ is mode-specific structural damping coefficient

*Rayleigh damping:*

$$C_\alpha = \alpha_\alpha + \beta_\alpha \omega_\alpha^2$$

Where $\alpha_\alpha$ and $\beta_\alpha$ are mass-dependent and stiffness-dependent Rayleigh damping coefficients, more active in the lower and higher frequencies respectively. Rayleigh damping coefficients calculated in this study will be based on the classic Rayleigh damping formulation [140], where for a specific mode of $\alpha$:

$$\xi = \frac{\alpha}{2\omega} + \frac{\beta\omega}{2}$$

In order to obtain values of $\alpha$ and $\beta$ one needs to input two experimental data points (hammer test for example) of damping ratio and frequency ($\xi, \omega$) to form a system of simultaneous

equations and solve for $\alpha$ and $\beta$ [140, 141]. Then the variables can be interpolated / extrapolated to obtain damping in the required frequency range. Based on the damping at each frequency, $\alpha$ and $\beta$ are calculated, and fed into the model.

Introducing all of these damping definitions into the equation above, equation of motion turns to be:

$$\ddot{q}_\alpha + 2\zeta_\alpha \omega_\alpha \dot{q}_\alpha + (\beta_\alpha + \alpha_\alpha \omega_\alpha^2)\dot{q}_\alpha + S_\alpha \omega_\alpha^2 q_\alpha + \omega_\alpha^2 q_\alpha$$

$$= \frac{1}{m_\alpha}(f_{1\alpha} + if_{2\alpha})\exp(i\Omega t) \qquad \text{Equation 10}$$

## 3.6. Application of Brake Shims - Methodology

Brake shims, applied to brake pads, are used for suppressing noise in disc brake units, typically in a specific frequency range. Also called brake insulators, they do so mainly by adding more damping to the system in the brake pad area. This reduces the likelihood of the energy transfer between the components which would cause modal coupling.

FEA, as a simulation and analysis technique, is widely used in the industry to perform squeal analysis as a part of the virtual development of new brake units. However, in most CAE simulations of brake noise, shims are modelled as thin sheets of steel or are not modelled at all. This introduces some inaccuracy due to ignoring the damping effect and flexibility of the rubber and adhesive material. Such inaccuracy in predicting system behaviour, in the virtual design stage, means the analyst may not be able to locate the right frequencies of any occurring instability in order to decide on a noise fix. Also, the over-prediction of instabilities by CEA adds to the inaccuracy of the process.

The shim provides flexibility between the piston and the brake pad and is therefore capable of changing modal response. Modelling of brake shim requires a comprehensive knowledge of material properties of different layers of the shim, some of which are not easy to measure. Also, precisely modelling the boundary conditions of the layers requires an in-depth understanding of how these layers interact with each other once in action [142-144].

Modelling shims along with other damping tuning techniques improves CAE analysis accuracy by eliminating instability over predictions. Accurate modelling of the shim is significant in assessing NVH performance of the brake unit, as it identifies instabilities which are caused by modal coupling where the shim is unable to provide enough damping to facilitate modal decoupling. This enables application of required structural noise fixing techniques in the CAE phase, before dynamometer or vehicle tests.

In order to obtain the actual level of damping in the shim they are tested and the data is reported on the shim map. Shim map, as seen in Figure 29, presents an estimated level of damping expected from the shim in a specific range of temperature and frequency.
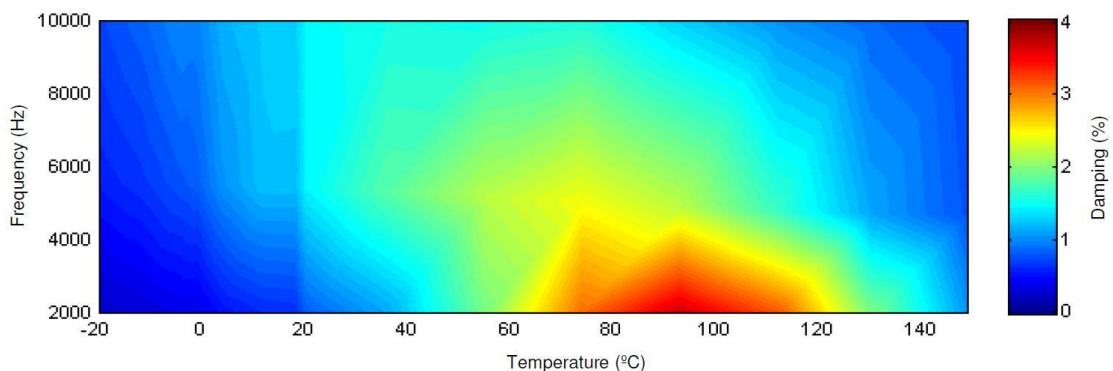


**Figure 29, Sample of shim damping map**

## 3.7.    Summary

Methodologies for the experimental and numerical investigations were reviewed. The brake noise experiments were explained, which were carried out using two methods of dynamometer test and full vehicle test. Experimental test results highlight the actual noisy frequency on the existing brake unit. The numerical investigation is aimed at improving the level of correlation of the existing model with the noise performance of the brake unit tested in the dynamometer.

The other experimental investigation is the modal experiments performed on the brake system components and assemblies. Modal experiments were aimed at confirming the correlation of the attributes of the individual components of the CAE model with the real parts. Furthermore, the damping characteristics of the components and assemblies were recorded which will be utilised for the damping tuning of the model. Modal extraction experiments were carried out using two methods of impact hammer test and shaker test.

The methodology of simulation of the brake model was reviewed, presenting the details of the CEA runs. This includes the theoretical background of the analysis as well as the damping tuning solutions. A mesh convergence study was performed to ensure the model is meshed with an optimally fine mesh. The analysis procedure was reviewed and the CEA results for the baseline model were presented.

The damping characteristics of the brake shim were also presented, highlighting the challenges in replicating the damping effect of the rubber material in the simulation.

As a conclusion, the study aims to improve the level of correlation of the CEA simulation in order to eliminate over-predicted instabilities and provide a clearer prediction of the noisy frequency.

# Chapter 4: System Damping

## 4.1. Introduction

Application of numerical analysis tools to simulate brake noise performance has become of interest since computers have become capable of performing complicated simulations using FEA techniques. This has resulted in a considerable improvement in designing brakes with better NVH performance. However, not all aspects of the phenomenon are easy to model yet, damping characteristics being a major challenge. CEA is an established tool for predicting brake instabilities potential to cause brake noise. However, CEA is known for over-predicting instabilities related to the noise occurrence [79].

In the CAE model, system damping plays a dominant role in simulating the potential modal couplings by replicating the realistic level of vibration amplitudes for the interacting components. Therefore it is significantly important to tune the system damping prior to performing the CEA. This also limits the instability over-prediction [79].

Assuming brake noise shows itself in the format of unstable coupled modes in the CEA results, the over-prediction of unstable modes is thought to be as a result of insufficient damping in the model compared with the real brake system. Lack of damping in the simulation causes the solver to assume higher energy levels for individual components at the resonant frequencies, resulting in easier energy transfer and modal coupling. This shows itself in the form of unstable coupled modes, reported as system instabilities and considered to cause noise. For this reason, the FEA model of the brake unit needs to be tuned in terms of damping characteristics to ensure that it replicates the system's attributes more realistically.

Individual components of the brake unit have specific levels of damping. In order to model this characteristic, which is generally related to the material properties of individual parts, an experimental study was performed to obtain the required data. Then components of the FEA model need were tuned with the corresponding level of damping based on the experimental data. Results of a squeal analysis based on such a model are expected to better correlate with the real-world NVH performance of the brake system.

This chapter aims to investigate the effects of CAE damping tuning on the accuracy of squeal analysis results. Over-prediction of instabilities by CEA is assessed from two perspectives of unstable frequency and the amplitude/repetition of instabilities at each unstable frequency. In order to achieve this aim, first modal experiments are performed in order to obtain the required data. Then different damping tuning techniques are reviewed and compared in terms of their performance or limitations. Based on the chosen technique, the FEA model is tuned using the damping values obtained from the experiments, and a squeal analysis is performed to investigate the effects of application of damping. Each analysis result is compared with the analysis of an un-damped brake model, aiming at eliminating over-predictions. Also, analyses results are assessed in terms of correct prediction of actual unstable frequencies based on the noise performance of the same brake tested in a dynamometer.

Finally, simulation of brake insulators is investigated, as the greatest source of damping in the system. Simulation of the brake shims is not a common practice in industry and shims are typically modelled as thin sheets of steel in order to keep the computing time at minimum. This is significant since a simplified yet accurate model of the shim can considerably enhance the accuracy of the analysis results and shorten the overall brake design and testing procedure [145].

## 4.2.    Modal Correlation and Component Damping Estimation

In order to validate the FEA model of the brake unit, individual components need to be correlated with the physical parts. This is to ensure that the FEA model represents the component geometry and material properties accurately. Another major outcome of the modal experiments is to identify the damping attributes of each component. The aim of the experimental study is to obtain an accurate estimation of the level of material damping for each component, as well as estimating the effect of contact damping. In order to achieve this, two experimental methods of hammer test and shaker test were practiced. Initially components were tested and the resonant frequencies were correlated with the CAE results. Then a case of comparison of the hammer test and the shaker test is conducted, both performed on a single part to correlate the results of both methods. Furthermore, in order to estimate the level of contact damping, an assembly of components is tested.

This section presents the correlation of the analytical and experimental results for the disc as a representative component, including resonant frequencies (and the relative frequency difference) and Frequency Response Function (FRF) graph. Experimental results for other individual components are provided in Appendix A.

The frequency difference $F(\%)$ is calculated as:

$$F(\%) = \frac{"Theoretical\ value" - "Experimental\ value"}{"Theoretical\ value"} \times 100$$
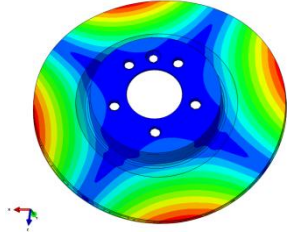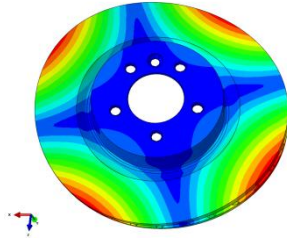
<div align="right">Equation 11</div>
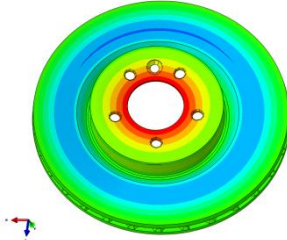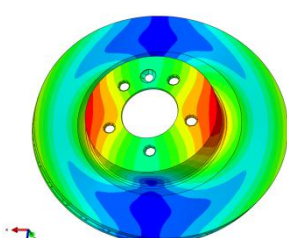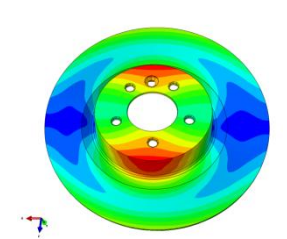
### 4.2.1. Disc

Two sets of hammer test were performed which were correlated with the CAE results. The tested disc with the numbered points is shown in Figure 30. The impact is imposed on either point 1 or 2 marked on the disc, and for each impact point data is recorded from 48 different points. For more accuracy, for each recording point the data is collected in 3 impacts and the response amplitude is averaged.
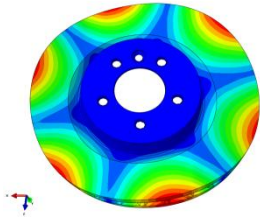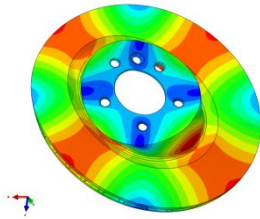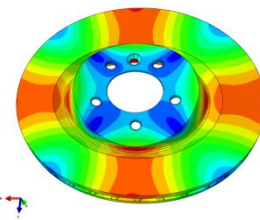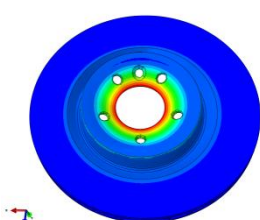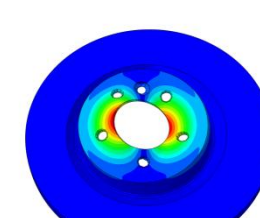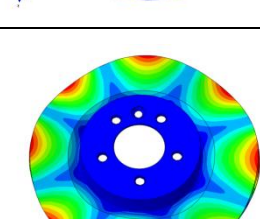


**Figure 30, Brake disc - hammer test markings**

Table 6 represents the resonant frequencies and mode shapes for the disc, obtained from the modal experiments. The hammer test was repeated several times and the best two sets of results were chosen. In this case $F(\%)$ is calculated based on hammer test 1.
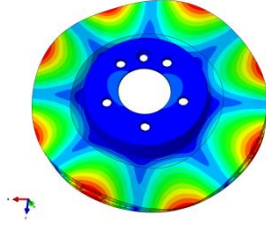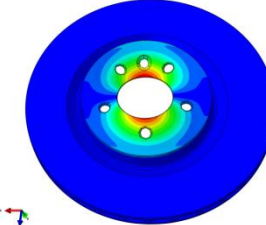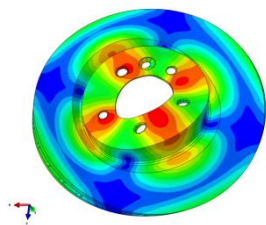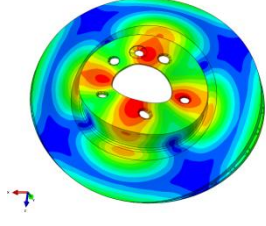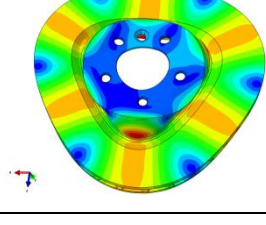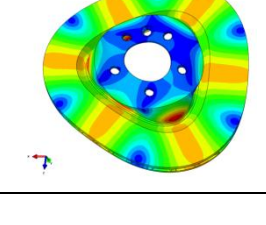
**Table 6, Disc modal correlation**

| CAE Resonant Frequency (Hz) | CAE Mode Shape | Hammer Test 1 Frequency (Hz) | Hammer Test 2 Frequency (Hz) | $F$ (%) |
|---|---|---|---|---|
| 695.21 |  | -- | -- | -- |
| 696.45 |  | 737.3 | 737.3 | 5.8 |
| 1,250.4 |  | 1,321 | 1,319 | 5.6 |
| 1,540.2 |  | -- | -- | -- |
| 1,543 |  | 1,656 | 1,661 | 7.3 |

| | | | | |
|---|---|---|---|---|
| 1,678.7 | | 1,737 | 1,739 | 3.4 |
| 1,907.5 | | -- | -- | -- |
| 1,909.2 | | 1,932 | 2,035 | 1.2 |
| 2,312.6 | | -- | -- | -- |
| 2,835.6 | | -- | -- | -- |
| 2,843 | | 2,926 | 2,933 | 2.9 |

| | | | | |
|---|---|---|---|---|
| 2,849.9 |  | -- | -- | -- |
| 2,871.4 |  | -- | -- | -- |
| 3,554.1 |  | -- | -- | -- |
| 3,566.3 |  | -- | -- | -- |
| 4,002.0 |  | -- | -- | -- |
| 4,002.2 |  | -- | -- | -- |

Correlation between the hammer test and the CAE results in Table 6 reveals some differences

in the modes. This can be explained by the fact that although shaker test and hammer test are

able to excite most of the modes, some modes are very difficult to excite and might require two simultaneous sources of excitation. It is possible to obtain most of the resonances from the hammer test by doing numerous series of tests after determining the critical hitting point locations using professional software built for this purpose [146]. Also, modes with very small difference in frequency might show themselves as a mixed mode in the experiment, usually with higher amplitude. On the other hand, FEA software also over-predicts some resonances which are obviously not visible with experiments. This is one of the major causes of over-prediction of modal couplings. The FEA software assumes virtual modes at frequencies where they do not exist, and these virtual modes couple with some other actual or virtual modes in the frequency range. Consequently the CEA over-predicts instabilities.

In conclusion, since all modes obtained from experiment are correlating with a very small frequency difference, it is a valid claim that the FEA model is a correct representation of the physical part. Figure 31 presents the experimental FRF prediction for the disc.
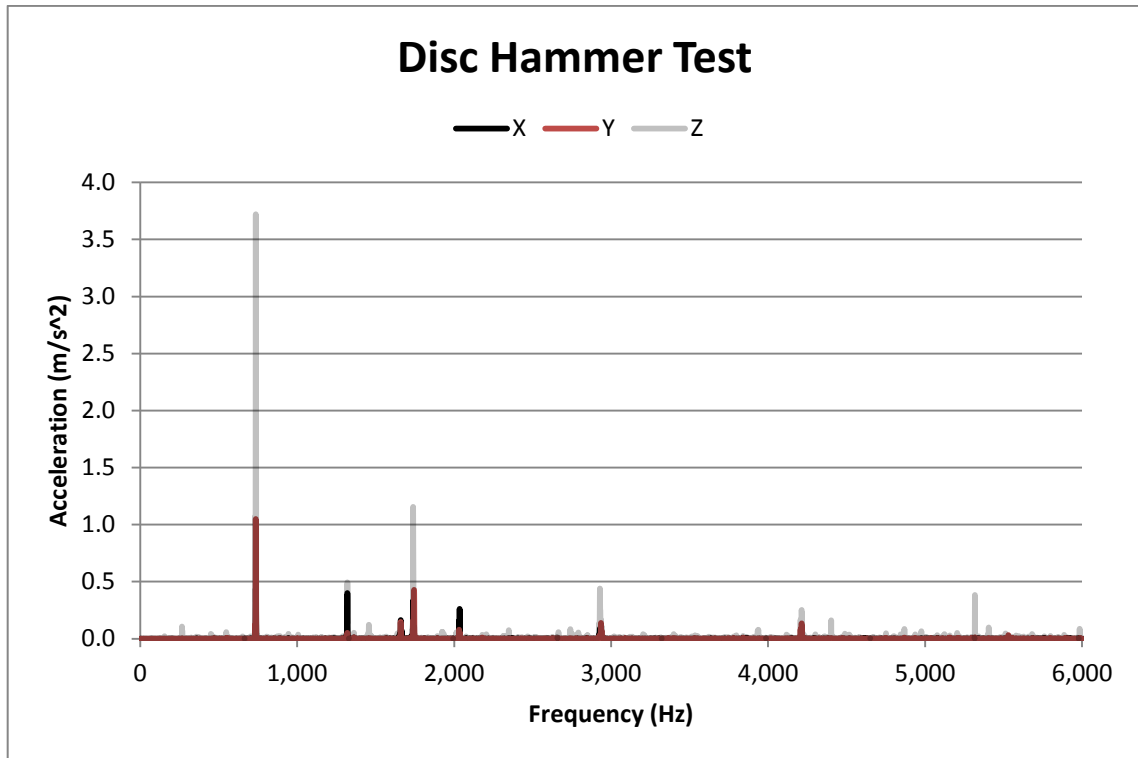
Figure 31, Disc experimental FRF - hammer test

Comparison of the peaks of the FRF graph which stand for the resonant frequencies with the CAE predictions confirms the correlation of the results.

### 4.2.2. Hub

The brake hub was hammer tested in a similar pattern to the disc. The impacts were from two points and data was recorded at 36 points. The hub had a simpler geometry compared with the disc, which enabled achieving a higher level of correlation of the natural frequencies.

### 4.2.3. Pad Assembly

The pad assembly is formed of a back-plate, friction material and shim. The friction material and shim required different testing procedures due to their material properties [147]. The major difficulty is the high level of damping in the friction material and the fact that the material is very brittle. Therefore, shim is removed from the pad assembly and the friction

material is machined in order to test the back-plate. Figure 32 shows the machined pad with hitting and data recording points for hammer test.
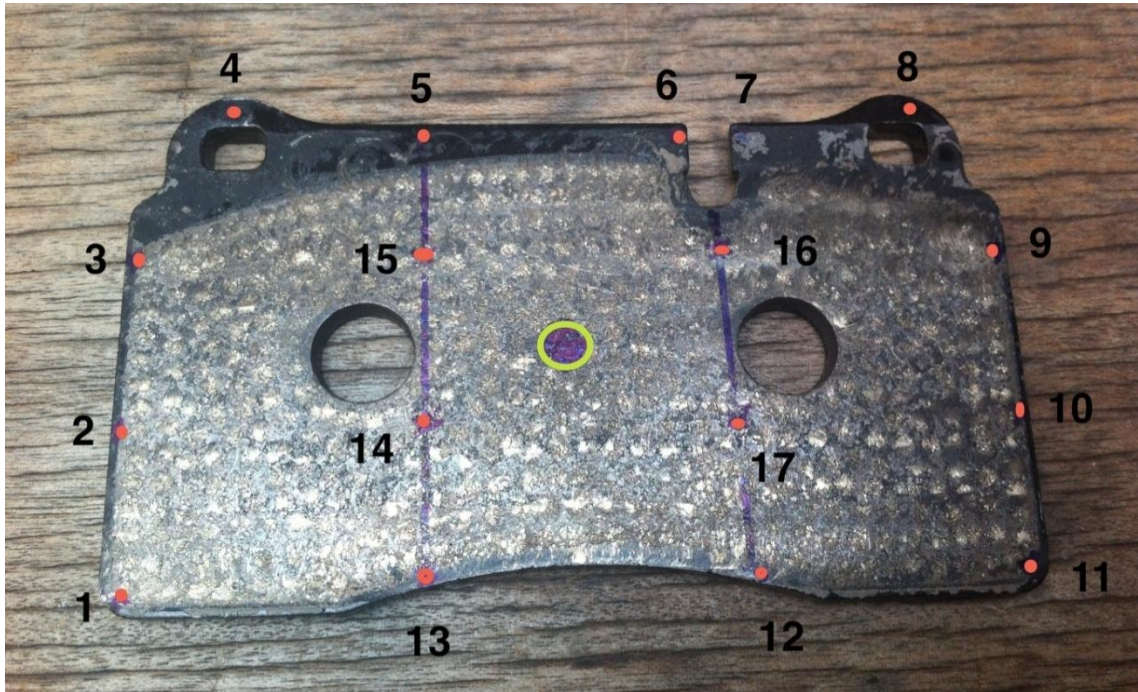


Figure 32, Machined back-plate - hammer test markings

### 4.2.4. Caliper

The caliper comes with the pistons and seals attached to it. Rubber seals surrounding the pistons can introduce lots of noise to the hammer test response, especially because the pistons themselves are made of steel and are relatively heavy. Therefore, in order to obtain a higher level of correlation all pistons and seals are removed from the caliper body. The lumped masses were however left attached since they were effective in shifting the resonant frequencies of the caliper body and were simulated as part of the caliper in the CAE model.

Figure 33, Brake caliper, hammer test markings (side)
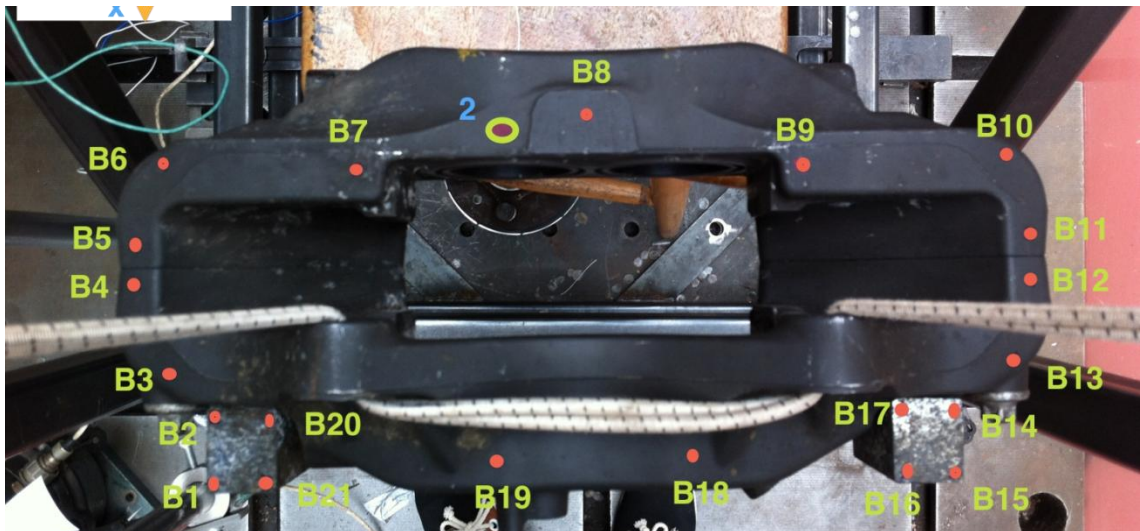


Figure 34, Brake caliper, hammer test markings (bottom)

## 4.2.5. Knuckle

The knuckle is chosen as the link between the hammer test and the shaker test, due to its mass distribution. Figure 35 shows the knuckle suspended from the test rig and being excited by the

shaker. There are also accelerators attached to the knuckle body to record the impact response.
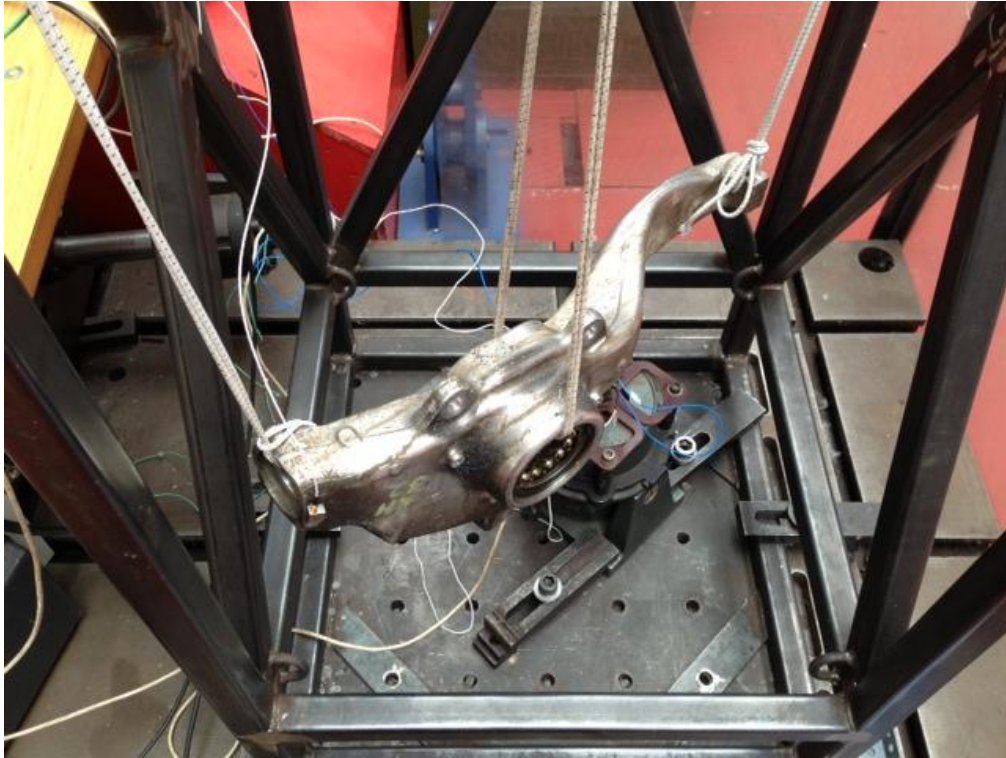


Figure 35, Knuckle, shaker test set-up

## 4.2.6. Component Tests Summary

Overall there was a good correlation for all the components for the specified range of frequency of [0.1, 6] kHz. Therefore the damping obtained from this test can be utilized for damping tuning of the CAE model.

Some mode shapes do not appear on the FRF graphs of the components. This is explained by the fact that CEA over-predicts the resonances, which itself is a reason for over-prediction of modal couplings of the assembled model. Also some modes are difficult to excite in the experiment, or two modes can appear as a mixed mode with high amplitude on the FRF graph.

### 4.2.7. Caliper + Knuckle Assembly

To obtain the system response at the assembly level, the caliper and knuckle were tested as an assembly. In order to perform this experiment, the caliper was assembled to the knuckle and mounted on the shaker test rig. The assembly was excited through the load cell attached to the knuckle. Then the response is recorded from caliper and the FRF is plotted. Table 7 presents correlation of the observed resonant frequencies with the CAE results.

Table 7, Knuckle + Caliper modal correlation

| CAE Frequency (Hz) | Shaker Test Frequency (Hz) | $F(\%)$ |
|---|---|---|
| 587.77 | 545 | 5.8 |
| 824.28 | 780 | 5.3 |
| 1,126.8 | 1,124 | 0.1 |
| 1,392.2 | 1,390 | 0.1 |
| 1,983.1 | 2,000 | 0.8 |
| 2,153.0 | 2,145 | 0.3 |
| 2,501.7 | 2,380 | 4.8 |
| 2,617.2 | 2,685 | 2.6 |
| 3,309.5 | 3,315 | 0.1 |
| 3,440.4 | 3,445 | 0.1 |
| 4,158.0 | 4,155 | 0.07 |

The CAE and shaker test results are in a good range of correlation. The relatively low frequency difference in the experimental and CAE results is discussed in the contact damping section. Figure 36 presents the FRF captured from the assembly.
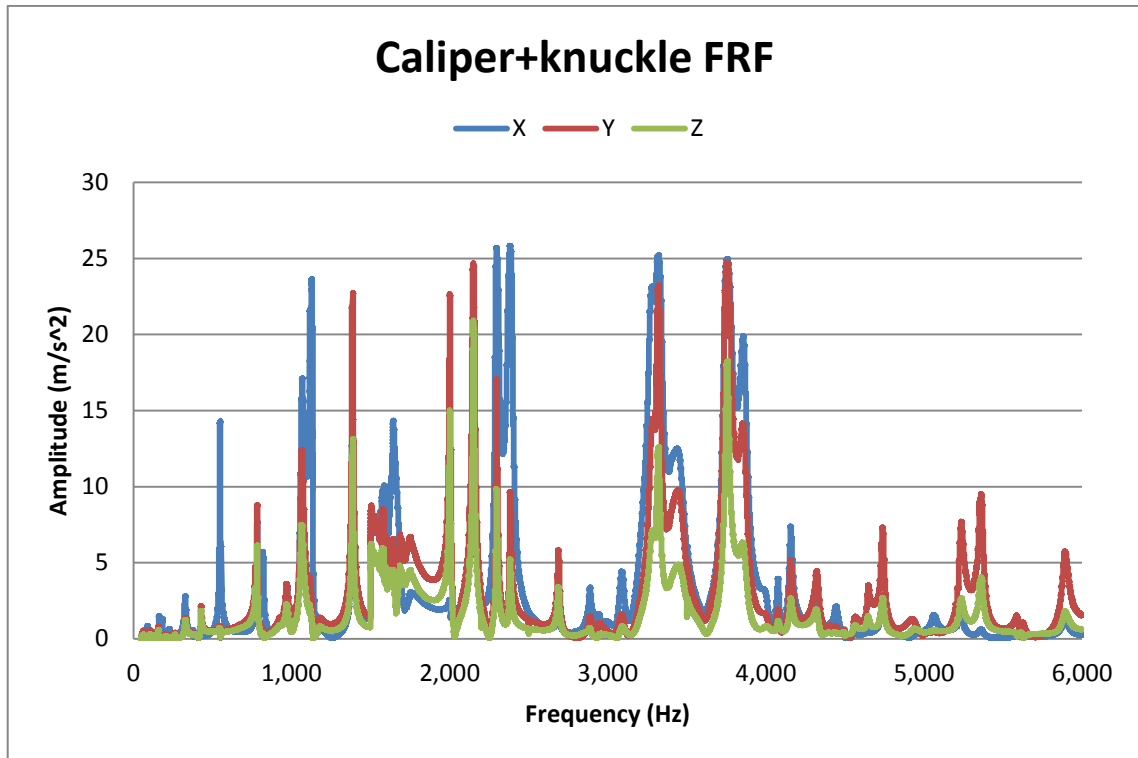
**Figure 36, FRF - caliper + knuckle assembly**

## 4.3. Contact Damping

### 4.3.1. Experimental Estimation of Contact Damping

As a part of the system damping estimation, a case study was performed to compare the significance of the contact damping with the material damping. Quantifying contact damping is difficult to achieve in terms of designing an experiment to measure it. Therefore contact damping is estimated indirectly by measuring the overall damping in an assembly and comparing that with the level of material damping of the individual components forming it. Assembly damping is made up of the material damping of the components plus the contact damping, and therefore can be used to estimate the significance of the contact damping. An investigation is carried out to compare the assembly damping of caliper and knuckle with the

material damping of the individual components. Figure 37 presents a comparison of the assembly damping and material damping.
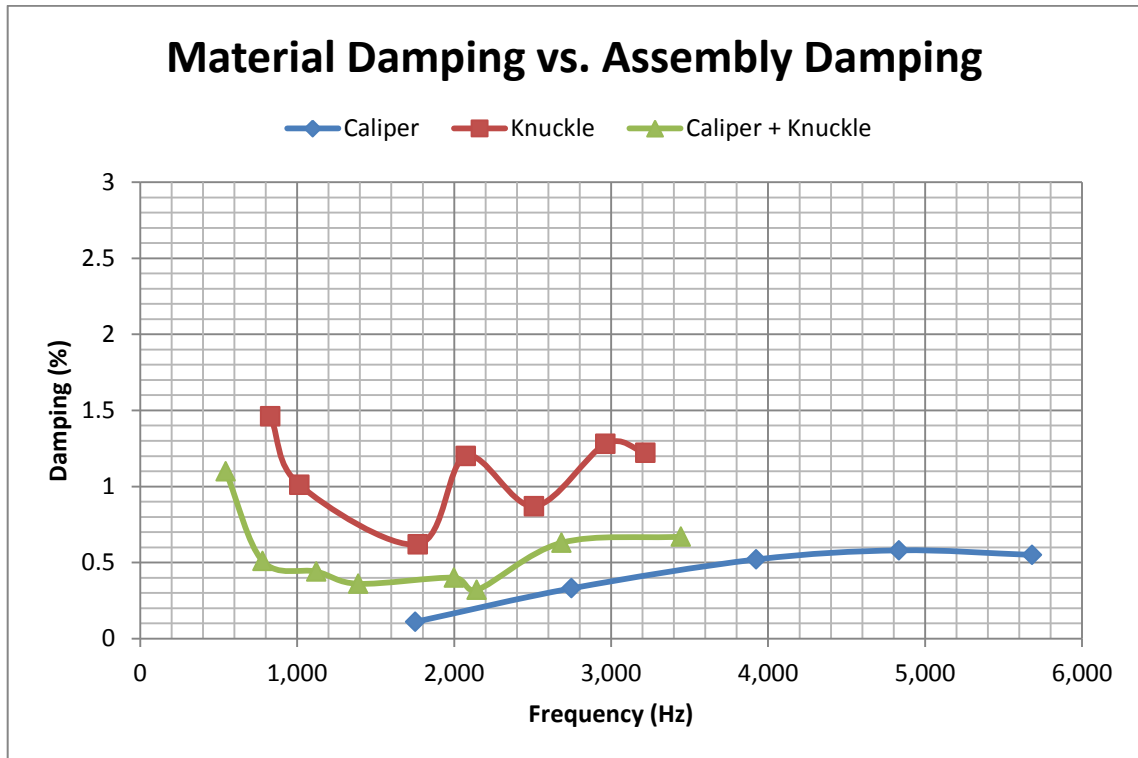


**Figure 37, Material damping vs. assembly damping - Study of contact damping**

Results show that although there is a certain level of contact damping in the assembly, but the level of the contact damping is relatively insignificant compared to the material damping of either component. However, measuring the exact level of contact damping is not possible using this technique.

Modal correlation of this assembly with the CAE model is presented in Table 7. The CAE model does not apply any damping to the contact interface and assumed two surfaces are fixed together. Also, both individual components are correlated with the CAE results individually. Consequently, the fact that the error margin in the assembly correlation is in the acceptable range of about 5% could be an indication that the CAE model for the assembly

without any contact damping is still a valid representative of the assembly. In other words, the actual contact damping is actually minimal.

### 4.3.2. Simulation of Bolted Joints

Bolted joints are a major contributor to the simulation of contact damping. Therefore, the best practice for simulation of the bolted joints is investigated. Three potential best practices were defined as follows:

- Case 1 - Beam-Rigid element bolts, no contact damping

- Case 2 - Solid bolts, no contact damping

- Case 3 - Solid bolts, 1% contact damping

A case study of comparing three different modelling techniques of the bolted joints is prepared. A full squeal analysis is performed for each case and results are compared. This is formed of friction levels of 0.3, 0.4, 0.5, 0.6 and 0.7; pressure levels of 2, 5, and 10 bar; and performed in both forward and reverse directions.

*Case 1 - Beam-Rigid Element bolts, no contact damping:*

In the first case 1D elements formed of beam elements connected to rigid elements are simulating bolts and nuts, without any damping. Figure 38 illustrates the beam elements forming this virtual bolt.
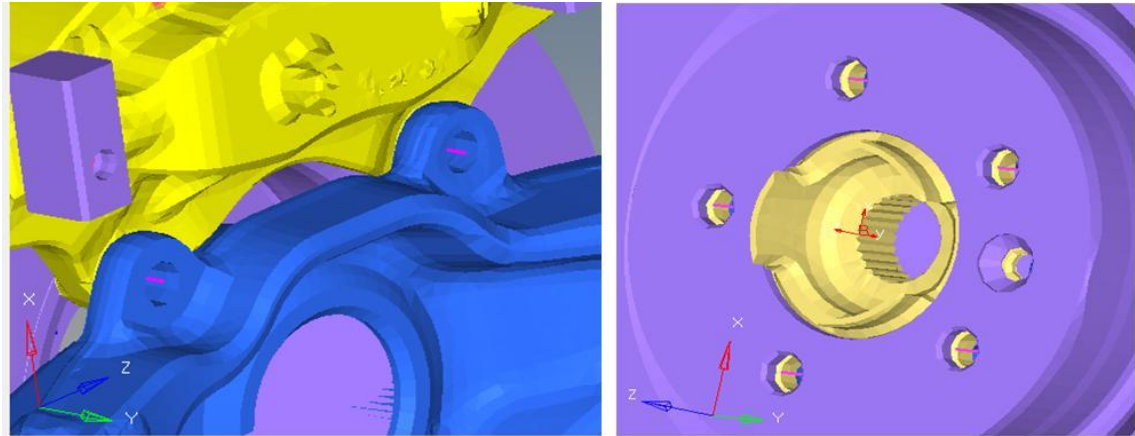
Figure 38, Beam elements as bolts (Left: caliper-knuckle - Right: disc-hub)

Also Figure 39 shows the rigid elements on the opposite side of the bolt, simulating the effect of a virtual nut fixing the two parts together. Obviously this is only required in order to connect the two sides of the contact together and the nut does not exist in the real brake unit.
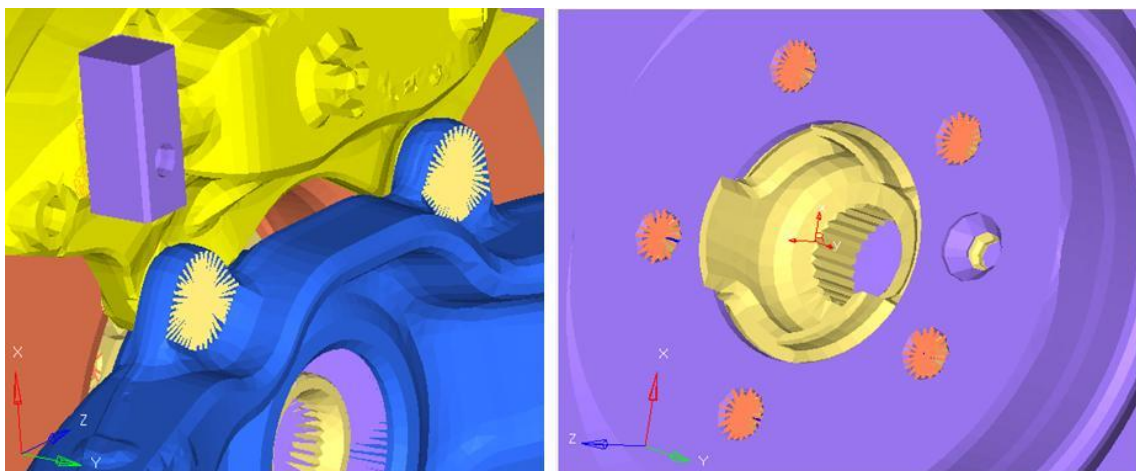


Figure 39, Rigid elements as nuts (Left: caliper-knuckle - Right: disc-hub)

*Case 2 - Solid bolts, no contact damping:*

In the second case bolts are modelled as solid hexahedral elements, with the geometry and material properties of the actual bolts. Figure 40 represents a schematic of the bolts modelled for the disc-hub and caliper-knuckle contact.
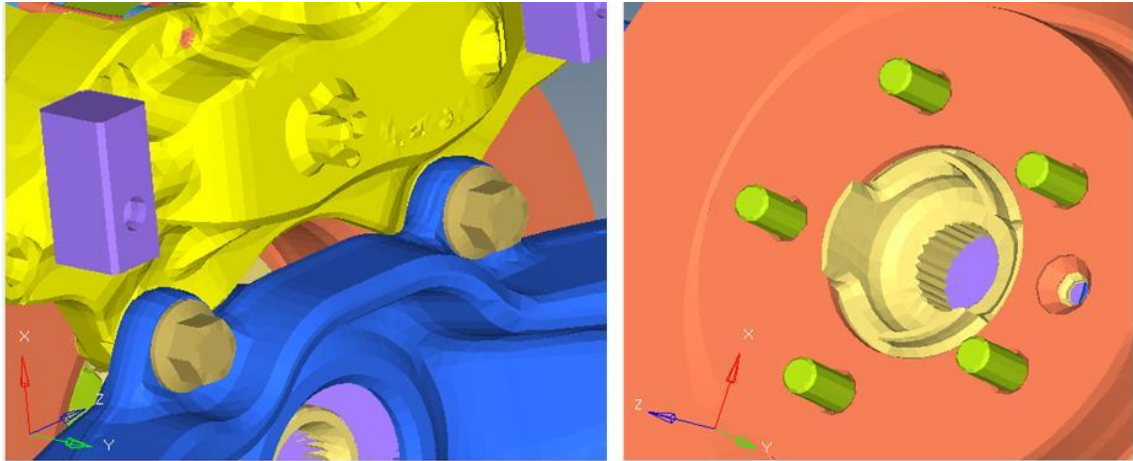
**Figure 40, Solid bolts – 1% contact damping (Left: caliper-knuckle - Right: disc-hub)**

*Case 3 - Solid bolts, 1% contact damping:*

Case 3 is similar to the case 2 with the only difference being that a contact damping of 1% is applied to the surfaces in contact, i.e. the bolt region only. The level of contact is only a general assumption in order to observe any differences in the results.

*Results and Conclusion:*

Figure 41 illustrates the analyses results which compares all 3 cases. Results show that the addition of the solid bolts to the model changes the instability prediction, but the addition of damping is not influential. Further investigation reveals that this is due to the order of steps in the FEA model, in which the squeal run is performed after the system clamp-up, which is likely to void the effect of applied contact damping. The clamp-up step is critical for performing the CEA as it ensures the contact between the nodes replicating the disc-pad contact interface.
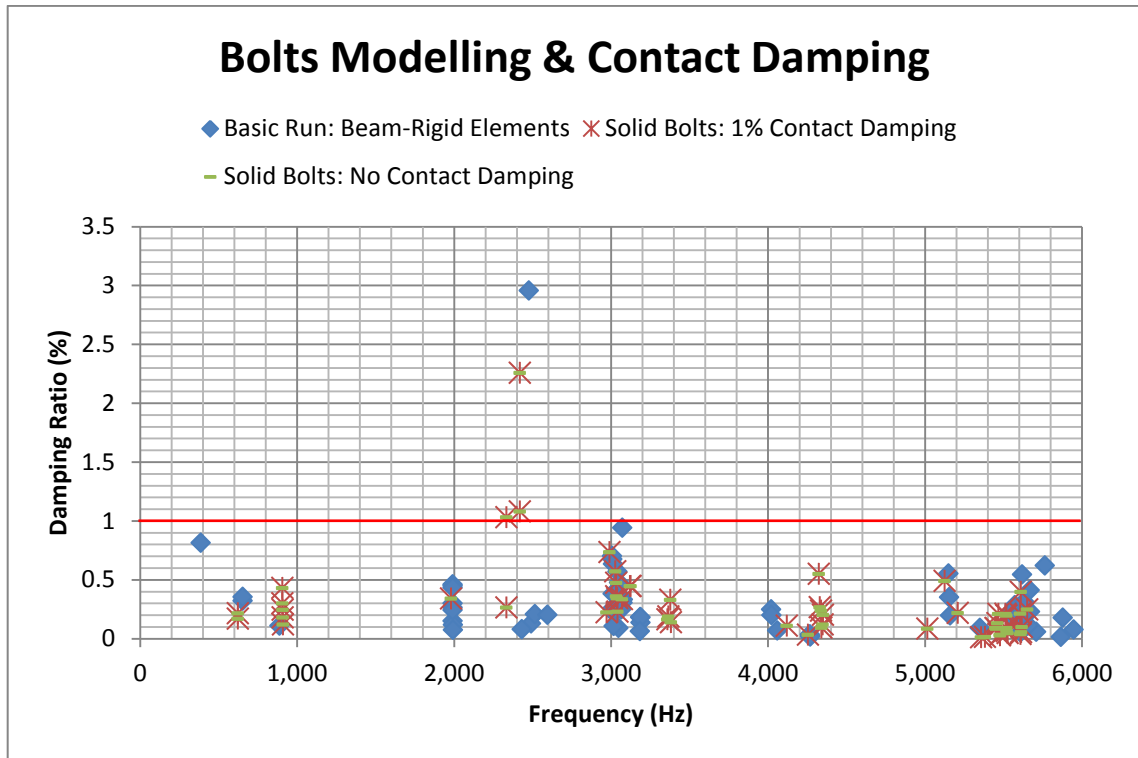
**Figure 41, Squeal analysis, bolts modelling and contact damping**

Also, instability prediction from the analyses results are assessed with the dynamometer. This comparison reveals that in terms of over-predictions, addition of rigid bolts is not making any significant improvement; the 0.8 kHz over-prediction is even stronger and there are even new over-predictions at 3.4 kHz and 4.3 kHz frequencies. As a conclusion, modelling of the bolted joints is at its optimum condition by assuming them as beam-rigid elements rather than solid parts, to avoid adding more complexity to the model.

### 4.3.3. Simulation of Bushes

Another major component connection method which has damping characteristics is bush joints. In order to evaluate sensitivity of bushes to damping, elemental damping of 1% is applied to all bushes. Results are compared with the basic run without any damping in the FEA model. Figure 42 compares application of 1% elemental damping with the basic run. The

comparison shows almost the same instabilities between two cases, except for a number of instabilities with very low damping ratio in frequencies less than 1 kHz.
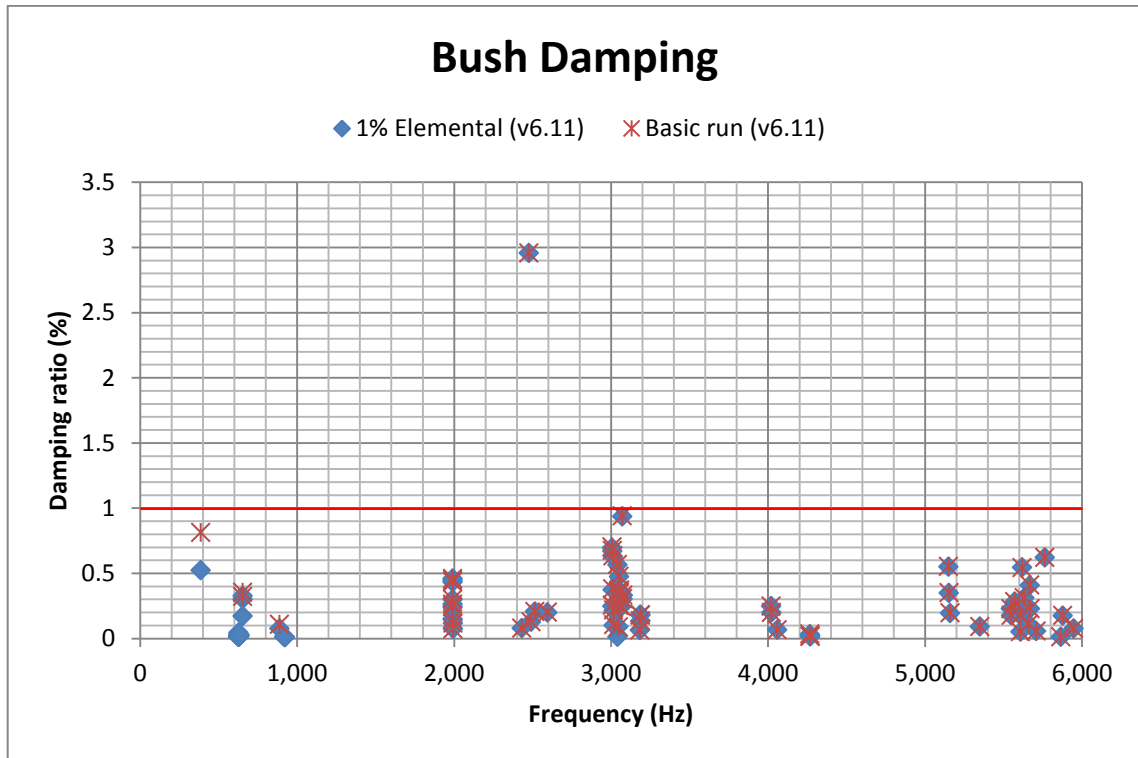


**Figure 42, Bush damping - 1% elemental damping**

### 4.3.4. Conclusions

Experimental estimation of the significance of contact damping is performed. Also the capability of the CAE model in taking contact damping - both bolted joints and bushes - into account is assessed. Considering both significance of the contact damping and also the FEA model's incapability in incorporating the contact damping into CEA, the study focuses on performing damping tuning of the FEA model based on the material damping of individual components. The best practice for conducting the CAE damping tuning is discussed in the next section.

## 4.4.    CAE Damping Tuning Solutions

In order to tune the damping attribute of the CAE model, possible software solutions are investigated considering a capable solution from instability prediction viewpoint . There are three different damping tuning solutions built into Abaqus CAE software package:

- Material Damping

- Modal Damping

- Rayleigh Damping

The optimum damping tuning solution needs to provide the appropriate level of damping for each material. Also, it is known that the level of damping observed from each component can vary slightly in the considered frequency domain. Therefore the optimum damping tuning solution needs to take these characteristics into account.

### 4.4.1. Material Damping

Material damping is significant as it is applicable to individual materials, hence providing each component with its corresponding damping. However, the applied damping will be consistent in the frequency range. Material damping is examined with a uniform damping of 1% applied to all materials (individual components). Results are compared with the basic run in Figure 43, which is showing an almost identical instability prediction, although damping level of 1% is quite significant.
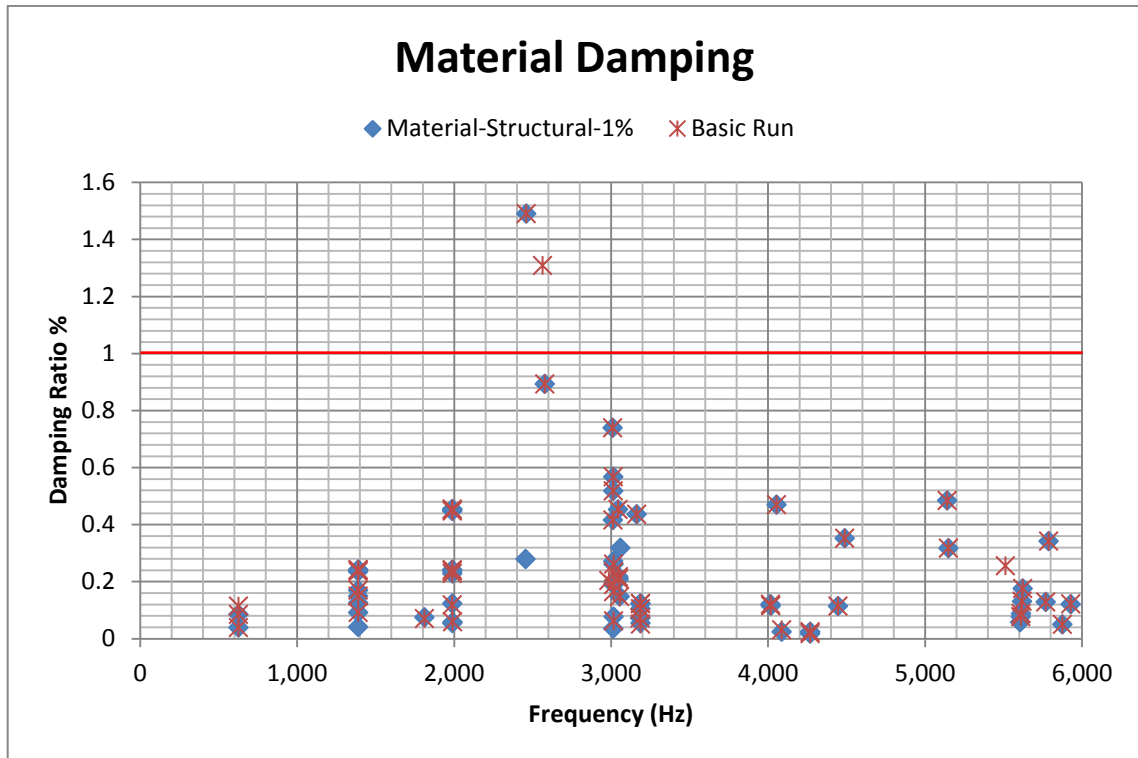
**Figure 43, Material damping vs. basic run**

Consequently, the next option which is modal damping is investigated in the continuation of the research.

### 4.4.2. Modal Damping

Modal damping is not as favourable as material damping because the damping applied is functional in a certain level at the specified frequency range on the entire structure. This means the same level of damping is assumed for all components. Modal damping of 1% is applied in the frequency range of [0.1, 6] kHz. Figure 44 illustrates results, compared with the basic run instabilities.
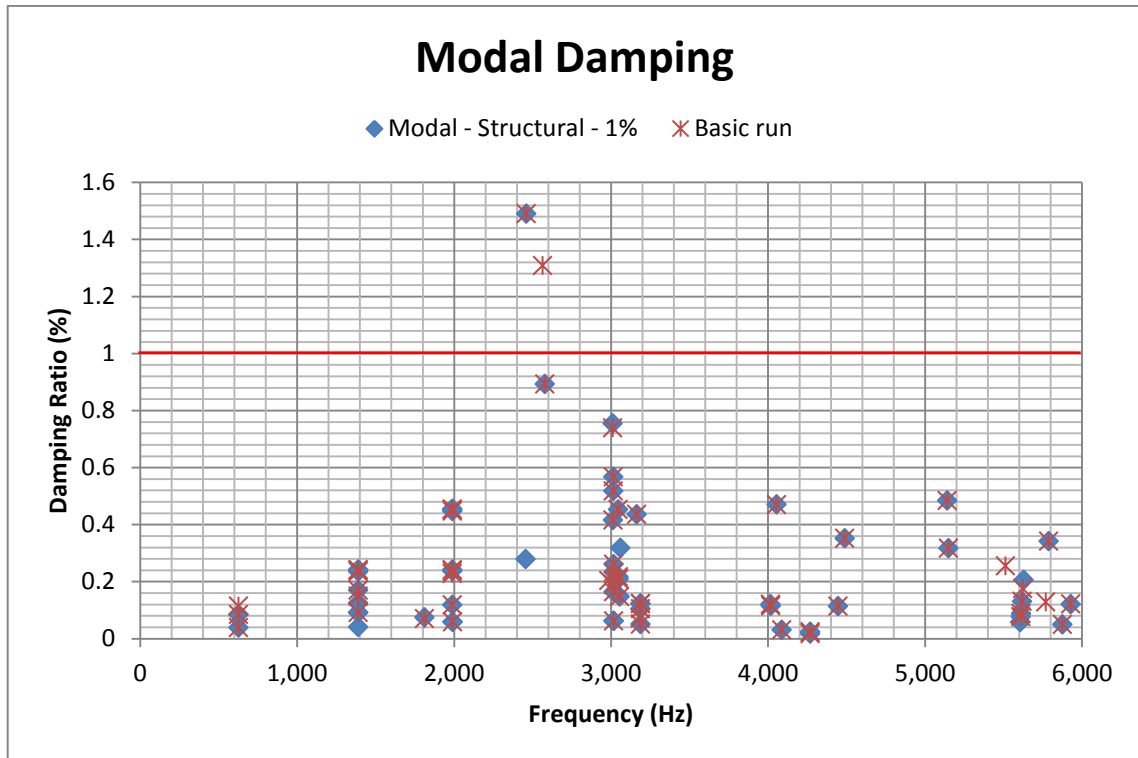
Figure 44, Modal damping vs. basic run

Analysis results do not demonstrate any significant difference with the basic run, hence not applicable to the damping tuning study. Further investigation of the reason behind ineffectiveness of both material damping and modal damping reveals the problem. Material damping and modal damping are not supported in the Complex Eigenvalue extraction procedure of Abaqus CAE software [139]. However, Rayleigh damping is supported as a frequency-based material damping.

### 4.4.3. Rayleigh Damping

Rayleigh damping offers the advantage of application of different levels of damping to each material, varying based on the frequency step. In other words, Rayleigh damping is a frequency-based material damping. Therefore, continuation of the study will be based on utilizing the Rayleigh damping technique.

Apart from model validation, the other aim of the modal experiments is providing the required data to perform an accurate damping tuning on the FEA model. Application of Rayleigh damping requires solution of two simultaneous equations (Equation 9) based on the experimental data. Table 8 shows the damping estimation for the disc, recorded from hammer test.

**Table 8, Disc hammer test - experimental material damping**

| Frequency (Hz) | Damping (%) |
|:---:|:---:|
| **737** | **0.14** |
| 1320 | 0.23 |
| 1656 | 0.36 |
| 1739 | 0.23 |
| **2035** | **0.25** |
| 2924 | 0.27 |

Solving Equation 9 for two data points of 737 Hz and 2,035 Hz returns coefficients of Rayleigh damping as $\alpha = 5.272148$ and $\beta = 3.59\text{E} - 07$. By obtaining $\alpha$ and $\beta$ which are constants of the Rayleigh damping equation, different frequencies can be substituted and the level of damping at the corresponding frequency is returned using the same equation.

Based on this technique, Rayleigh damping for major components of the brake unit is calculated. This includes brake disc, pad back-plates, caliper and knuckle. Figure 45 to Figure 48 visualise the Rayleigh damping estimation compared to the material damping obtained from the modal extraction experiment for these components.
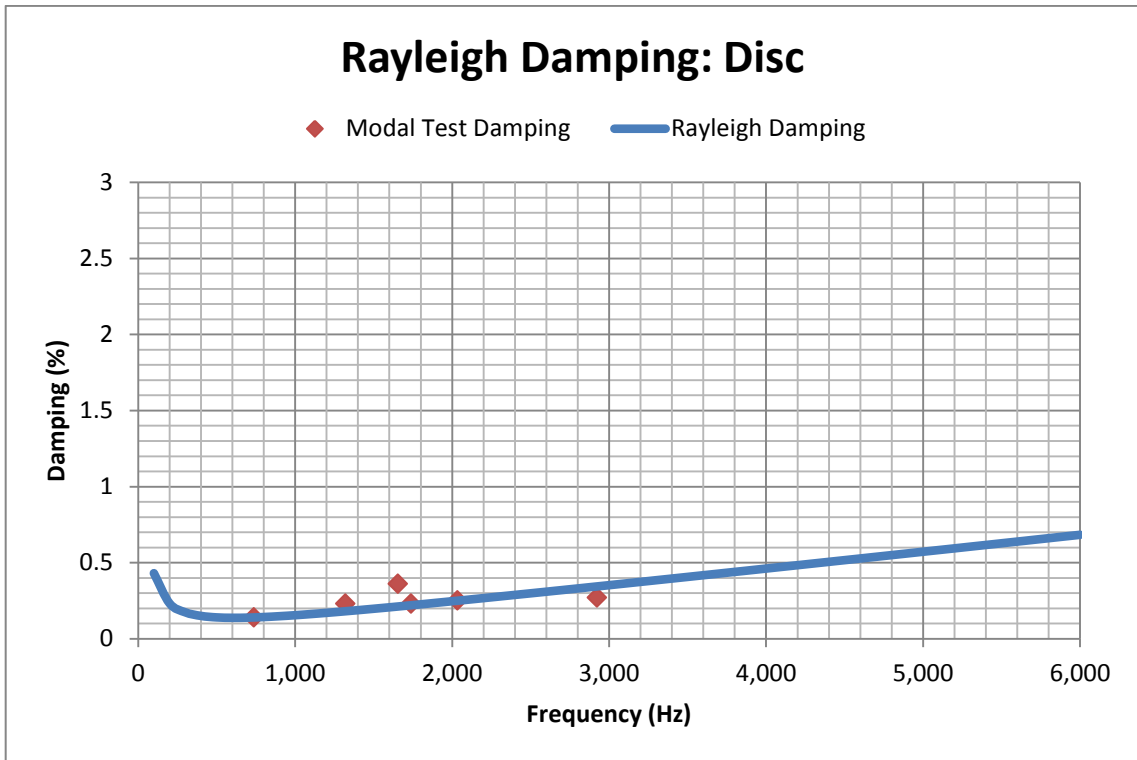
**Figure 45, Rayleigh damping curve vs. actual test data - disc**
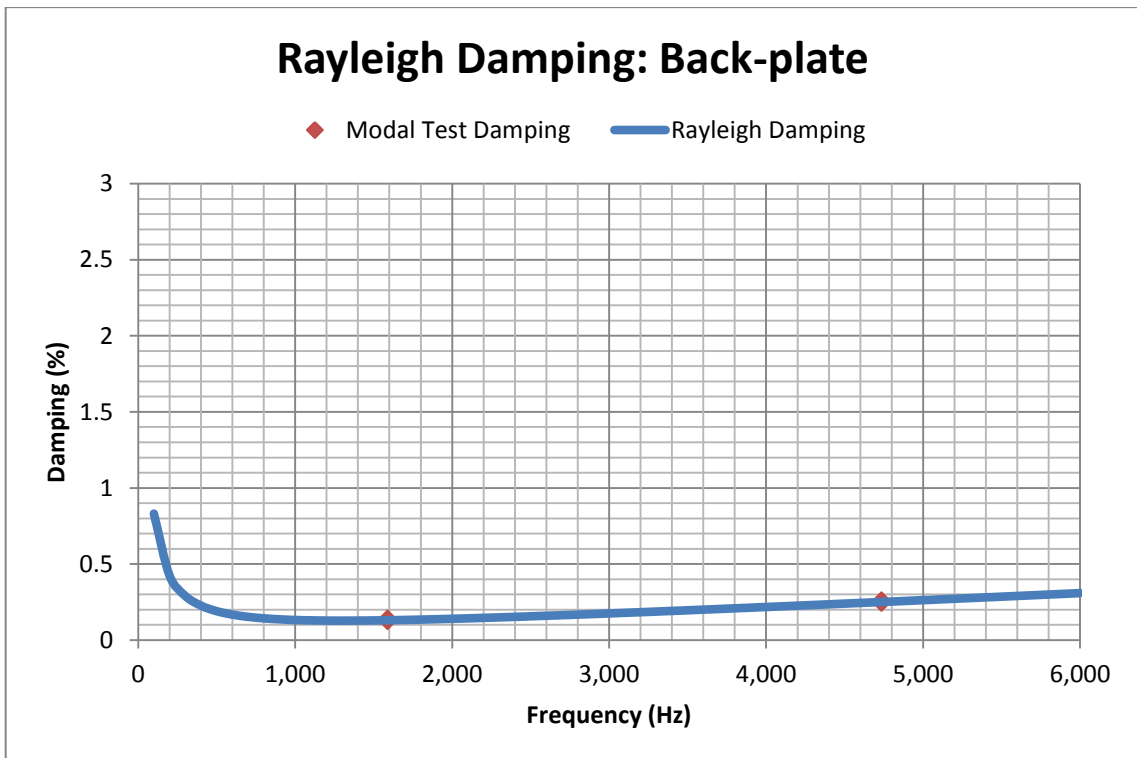


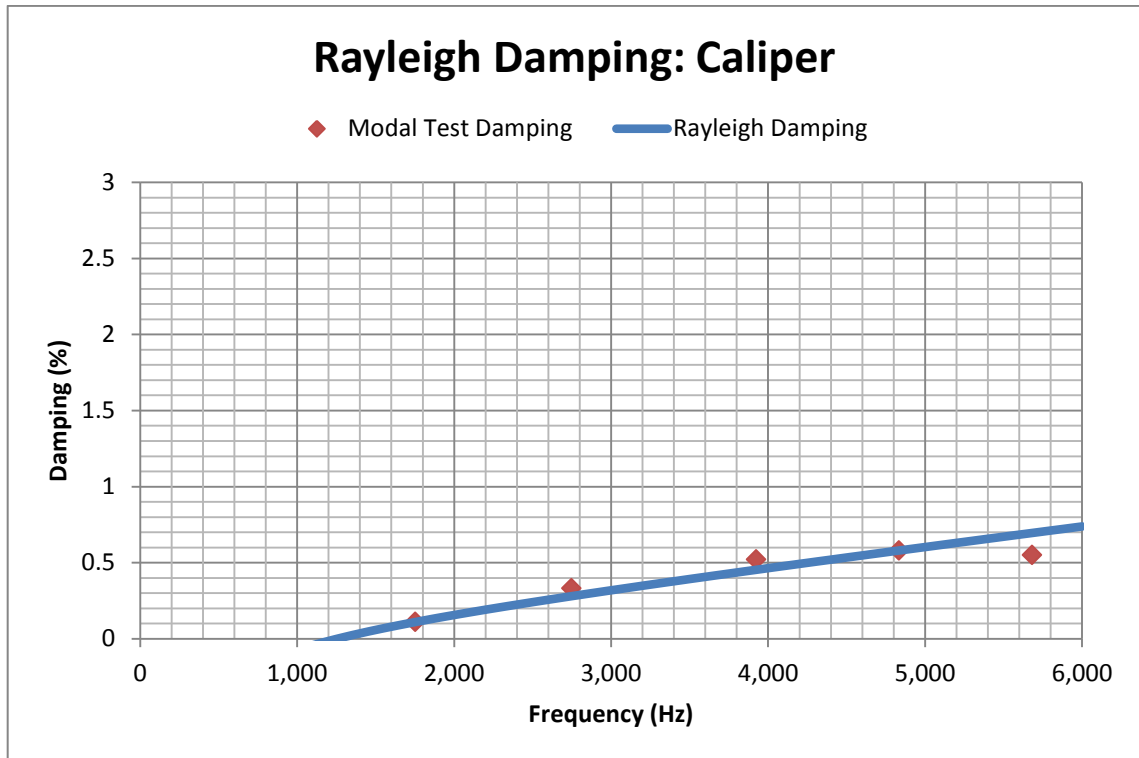**Figure 46, Rayleigh damping curve vs. actual test data - back-plate**

**Figure 47, Rayleigh damping curve vs. actual test data - caliper**
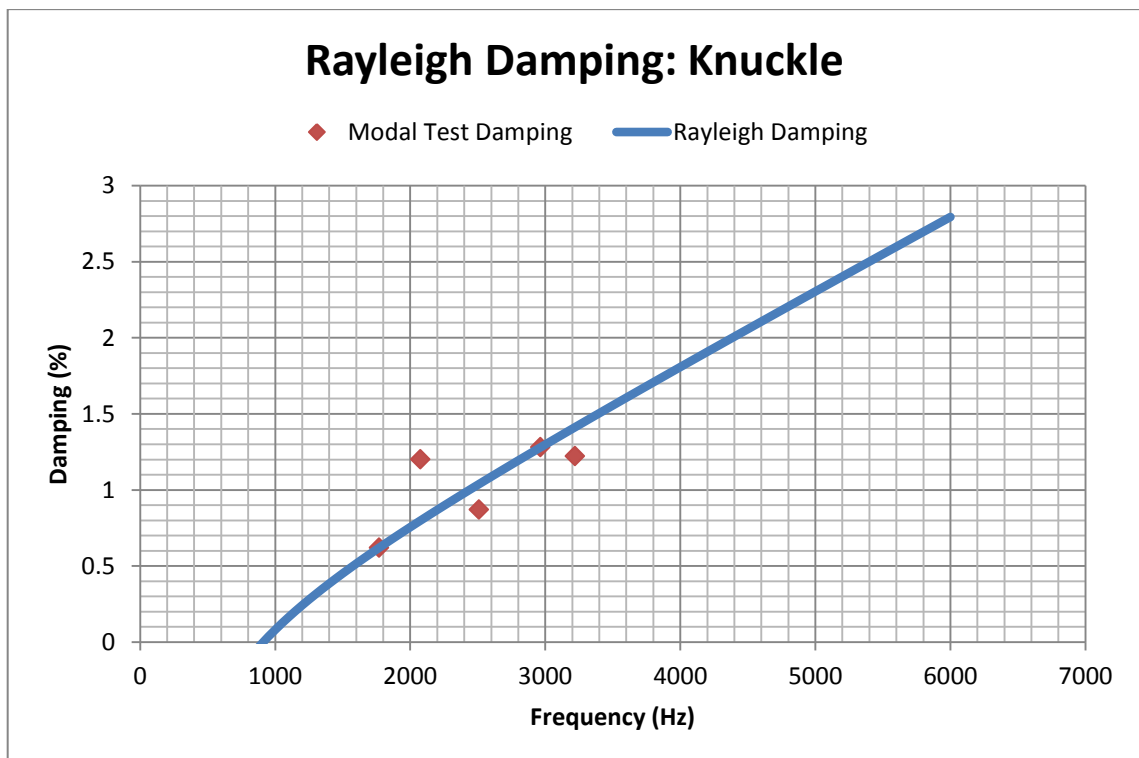


**Figure 48, Rayleigh damping curve vs. actual test data - knuckle**

This comparison demonstrates that the estimated Rayleigh damping is within an acceptable range of variation from the experimental data. However, level of damping at different frequencies depends on the formulation of Rayleigh damping and the current Rayleigh damping graphs are the best curve fitting based on the experimental data.

By examining and evaluating all possible damping application methods in the Abaqus CAE package, Rayleigh damping is preferred as the best approach for damping tuning of the disc brake model. Also Rayleigh damping coefficients are formulated. The next step is application of all experimental damping values on the CAE model and performing the squeal analysis. However, there is also another major source of damping in the system, being brake insulator which is discussed in the next section.

## 4.5.    Damping from Brake Insulators

Brake shims are one of the most important contributors to the damping attribute of brake systems. Damping sourced from the shim can balance the energy of modes potential to couple as an unstable mode. While a basic-specification shim can be very useful to damping out minor unstable frequencies, there are also more advanced shims applied for specific frequency ranges or functional temperatures. The greatest source of damping in the shim is the rubber part (the other is the adhesive), and rubbers exhibit relatively different levels of damping as temperature varies (see shim map in Figure 29). Therefore the most suitable shim can be selected based on the specifications of the rubber applied to it. Despite these purpose-built shims, basic shims usually have similar characteristics (often referred to as base-line shims).

On the other hand, selection of the right shim is an expensive and time consuming process, as it requires numerous dynamometer (or vehicle) tests which are only possible once the

component design is finalised and a prototype exists. All brake components can be designed and tested for NVH attributes in the CAE phase, before any prototype exists. Damping tuning of the model can also contribute greatly to this, as it can potentially eliminate most of the over-predicted instabilities. This is where a simple yet representative CAE model for the shim which can demonstrate the damping attributes becomes significant. This can result in significant improvement in the accuracy of instability prediction. Consequently, the modes forming the unstable frequency can be shifted (modal decoupling) by performing geometrical alterations or changes in the material properties. Various modal decoupling techniques are practiced in designing brakes applicable based on the specific frequency range of the modal coupling and the components involved [148].

Shims are formed of rubber material, adhesive, and usually a sheet of steel in the middle [149]. A basic model of shim is developed which comprises of a central steel section and two rubber layers on sides. Figure 49 represents a schematic of the shim model developed.



Figure 49, Schematic of three layer shim design

The adhesive material is not simulated in this model. Rubber parts are modelled as hyper-elastic materials in order to replicate the nonlinear elastic behaviour. Hyper-elastic material property does not account for the material damping; however, it does account for the flexibility of the material. The shim is initially modelled without any material damping, and then the hyper-elastic rubber material is damped in order to achieve a more accurate estimation of strength of instability from the simulation. Rubber material damping can be

obtained by performing stress relaxation experiments [142]. This study uses Rayleigh damping technique and assumes damping level of $\alpha = 0$ and $\beta = 3.75 * 10^5$ [142]. Effectiveness of this shim design is assessed by performing a full set of CEA squeal analysis. Initially the shim is modelled without any damping in the rubber section, and then application of damping to the rubber is analysed.

## 4.6.      Squeal Analysis of CAE Model with Damping Tuning

The most effective software technique for application of damping on the CAE model is identified to be Rayleigh damping. Based on the experimental data, required coefficients are calculated for major components of the system. Also, a modelling technique is developed for simulation of brake shims, which is capable of representing the damping attributes of the shim incorporated into the rubber material. In order to assess the effect of damping tuning on the instability prediction by CEA, the analysis is initially performed on the baseline model with no damping. Although there are over-predictions in the Baseline analysis results, but it is still a reliable way of analysing the brake. It shows all possible unstable frequencies, some of which may be over-predictions. Therefore the damping tuning is also assessed based on the dynamometer results, showing the unstable frequency at 2.5 kHz.

For the first case of comparison, major components of the system are tuned with their corresponding level of damping. This includes disc, hub, caliper, knuckle and back-plates. Figure 50 illustrated this comparison.
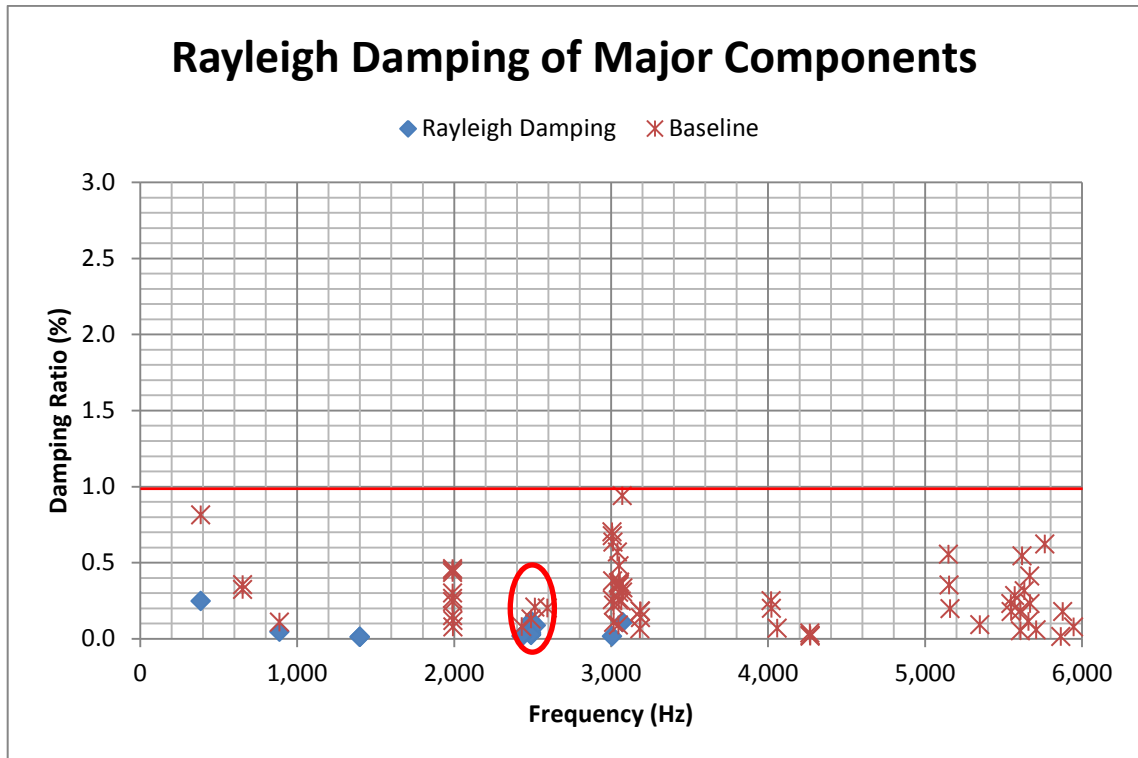
**Figure 50, Squeal analysis: damped model vs. baseline**

Considering the NVH performance of the brake unit on dynamometer (Figure 3), the new model with Rayleigh damping is an improvement on the instability prediction as it eliminates majority of the over-predictions except for the 3 kHz frequency range and some minor instabilities at the lower frequencies. However, although the repetition of instabilities at 2.5 kHz can be an indication of an unstable frequency, the strength of any of the predicted instabilities is not significant enough to demonstrate that. Also, considering all major components have been tuned for damping, there is an inconsistency in the model because of lack a major source of damping - the brake shim.

In the next set of analysis, the 3 layer shim is added to the FEA model which is tuned using the Rayleigh damping technique. Figure 51 compares the squeal analysis results of the new model with the baseline model.
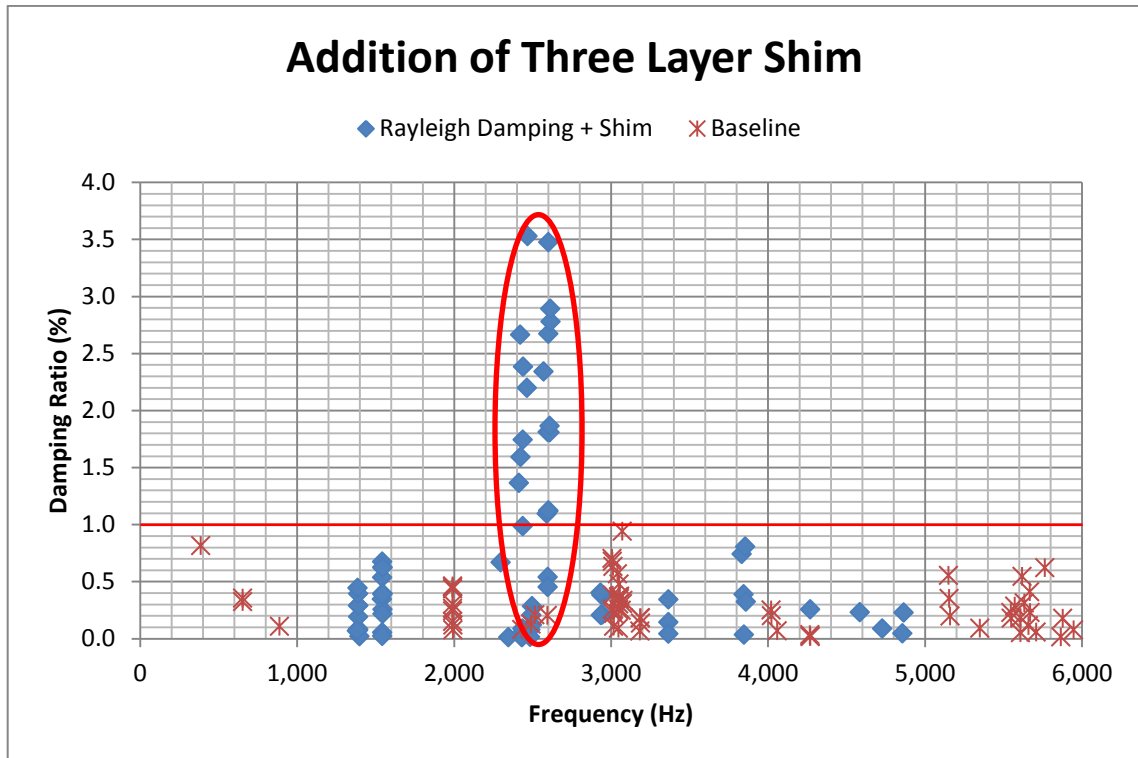
**Figure 51, Three layer shim without damping tuning on the damped model vs. baseline**

As seen in the results, the noisy frequency (2.5 kHz, compared to Figure 3) is tangible in the new model with relatively high amplitude and significant repetitions in the same frequency range. However, there are still some over-predictions despite their relatively low amplitude. An example of this is 1.4-1.5 kHz frequency range, where new over-predicted instabilities are added. The next step is damping tuning of the rubber section to fully demonstrate the characteristic of the shim. The steel section has a less significant damping compared to the rubber part. Therefore, in order to minimise the required computing, the steel section is not damped. Application of damping on the shim can reduce the strength or number of repetition of over-predictions. Figure 52 illustrates comparison of analysis results of this model with the baseline.
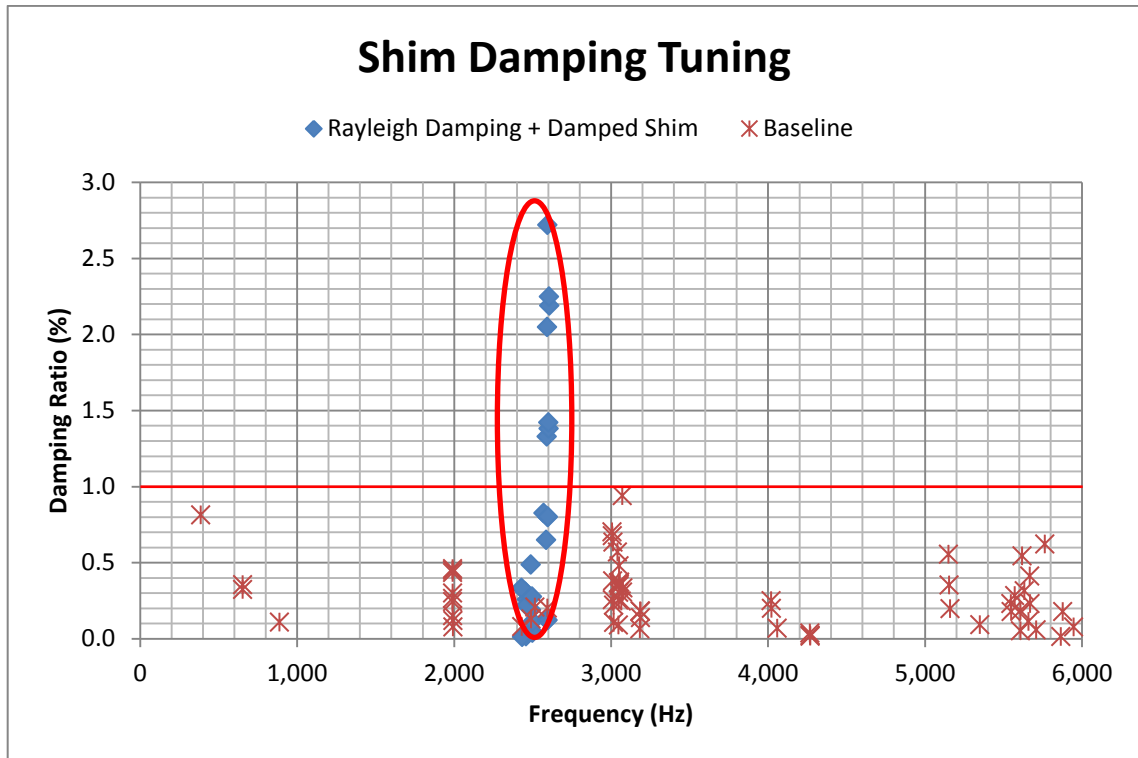
Figure 52, Three layer shim with damping tuning on the damped model vs. baseline

As seen in Figure 52, application of damping on the rubber section significantly improves the instability prediction, and the CAE results are now thoroughly correlating with the dynamometer results. The over-predicted instabilities are completely eliminated, especially those at 1.4-1.5 kHz and 3.8 kHz which seemed to be mainly due to lack of damping in the shim.

## 4.7.    Summary

System damping and application of damping characteristics to the CAE model were investigated. Initially the CAE model was validated by modal correlation with the prototype. Different aspects of damping including material damping, contact damping and shim damping were investigated. Also, simulation solutions for application of damping to the CAE model were reviewed and Rayleigh damping was selected for performing damping tuning. Rayleigh

damping coefficients were calculated based on the component damping levels obtained in the modal experiments.

Other aspects of the CAE model relating to damping were also evaluated, including modelling of bolted joints and bushes. The level of contact damping was compared with the material damping based on a DOE study.

A simplified yet representative modelling technique for the brake shim was introduced. The new modelling technique demonstrated the damping characteristic of the shim without adding unnecessary complexities to the system. The damping tuning eliminated the majority of over-predicted instabilities and enhanced the prediction of the actual unstable frequency.

# Chapter 5: On the Significance of Friction

## 5.1. Introduction

Frictional forces are a significant factor in brake noise. The frictional force in the disc-pad contact interface is a known factor for facilitating initiation of modal coupling [12]. Moreover, friction materials have been a topic of research since the early years of disc brake development. However the work linking friction material properties to brake noise has not yet yielded a practical brake pad design solution to eliminate brake noise.

Braking torque of a brake unit reflects its most significant functionality and there is a direct relation between the frictional force and the braking torque. Therefore, the friction material used for this purpose is also of high significance. There are two conflicting factors to be considered in selecting friction materials based on the Coefficient of Friction (COF). Firstly high COF to give adequate braking performance [29, 80], and secondly low COF which promotes low brake noise [150]. Hence, any variation of the COF should be carried out with further attention, since decreasing it can affect the braking performance and increasing it can introduce even more instabilities into the system [132].

The conventional design for brake pads uses a homogenous composite friction material throughout the frictional surface of the pad. This specific composite material - also referred to as the friction material or friction powder (in the manufacturing process) - is chosen based on the expected attributes of the brake system. The required braking torque and NVH performance are the most significant attributes of a brake system when it comes to friction material selection.

The composite material, due to the size and material properties of its ingredients, can show slightly different microscopic local behaviours. This is a known issue referred to as clusters of composite which generate local different COF or even different temperatures (consequently causing hot spots). However, this is in the microscopic scale and also the variation in the COF or temperature is minimal. This is considered as a quality problem which has improved significantly in the recent years. The issue is resolved by a more homogeneous friction powder and better mixtures. The fine friction material produced from the high quality friction powder composite is expected to demonstrate more consistent technical attributes, frictional coefficient being one of them.

## 5.2.    Concept of Partitioned Brake Pad

Assuming the brake disc rotates at a constant rotational velocity, this results in different local tangential velocities at different distances from the centre of rotation in the disc-pad contact interface ($v = rw$). The stationary side of the contact is the brake pad, which is assumed to be produced from a fine friction material and has microscopically-uniform COF.

The disc's surface with different local tangential velocities once in contact with the uniform frictional force from the brake pad can cause stick-slip across the contact interface. In this interaction, the uniform friction material will cause different local frictional forces and slip rates at different distances from the centre of rotation. Since slip is known to cause instability [27], and it is varying radially [151], one can understand that the uniform friction material undergoing this different local slip over its surface can be a reason for the mentioned instabilities. This is where the hypothesis of a new brake pad design becomes meaningful.

A new brake pad design was introduced based on the hypothesis that variation of the friction material based on a pattern can normalize the distribution of frictional forces relative to the local tangential velocity. This may counteract stick-slip. This concept is based on the hypothesis that variation of COF over the radius of the brake pad is effective in reducing the susceptibility of the brake instability to cause brake squeal.

Partitioned Brake Pad (PBP) is a brake pad with radially increasing level of COF. The contact interface is divided into a few radial sections, each of them with a friction material with a different COF. Partitions coincide with each other on radial boundaries in a way that the entire surface of the pad is covered with the friction material. The level of COF increases from the lower section (closer to the disc centre) to the higher section. This concept is mainly based on the variation of the COF over the radius of the brake pad, and how that can reduce the propensity of brake system instabilities. Partitions with different friction material are aimed at replicating the smooth increase in the COF in the radial direction. A cross-section view of the brake assembly model with a five partitioned pad is shown in Figure 53.
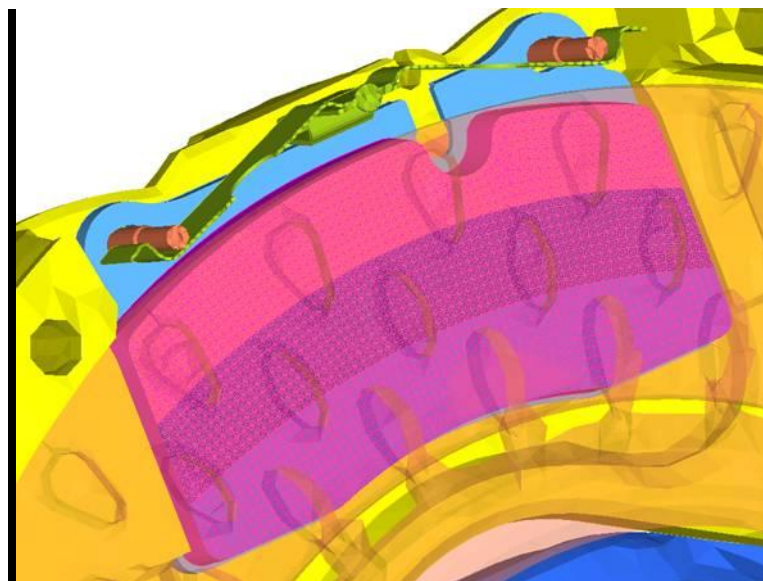


**Figure 53, Cut-away view of PBP assembled to the brake unit**

In order to evaluate the PBP concept and compare the idea with other possible layouts of variation of COF, different scenarios of PBP were proposed. Each case was simulated and analysed in terms of NVH instabilities using CEA technique. The first set of PBP simulated and tested were the radially partitioned pads, with different number of partitions. The friction material surface was divided into partitions with equal widths. Figure 54 shows a PBP with three radial partitions.
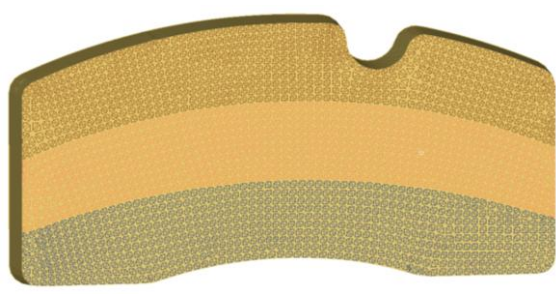


**Figure 54, Schematic of radially partitioned friction material**

The other possible layout of the PBP could be the circumferentially divided pad. This was based on the hypothesis that the nature of the contact may vary from the leading edge to the trailing edge. Figure 55 shows schematic of the pad divided into three circumferential partitions.



**Figure 55, Schematic of circumferentially partitioned friction material**

Apart from the pattern on the pad COF, the number of partitions was also a considerable factor. The original concept recommended a smooth variation in the COF, which could be achieved by higher number of partitions. On the other hand, the difficulty in manufacturing

such a pad was foreseeable. Therefore, the minimum number of partitions which could provide the advantages of the concept was desirable. Consequently, both radially partitioned and circumferentially partitioned pads were simulated with 3 and 5 partitions.
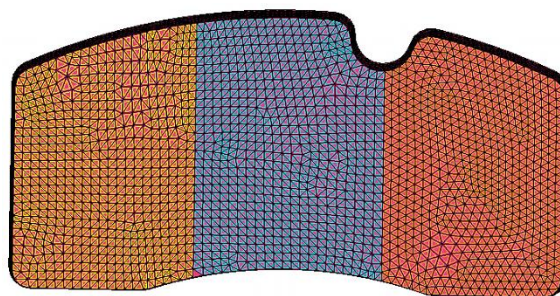
Typical value of COF in the brake system of a commercial vehicle is in the range of 0.4 to 0.5. However, brake pads with a COF in the range of 0.3 to 0.7 [79] are available in the automotive industry. Although both lower and higher end of the range are for specific applications, the formulation of a friction material to demonstrate those levels of friction is available. Pads with higher COF are commonly utilised for race and high performance cars, and motorcycle brakes usually have pads with lower COF [44, 152]. This is the range where the different friction materials forming the Partitioned Brake Pad were chosen from.

The other aspect of the COF level was its variation from one partition to the other. Theoretically, great variation of COF from one partition to the other could cause uneven temperature distributions and consequently cracks on the pad surface. This was one of the aspects of the concept which needed to be investigated experimentally. Also, small variation in the COF seemed difficult to achieve in the friction powder formulation, and would not cover the entire range and result in lower braking torque. The other concern was the accuracy of the COF resulting from each friction powder and how fine the boundaries of the partitions could be, to demonstrate the variation, considering the entire variation was minor.

Although the original concept and the theory forming this hypothesis suggested radially increasing COF, other patterns were also simulated. This helped in investigating the sensitivity of the instabilities (causing brake noise) to the COF pattern. Patterns simulated for this reason were radial and circumferential increase and decrease in the COF, as well as the case with the highest COF in the middle. The latter was aimed at investigating the effects of

higher local pressure in the middle section of the pad, based on the pressure applied to the brake pad through the pistons.

## 5.3.       Proof of Concept: CEA of Partitioned Brake Pad

In order to evaluate each case of the PBP designs, each particular pattern was simulated on the brake pad and assembled to the complete corner unit model. A complete set of CEA was performed for different pressures and directions, to assess the stability of the system with the new brake pad. Instabilities were ranked by the damping ratio determined from CEA. A value of 0.5% was assumed as the limit for the damping ratio below which brake instability is assumed to be suppressed.

Performance of the different configurations of the brake pad applied to each case of the study and possible improvements were judged by comparing their results with the baseline model, i.e. uniform brake pad COF. Figure 56 shows instabilities predicted under the baseline conditions as previously mentioned in Chapter 3, highlighting instabilities in the unacceptable damping ratio region in frequency neighbourhoods of 2, 2.5, 3.0 and 5.1 kHz.
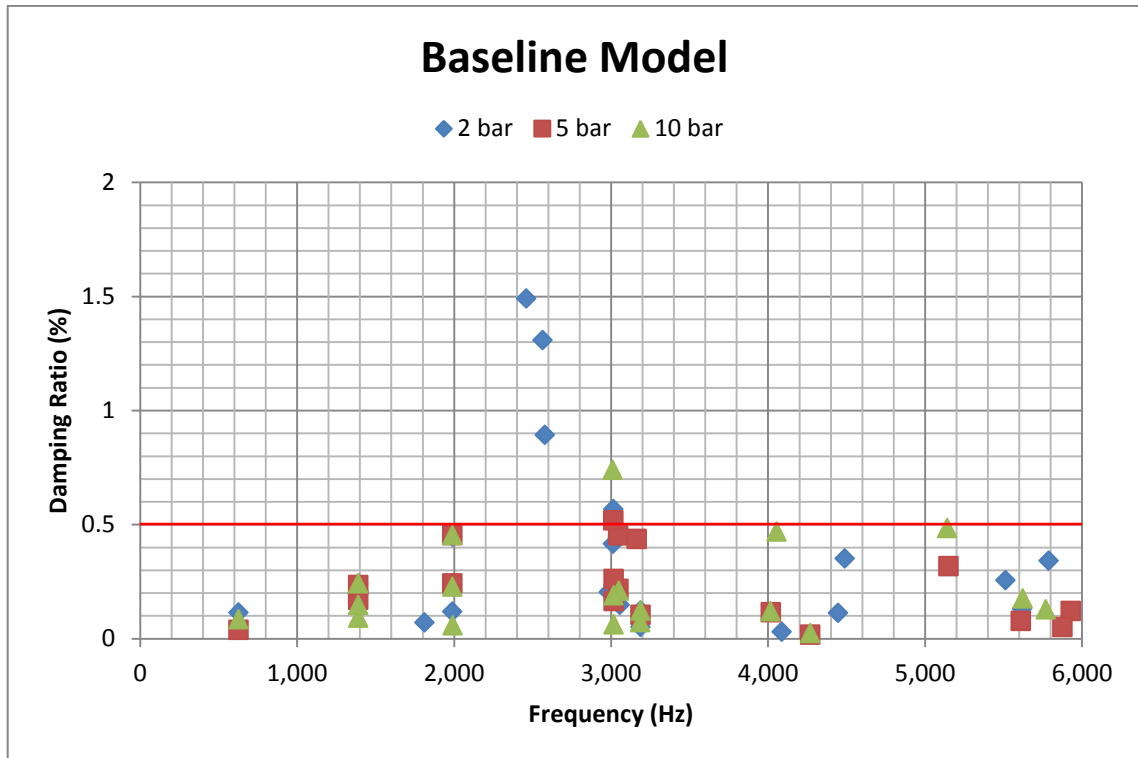
Figure 56, CEA instability prediction for the baseline model

### 5.3.1. Radially Partitioned Pad

In order to compare the different possible patterns of COF variation on the brake pad, different cases were defined. The radially partitioned brake pad was assigned different COF patterns where the COF increased radially (Figure 57 and Figure 58), decreased radially (Figure 59 and Figure 60) or was higher in the middle partition (Figure 61 and Figure 62).
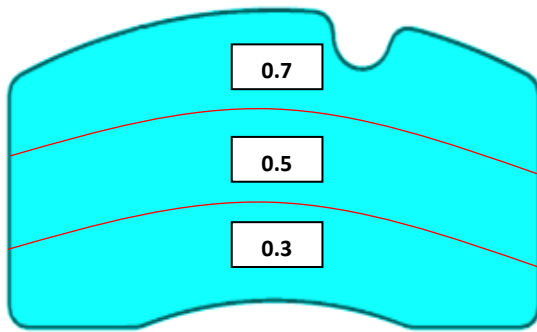
**Figure 57, Case 1: Three partitions, radially increasing COF**
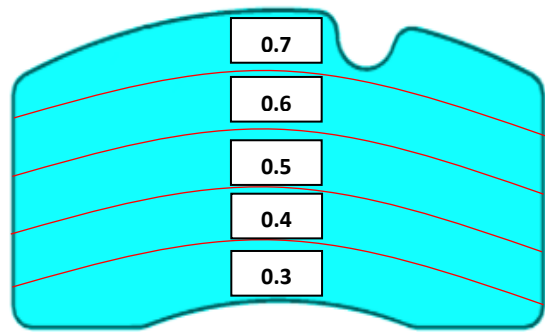


**Figure 58, Case 2: Five partitions, radially increasing COF**
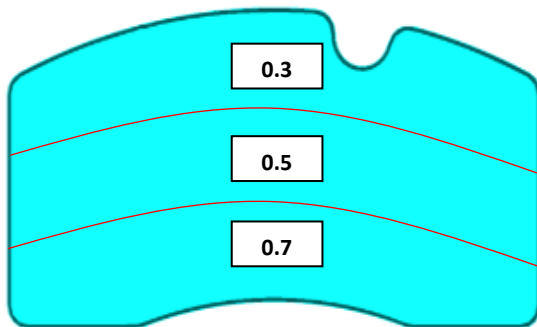


**Figure 59, Case 3: Three partitions, radially decreasing COF**
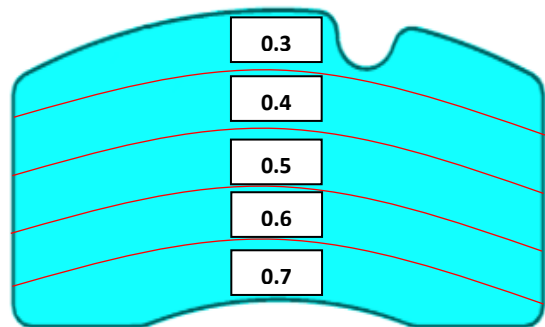


**Figure 60, Case 4: Five partitions, radially decreasing COF**
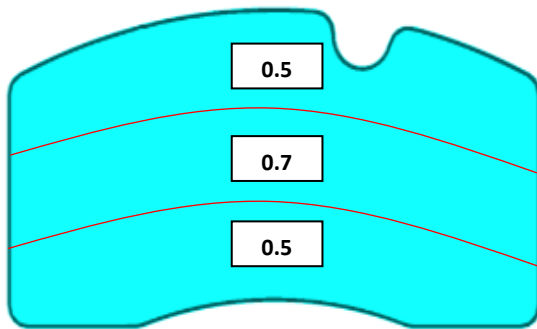


**Figure 61, Case 5: Three partitions, higher COF in the middle**
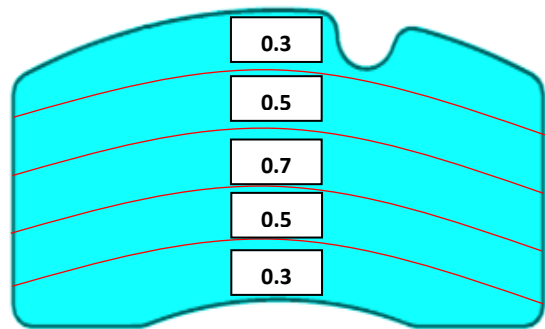


**Figure 62, Case 6: Five partitions, higher COF in the middle**

The FEA squeal analysis was performed for each of the 6 cases mentioned above, each undergoing pressures of 2, 5 and 10 bar, simulated in both in forward and reverse directions. Figure 63 and Figure 64 present results for cases 1 and 2, sharing the same pattern with

different number of partitions. Case 2 confirms the hypothesis of the concept, i.e. the smoother increase of COF results in a more stable contact.
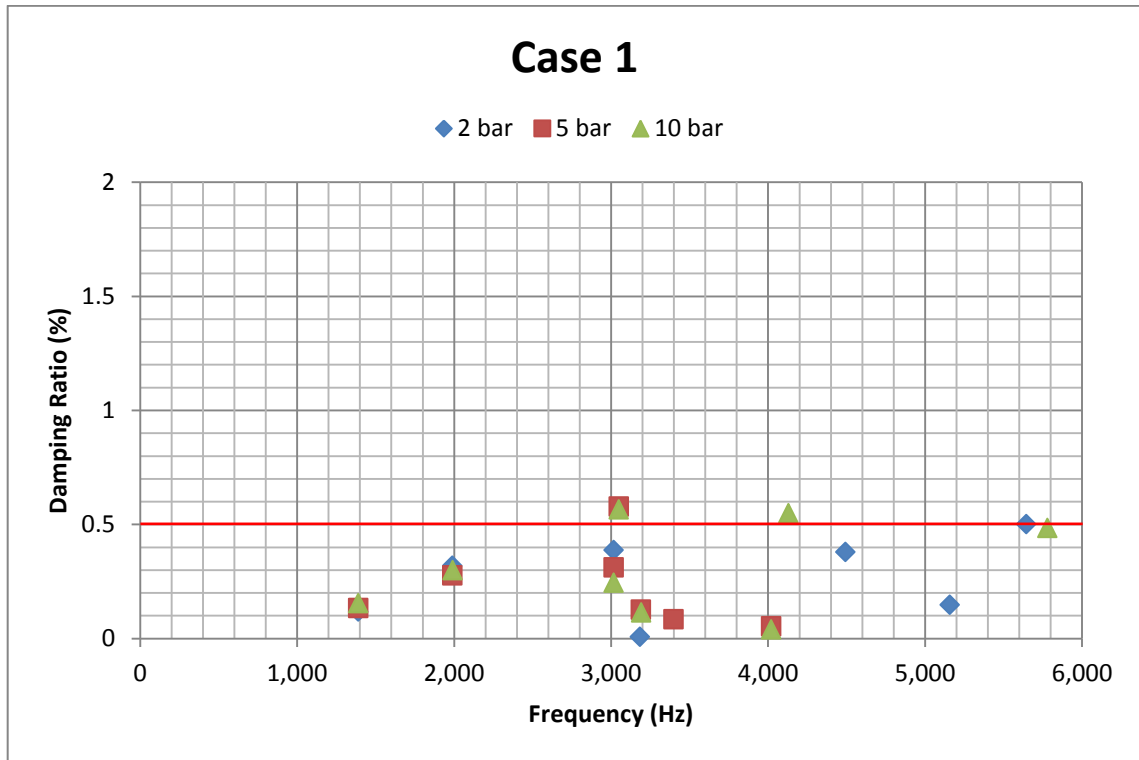


Figure 63, CEA of PBP, Case 1
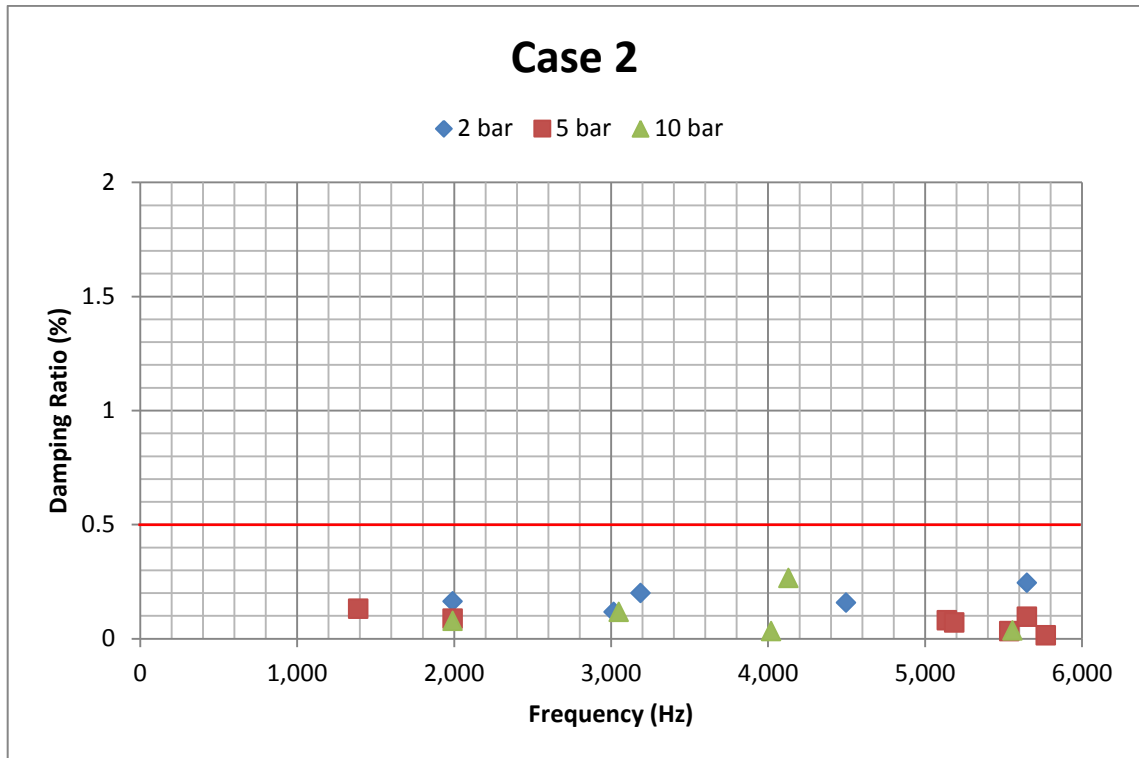
Figure 64, CEA of PBP, Case 2

The analysis results of radially increasing COF are in cases 1 and 2 (Figure 63 and Figure 64 respectively). On the other hand, radially decreasing COF was analysed in cases 3 and 4 (Figure 65 and Figure 66 respectively). Comparison of these two patterns highlights that radially increasing COF is a relatively more stable pattern.
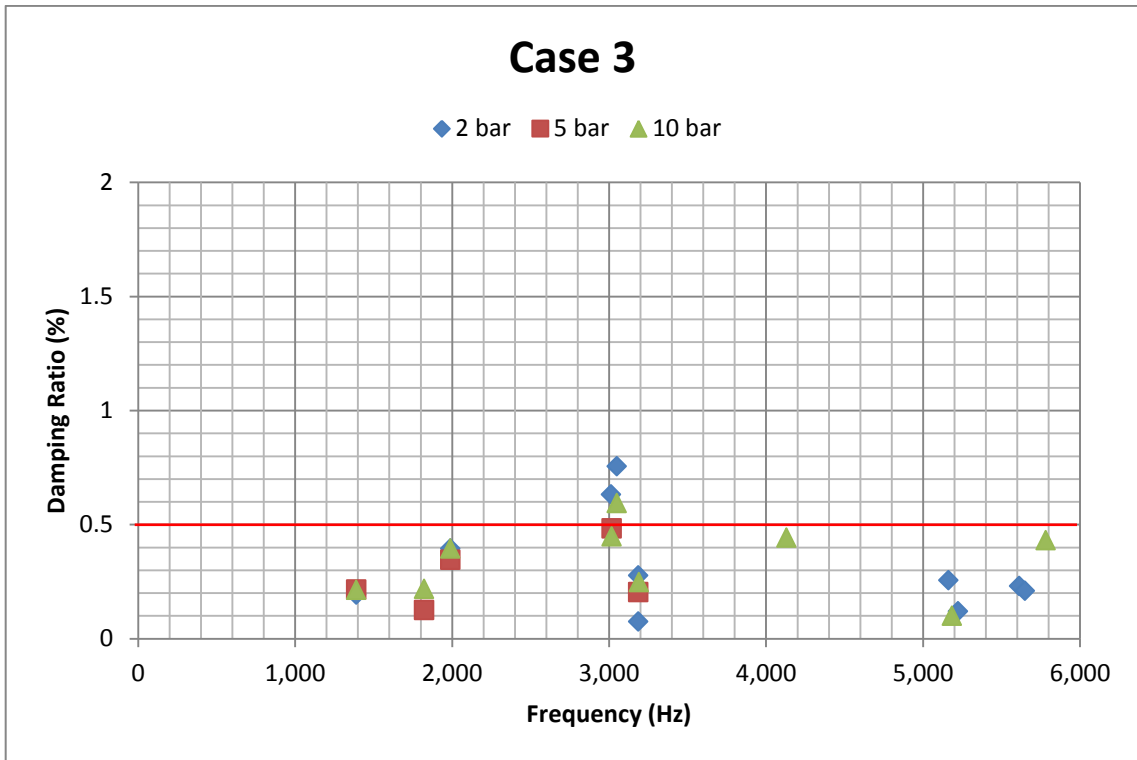
**Figure 65, CEA of PBP, Case 3**
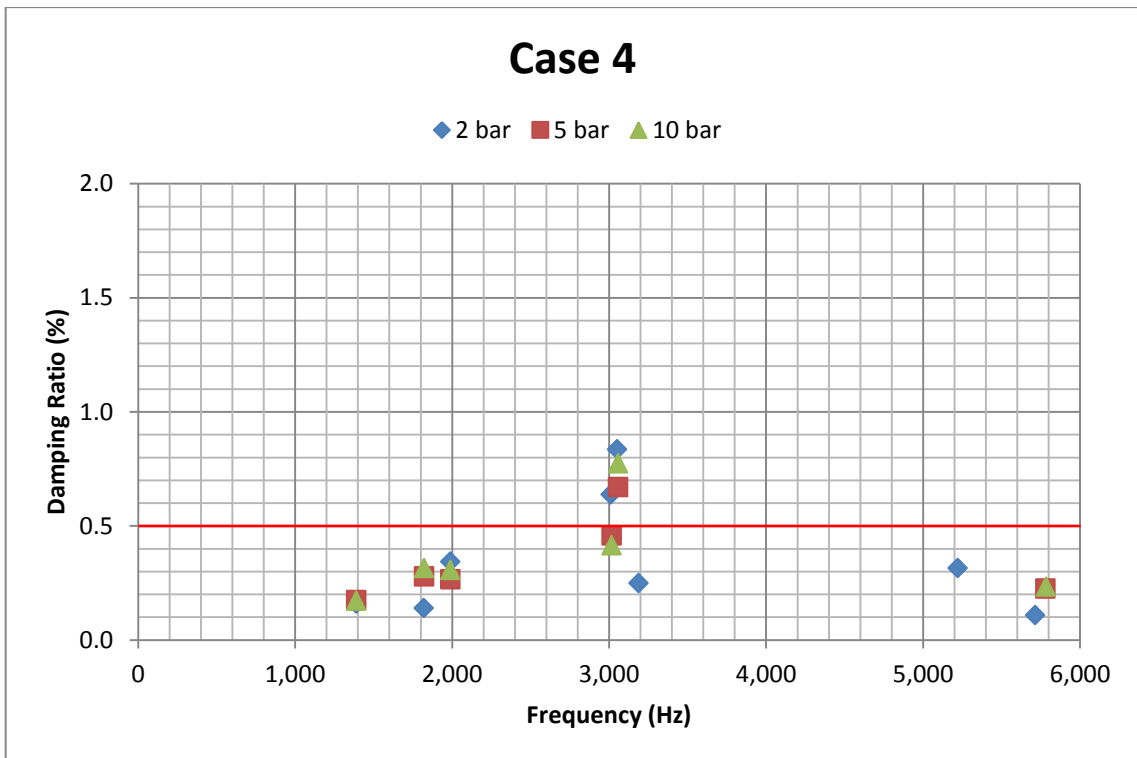


**Figure 66, CEA of PBP, Case 4**

Cases 5 and 6 were both pads with a higher COF in the middle partition. Case 5 (shown in Figure 67) clearly shows an unstable frequency at 3 kHz. This is less visible in case 6 (Figure 68). However, the relatively high repetition of instabilities in the same frequency domain in case 6 could be an indication of an instability potential to cause brake noise.
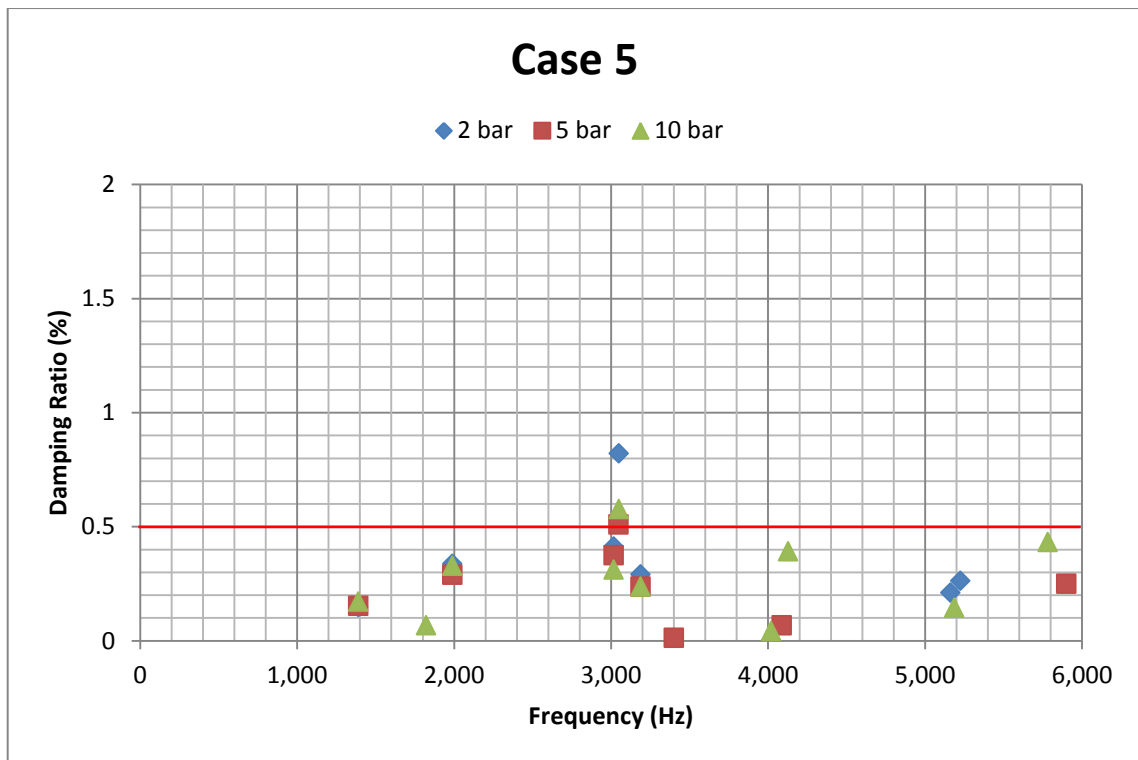


Figure 67, CEA of PBP, Case 5
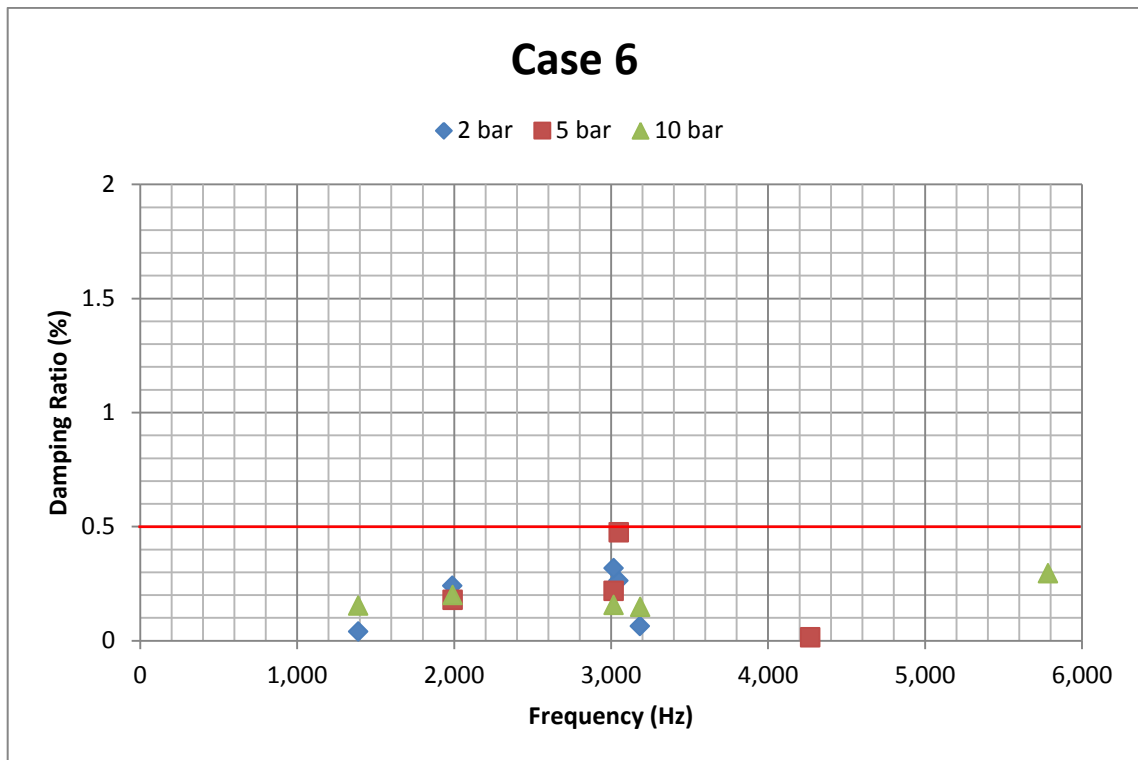
Figure 68, CEA of PBP, Case 6

Comparing results from different cases of radially partitioned pads revealed that Case 2 (five partitions and radially increasing COF) shows the most stable behaviour. Although case 2 shows instabilities happening at various frequencies, the majority of them have a very low damping ratio, with the highest being 0.266% at a frequency of 4129.79 Hz.

Hence case 2 was selected as the most successful scenario, showing instabilities with a damping ratio mostly lower than half the target set, i.e. 0.5%. Consequently, compared to other cases of radially partitioned pads, the pad with the radially increasing COF over 5 partitions showed significantly lower strength of instability.

### 5.3.2. Circumferentially Partitioned Pad

The next step of the investigation was introducing circumferential partitions, to investigate the effect of variation of COF between the leading and trailing edges. The circumferential partitioning of the brake pad was conducted in different cases with higher COF at the leading

edge (Figure 69 and Figure 70), higher COF at the trailing edge (Figure 71 and Figure 72) and

the higher COF in the middle partition (Figure 73 and Figure 74).
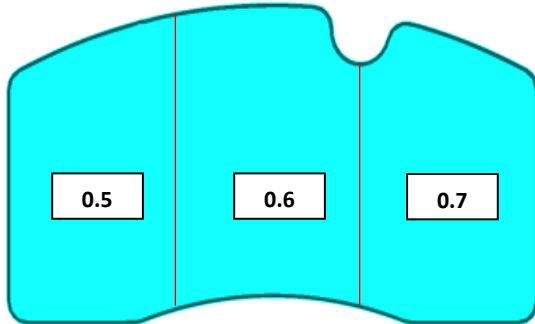


**Figure 69, Case 7: Three partitions, higher COF at trailing edge**
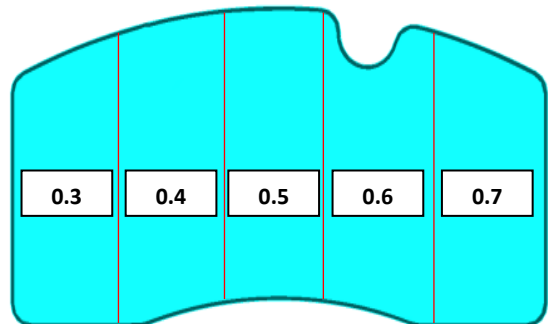


**Figure 70, Case 8: Five partitions, higher COF at trailing edge**
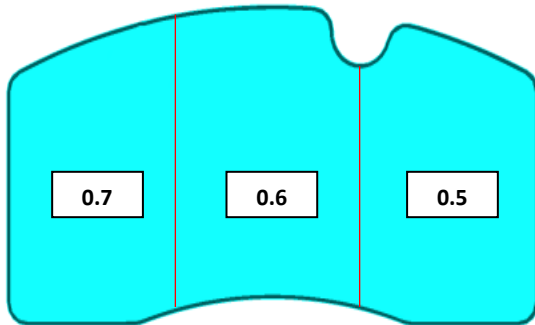


**Figure 71, Case 9: Three partitions, higher COF at leading edge**
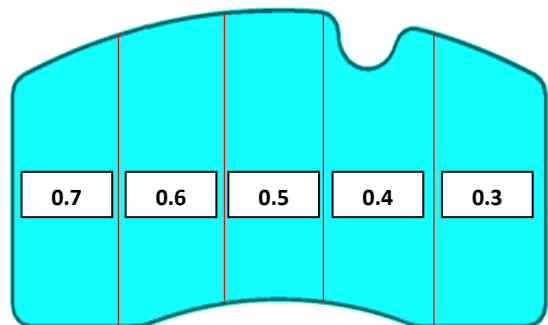


**Figure 72, Case 10: Five partitions, higher COF at leading edge**
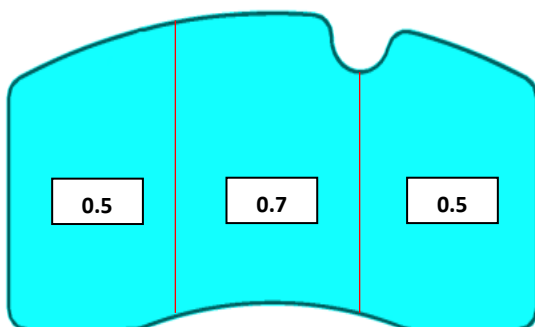


**Figure 73, Case 11: Three partitions, higher COF in the middle**
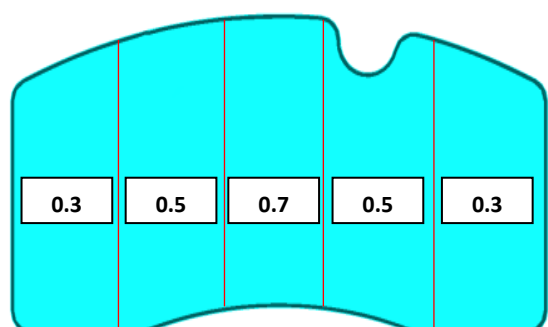


**Figure 74, Case 12: Three partitions, higher COF in the middle**

Cases 7 and 8 both had the same COF pattern, i.e. higher COF on the trailing edge, with the

difference being in the COF range. Once analysed for brake noise instabilities, both case 7 (in

Figure 75) and case 8 (in Figure 76) showed repeated instabilities in the 3 kHz frequency range. Instabilities at this frequency range were reported for different pressures which is an indication of likelihood of brake noise at this frequency.
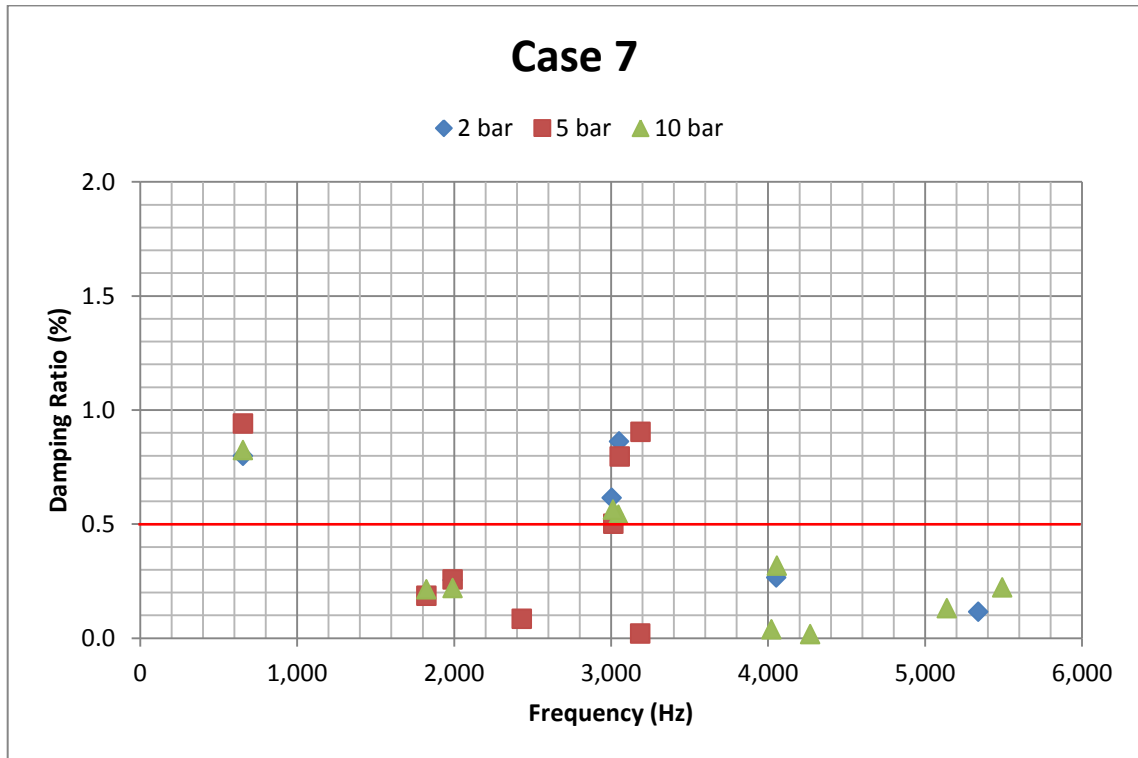


**Figure 75, CEA of PBP, Case 7**
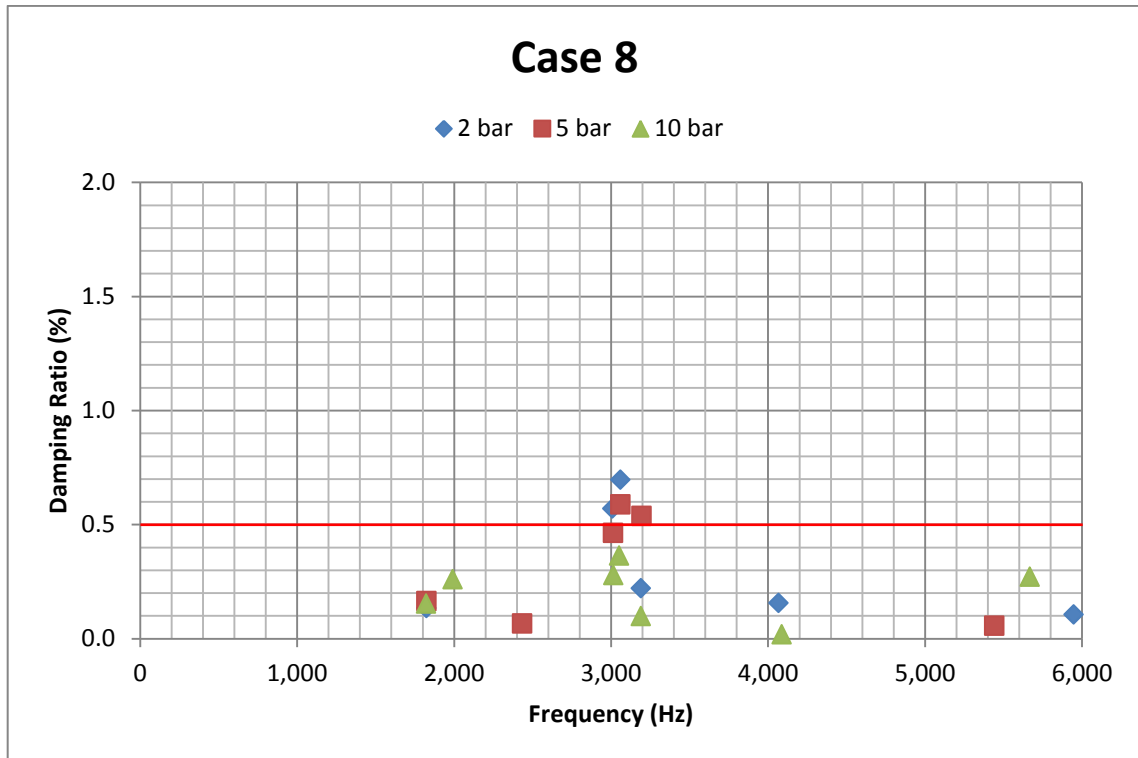
**Figure 76, CEA of PBP, Case 8**

The next set to be tested was cases 9 and 10 (in Figure 77 and Figure 78 respectively) with three and five partitioned pads having a higher COF in the leading edge. Case 9 showed the same unstable frequencies as case 7 (650 Hz and 3 kHz). Although the instabilities at 3 kHz in case 10 were just below the target line, it was also showing instabilities at 5.7 kHz range.
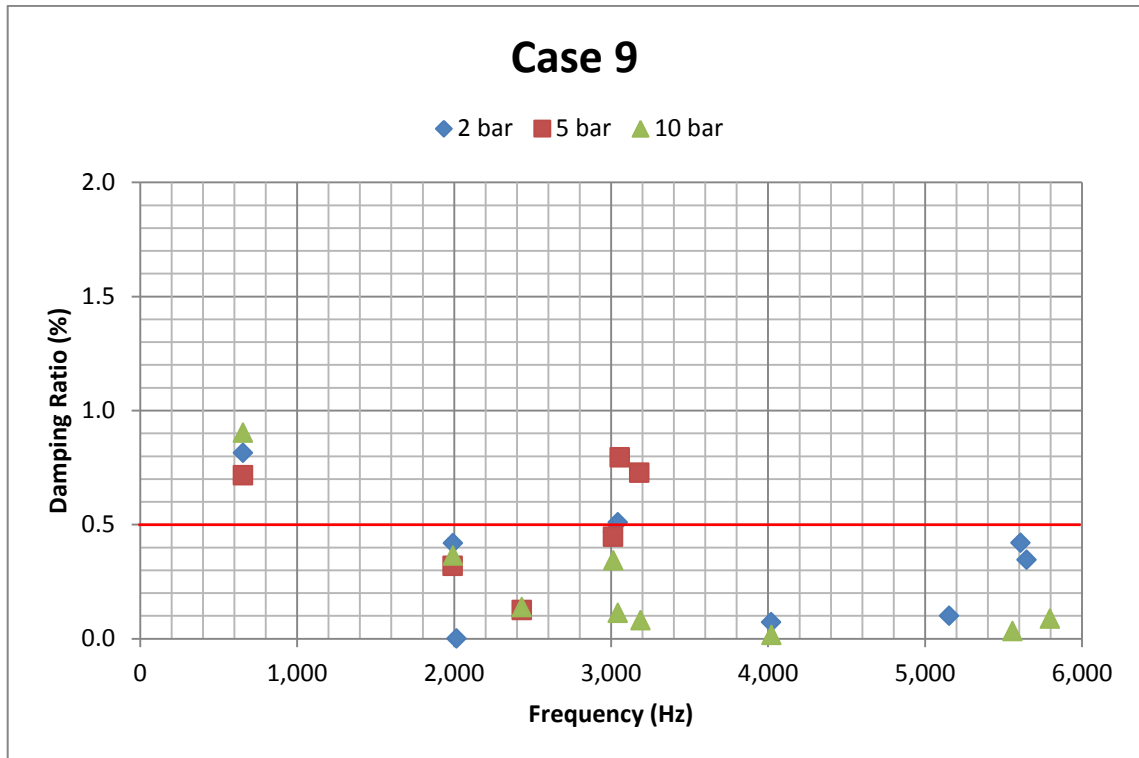
Figure 77, CEA of PBP, Case 9
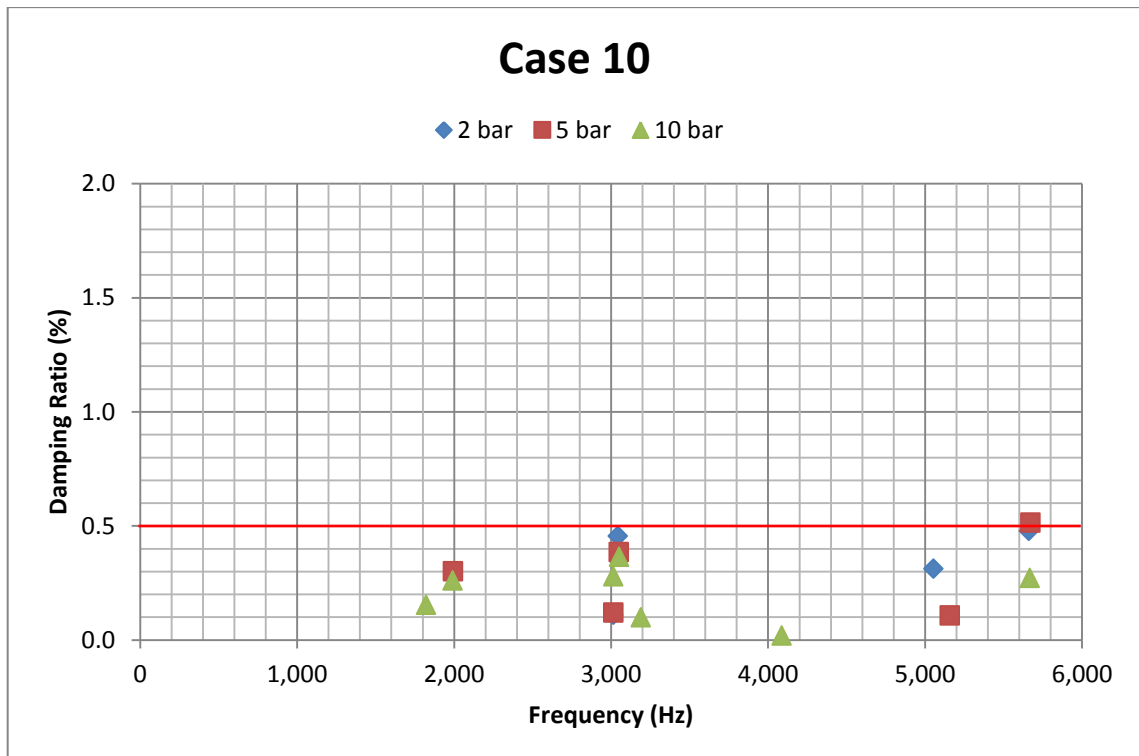


Figure 78, CEA of PBP, Case 10

The last set of circumferentially partitioned pads was where the middle partition was assigned the highest COF; cases 11 and 12. The analysis results for these cases are presented in Figure 79 and Figure 80 respectively. They both exhibit instabilities at 3 kHz frequency while case 11 is also unstable at 650 Hz range, similar to cases 7 and 9.
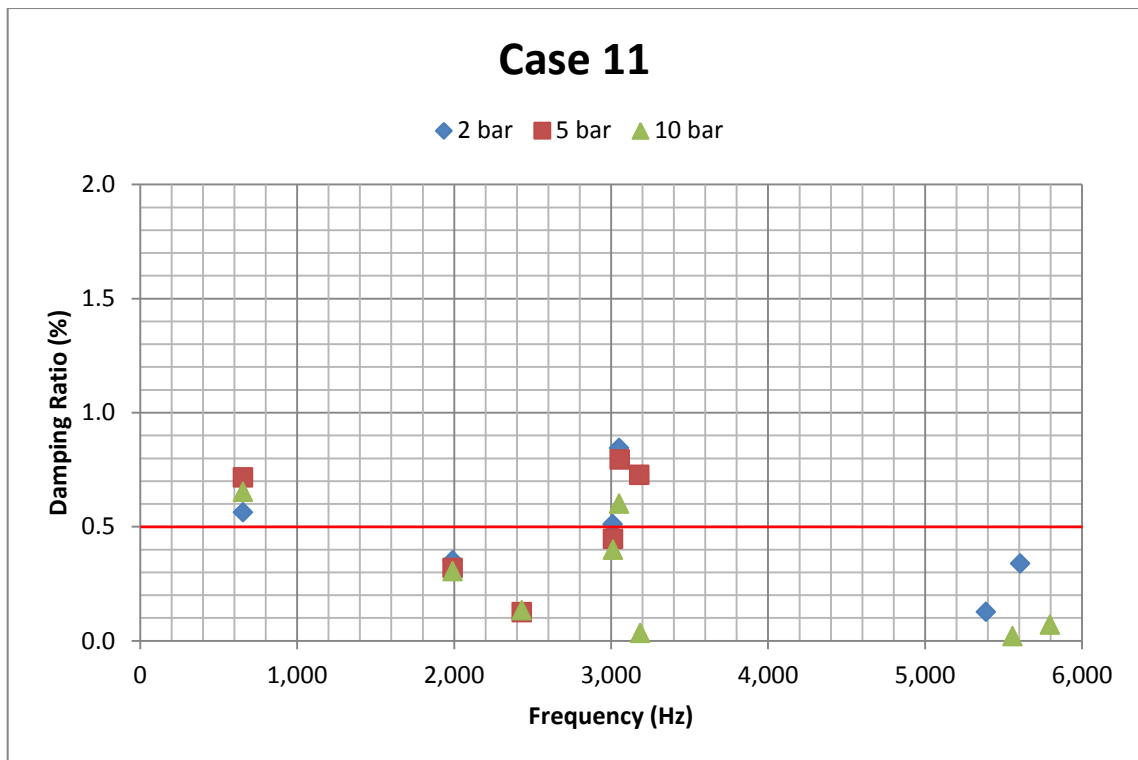


Figure 79, CEA of PBP, Case 11
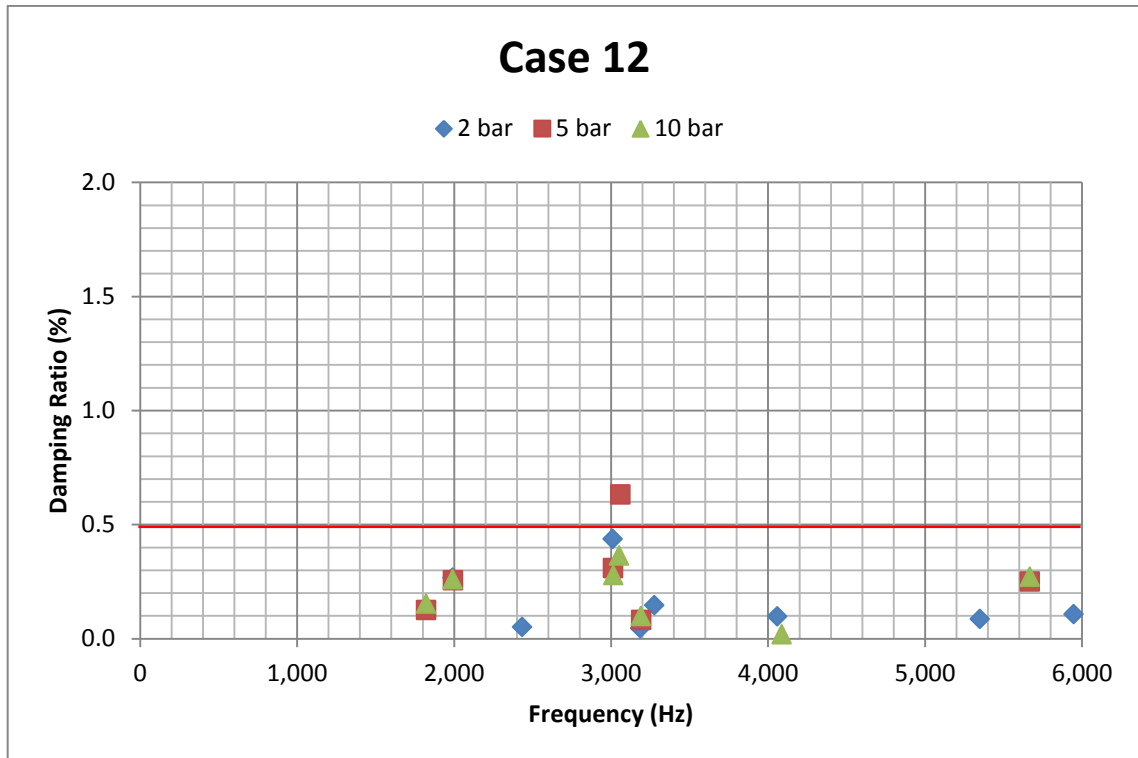
**Figure 80, CEA of PBP, Case 12**

12 cases of different possible scenarios of PBP were simulated and analysed in terms of vibrational instabilities. Interestingly, the analysis results confirmed the hypothesis and highlighted that the case replicating the original concept (case 2) shows minimal instabilities. PBP with radial increase of COF over 5 partitions showed minor instabilities with very low strength. On the contrary, circumferential partitioning did not seem effective in supressing instabilities. Both radial and circumferential patterns confirmed that higher number of partitions results in less number of instabilities with relatively lower strength.

The successful case was selected for the continuation of the study, where PBP refers to this case. The next step was estimation of braking torque and consequently building prototypes and testing the concept in a dynamometer.

## 5.4.     Estimation of Braking Torque

A lower COF is a recommended method of supressing brake noise. Since the concept of PBP was directly targeting the COF to achieve the desired NVH performance, a significant aspect of the concept was ensuring the pad can provide sufficient braking torque. In order to evaluate this, the normal pad with nominal COF of 0.45 was taken as an example, and the PBP was compared with that in terms of braking torque. The braking torque comparison was conducted under uniform piston pressure of 5 bar, and both inboard and outboard pads were taken into consideration. The braking torque ($T$) was obtained by the frictional force ($F$) multiplied by the effective (or average) radius ($R_e$). This is formulated in Equation 12:

$$T = F_{friction} \cdot R_{effective}$$

<div align="right">Equation 12</div>

The total frictional force effective in the defined area was obtained from Abaqus using CFSM output (a surface variable output from the software). Also, the total area in contact was reported using CAREA command. The braking torque was calculated as multiplication of the returned value for CFSM and the effective radius.

For the uniform pad, the effective radius was assumed to be the mid-point in pad's width, and for the partitioned pad the same was done for each partition. Figure 81 shows the method for measuring the effective radius.
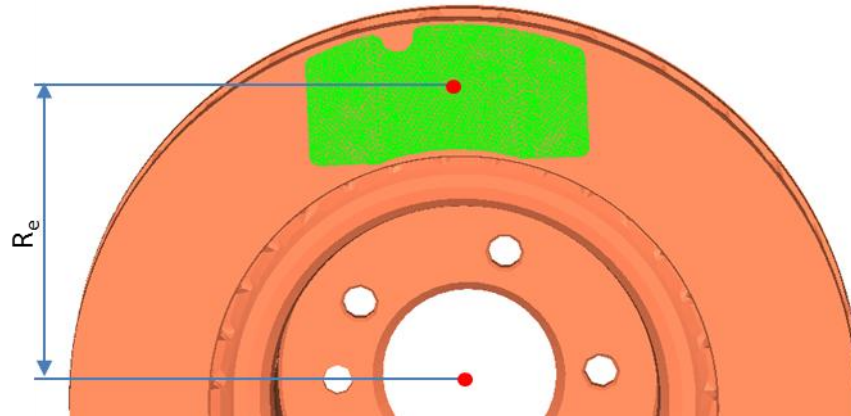
**Figure 81, Measuring the effective radius for calculation of braking torque**

By conducting the analysis and obtaining the required values for each case, the braking torque was calculated for the uniform pad as 166.60 Nm. Table 9 presents the details of this calculation:

**Table 9, Braking torque calculation for the uniform pad**

| Section name | CAREA $(mm^2)$ | CFSM $(N)$ | Effective Radius $(mm)$ | Torque $(Nm)$ |
|---|---|---|---|---|
| Inner Pad | 2184 | 560.7 | 148.6 | 83.34 |
| Outer Pad | 4724 | 560.1 | 148.6 | 83.25 |
| Total | 6908 | 1120.8 | -- | 166.60 |

On the other hand, the PBP was also assessed for the braking torque. Table 10 presents the details for each partition and reports the total braking torque of 221.15 Nm for this pad.

**Table 10, Braking torque calculation for the uniform pad**

| Section name | CAREA $mm^2$ | CFSM $(N)$ | Effective Radius $(mm)$ | Torque $(Nm)$ |
|---|---|---|---|---|
| Inner Pad (0.7) | 1038 | 118.2 | 173.11 | 20.46 |
| Inner Pad (0.6) | 1024 | 213.8 | 160.34 | 34.28 |

| | | | | |
|---|---|---|---|---|
| Inner Pad (0.5) | 863.1 | 169.5 | 148.59 | 25.18 |
| Inner Pad (0.4) | 949.2 | 145.7 | 136.82 | 19.93 |
| Inner Pad (0.3) | 708.1 | 58.66 | 125.12 | 7.34 |
| Outer Pad (0.7) | 1184 | 143.1 | 173.11 | 24.77 |
| Outer Pad (0.6) | 1368 | 233.6 | 160.34 | 37.45 |
| Outer Pad (0.5) | 1352 | 199.6 | 148.59 | 29.65 |
| Outer Pad (0.4) | 1204 | 131.8 | 136.82 | 18.03 |
| Outer Pad (0.3) | 459.2 | 32.2 | 125.12 | 4.02 |
| Total | 10149.6 | 1446.16 | -- | 221.15 |

The calculations mentioned in Table 9 and Table 10 confirm that the braking torque for the PBP was 32% higher than the nominal pad, which predicts a significantly higher braking torque once the pad is prototyped and tested in practice.

## 5.5. Prototyping and Experimental NVH Investigations

Friction material development is already at a reasonably well advanced level [96, 153], from the points of view of both knowledge of the friction material itself and the manufacturing processes, whereby manufacturers can limit the frictional behaviour of the brake pad to a certain value or range, within a reasonable margin of accuracy. Hence, manufacturing a brake pad with a pattern of COF variation was a realistic proposition. In order to investigate the possibility of laying different friction powders in the mould and making the pad, initially a brake pad with two different friction levels was manufactured. This was a brake pad with two radial partitions, with the lower COF of 0.33 and the higher COF of 0.65. Figure 82 shows this simplified version of the PBP.
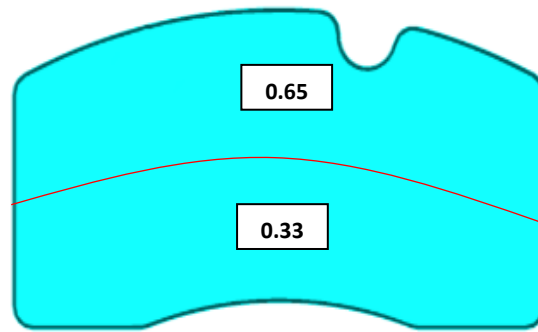
**Figure 82, Schematic of two partitioned pad**

The main aim of the two partitioned pad was to ensure possibility of manufacturing the pad. Also, the temperature distribution and wear pattern were significant concerns to address. Figure 83 shows the brake pad before the dynamometer test.



**Figure 83, First prototype - Partitioned Brake Pad – 2 Partitions**

The pad was tested in a dynamometer in a test procedure replicating a NASCAR race. The reason for that being the source of the friction material assigned to the top partition with the higher COF. Furthermore, this test was not aimed at evaluation of the NVH performance, and was investigating the material integrity of the pad with different levels of COF under severe

braking applications. The pad underwent the extreme braking cases and yet kept its material integrity. The pad after the test can be seen in Figure 84.



Figure 84, Post-test brake pads – 2 partitions

The initial prototypes seemed to wear in a very normal pattern. The disc tested with the set of brake pads also didn't show different radial wear pattern, which can be seen in Figure 85.

**Figure 85, Post-test brake disc**

Following the successful manufacturing and testing of the simplified two-partitioned brake pads, the three-partitioned prototypes were manufactured and tested. This was aimed at replicating Case 1 (shown in Figure 57). The pads are shown as manufactured (pre-test) in Figure 86 and comparison of this with the two partitioned pad (seen in Figure 83) shows that there is no visual distinction between the PBP and a uniform pad.

Figure 86, Partitioned Brake Pad – 3 Partitions

This pad was tested under the SAE J2521 dynamometer test procedure, and the results were compared with the uniform pad. Figure 87 presents the dynamometer test results of the uniform brake pad.
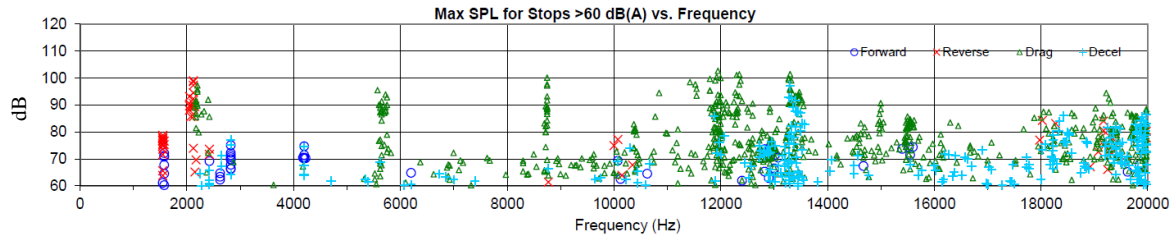
Figure 87, Uniform brake pad - dynamometer test results - SAE J2521 (JLR)

Figure 88 is the test results for the three partitioned brake pad.
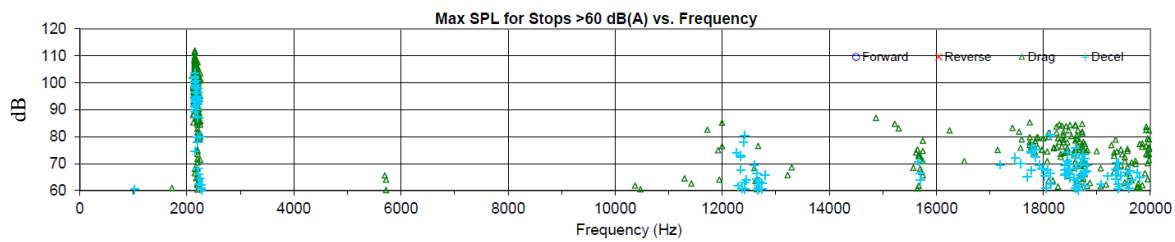


Figure 88, Three partitioned brake pad - dynamometer test results - SAE J2521 (JLR)

The dynamometer tests of the uniform pad and the three-partitioned one indicate significant improvement of the NVH attributes in the PBP. Experiment results satisfied the expectations based on the CAE instability predictions and encouraged the expectation that the five-partitioned pad will be relatively quieter. Although the uniform brake pad is considerably noisy in different frequencies, the partitioned pad with three partitions eliminates a significant part of them.

Considering the significant improvement from the uniform brake pad to the three-partitioned pad, the full scale Partitioned Brake Pad with five partitions is expected to be considerably quieter. However, the five partitioned pad is not tested as the prototyping process was delayed beyond the time-scale of this research.

## 5.6.    Summary and Conclusions

This study is based on the hypothesis that variation of the pattern of distribution of frictional coefficient over the radius of the brake pad is effective in reducing the strength of the brake instability. Results of the investigation suggest that variation of frictional coefficient over the radius of the brake pad is effective in reducing the strength of brake instability. More specifically, increasing the COF radially over the disc radius in the specified steps produces instabilities with an effective damping ratio well within the acceptable range. This low predicted damping ratio is an indication that there is less likelihood that noise will be generated from the brake system, when tested as a prototype.

Various patterns of distribution of COF over the disc pad contact interface were investigated. The successful scenario recommends that increasing the COF radially over the disc radius will lead to instabilities with an effective damping ratio in the acceptable range. The variation in the COF is set to cover the entire range of COF used in different applications of different brake systems, varying from $\mu = 0.3$ to $\mu = 0.7$.

Based on the various simulation cases, as well as the two simplified prototypes, this study suggests that the uniform brake pad friction material is not the best approach from the brake noise point of view. The proposed friction material distribution pattern can contribute to reducing the fugitive nature of the brake noise problem, by reducing the strength of all predicted instabilities to a value much lower than the target value of 0.5%. This suggests that instabilities predicted for the brake system using the proposed pad material design will reduce the propensity for brake noise.

Although the proposed friction material patterns are not easy to manufacture compared to conventional brake pads, there are manufacturing processes which make it possible. However, these are beyond the context of this research.

# Chapter 6: Co-simulation: A Hybrid Analysis Technique for Squeal Analysis

## 6.1.    Introduction

In the simulation and analysis of brake noise, computational time is a significant factor. CEA is the most common analysis method of brake noise mainly because it can provide a quick prediction of the noisy frequency [7]. On the other hand, the Explicit analysis can provide a more comprehensive understanding of the system by taking into account non-linear variables of the system in the time domain. Although both frequency domain and time domain analyses offer significant advantages, they both have their own disadvantages too.

Most non-linear behaviours of the system are simplified in order to achieve a quick result in the frequency domain, and performing an Explicit analysis is expensive in terms of computing time and costs. Co-simulation solves this problem by limiting the nonlinear analysis only to the dynamic parts, and analysing the static parts using the linear frequency domain solver.

The aim of the study was to investigate the suitability of Implicit-Explicit co-simulation for brake NVH evaluations. Co-simulation is a hybrid Implicit/Explicit FEA method which efficiently combines frequency domain and time domain solution schemes. In the application of co-simulation technique to the investigation of brake noise, the time/frequency domain co-simulation analysis simulates the brake unit partly in Implicit and partly in Explicit domain, and combines the results. For this study a different brake set-up was investigated, and the CAE model was correlated with dynamometer test results.

## 6.2.    The Concept of Hybrid Analysis

### 6.2.1. Debate: Implicit vs. Explicit

There has been a long debate in comparing the time domain and the frequency domain analyses, discussing their respective virtues [83]. The outcome of this debate in the literature recommends that probably the most reliable, accurate and comprehensive solution could be performing simulations using two different numerical approaches to identify the squeal mechanism; one being the CEA and the other one being the nonlinear time domain analysis. CEA of the brake system defines its eigenvalues, and relates them to the squeal occurrence. On the other hand, the nonlinear analysis focuses on the contact problem and the friction between deformable bodies, namely disc and friction materials (pads). Finally, the findings of the two approaches are compared, and the onset of squeal is predicted both in the frequency domain by the linear model and in the time domain by the nonlinear one [79].

In the Implicit approach a solution to the set of CEA equations is obtained by iterations for each time increment, until a convergence criterion is obtained. The frequency domain results present the behaviour of the system over the range of frequency, in one step of time ($t = t_i$). The Implicit technique is ideally suited for long duration problems where the response is moderately nonlinear. In the case of analyses involving large element deformation, highly non-linear plasticity or contact between surfaces, the Implicit solver is known to face problems in converging to a correct solution. While each time increment associated with the Implicit solver is relatively large, it is computationally expensive and may pose convergence challenges.

In the Explicit method, the non-linear properties of the system are taken into account at the cost of computing time. The system of equations is reformulated to a dynamic system and is

solved directly to determine the solution at the end of the time increment without iterations, providing a more robust alternative method. The Explicit technique is very robust and ideal for modelling short duration, highly nonlinear events involving rapid changes in contact state and large material deformation.

Implicit or Explicit, each of them has specific advantages and disadvantages. However, there is possibility of combining these two into a hybrid analysis, called co-simulation. Co-simulation is the coupling of different simulation systems where different substructures of a model exchange data during the integration time. The Co-simulation technique allows combining heterogeneous solvers and is less time consuming when different load and model cases require different amounts of time for the solution between two different solvers.

In the case of brake noise analysis, co-simulation capability combines the unique strengths of Abaqus Standard and Abaqus Explicit to more effectively perform complex simulations. Implicit/Explicit co-simulation allows the FEA model to be strategically divided into two parts, one to be solved in the frequency domain and the other in the time domain. The two parts are solved as independent problems and coupled together to ensure continuity of the global solution across the interface boundaries [154-156].

### 6.2.2. Implicit Solution Method

The equation of motion of a vibrating system, as well as the concept and formulation of the complex eigenvalue problem are repeatedly discussed in the published literature [7, 40, 83, 84, 132-138] which was reviewed in the literature review chapter. However, there are specific differences in the CEA when it is paired with the Explicit model for a co-simulation.

In the Implicit method the state of the FEA model is updated from time $t$ to $t + \Delta t$. A fully Implicit procedure means that the state at time $t + \Delta t$ is determined based on the information at time $t + \Delta t$. On the other hand, the Explicit method solves for time $t + \Delta t$ based on information at time $t$ [157]. There are different solution procedures used by Implicit FEA solvers. A form of the Newton–Raphson method [158] is the most common and is employed by Abaqus. In order to solve a quasi-static boundary value problem, a set of non-linear equations is formed as:

$$G(u) = \int_v B^T \sigma(u)dV - \int_S N^T t dS = 0$$

<div align="right">Equation 13</div>

where $G$ is a set of non-linear equations in $u$, the vector of nodal displacements. $B$ is the matrix relating the strain vector to displacement. $\sigma$ is the stress vector, and the product of $B^T$ and $\sigma$, is integrated over a volume, $V$. The matrix of element shape functions is defined as $N$ and is integrated over a surface, $S$.

Equation 13 is solved in increments, where different displacements are applied in various time steps of $\Delta t$ to reach the ultimate time of $t$ and the state of the analysis is updated at each increment. An estimation of the roots of Equation 13 is obtained, such that for the $i^{th}$ iteration:

$$\delta u_{i+1} = u_{i+1}^{t+\Delta t} - u_i^{t+\Delta t} = -\left[\frac{\partial G(u_i^{t+\Delta t})}{\partial u}\right]^{-1} G(u_i^{t+\Delta t})$$

<div align="right">Equation 14</div>

where $u_i^{t+\Delta t}$ is the vector of nodal displacements for the $i^{th}$ iteration at time $t + \Delta t$. The partial derivative on the right-hand side of the equation is the global stiffness matrix $K$. Equation 14 is manipulated and inverted to produce a system of linear equations:

$$K\left(u_i^{t+\Delta t}\right)\delta u_{i+1} = -G\left(u_i^{t+\Delta t}\right)$$

<div align="right"></div>

Equation 15 is solved for each iteration, where the incremental displacements $\delta u_{i+1}$ vary. In order to solve for $\delta u_{i+1}$ the stiffness matrix $K$, is inverted [157]. Following the iteration $i$, $\delta u_{i+1}$ is determined and a better approximation of the solution is made as $u_{i+1}^{t+\Delta t}$ , through Equation 14. This is used as the current approximation to the solution of the subsequent iteration $i$.

The accuracy of the solution is confirmed by the convergence criterion for $G$, which must be less than a predefined tolerance value. Computing time can significantly vary for different complex analyses and it can be difficult to predict.

Abaqus Standard uses a form of the Newton-Raphson iterative solution method to solve the incremental set of equations. Formulating and solving the Jacobian matrix (stiffness matrix $K$) requires the highest computing power and time. The modified Newton-Raphson method is the most commonly used alternative and is suitable for non-linear problems. In this method the Jacobian is only recalculated occasionally since when the Jacobian is unsymmetrical it is not necessary to calculate an exact value for it [157].

### 6.2.3. Explicit Solution Method

The Explicit method is best applicable to solve dynamic problems where deformable bodies are interacting. The Explicit method is ideally suited for analysing high-speed dynamic events where "accelerations and velocities at a particular point in time are assumed to be constant during a time increment and are used to solve for the next point in time" [159, 160]. The Explicit solver in Abaqus uses a forward Euler integration scheme as follows:

$$u^{(i+1)} = u^{(i)} + \Delta t^{(i+1)} \dot{u}^{(i+\frac{1}{2})}$$

$$\dot{u}^{(i+\frac{1}{2})} = \dot{u}^{(i-\frac{1}{2})} + \frac{\Delta t^{(i+1)} + \Delta t^{(i)}}{2} \ddot{u}$$

where $u$ is the displacement and the superscripts refer to the time increment. In the Explicit method it is assumed that values for the velocities $\dot{u}$ and the accelerations $\ddot{u}$ are constant across the half-time intervals, and the state of the analysis is updated at each increment by calculating the acceleration rates using:

$$\ddot{u} = M^{-1} . (F^{(i)} - I^{(i)})$$

where $F$ is the vector of externally applied forces, $I$ is the vector of internal element forces ($Q$ in some notations) and $M$ is the mass matrix [157]. The stability criteria for the Explicit integration operator can be shown using:

$$\Delta t \leq \frac{2}{\omega_{max}}$$

where $\omega_{max}$ is the maximum element eigenvalue. The Explicit procedure is ideally suited for analysing high-speed dynamic events [159].

## 6.2.4. Implicit - Explicit Co-simulation Method

A co-simulation (also referred to as co-execution) is the simultaneous execution of two analyses that are executed in Abaqus CAE in synchronization with one another using the same functionality with two different solvers. In the co-simulation analysis the FEA model is split into two sections, the Implicit section which is solved in the frequency domain and the

Explicit section which is solved in the time domain. The analysis procedure in the Implicit section is very similar to the normal CEA procedure, with the major difference being interactions with the other solver in the predefined time increments.

For a co-simulation analysis comprising of Abaqus Standard and Abaqus Explicit, the interface region and coupling schemes for the co-simulation need to be specified. A common region is defined for both Implicit and Explicit models, referred to as the interface region. Interface region is the section for exchanging data between the two sections of the model and the coupling scheme is the time incrementation process and frequency of data exchange. An interface region can be either node sets or surfaces when coupling Abaqus Standard to Abaqus Explicit. The Implicit region provides the boundary condition and loadings to the Explicit region through these nodes.

In the FEA model, an Implicit-Explicit co-simulation interaction is created to define the co-simulation behaviour. Only one Implicit-Explicit co-simulation interaction can be active in a model. The settings in each co-simulation interaction must be the same in the Abaqus Standard model and the Abaqus Explicit model. The solution stability and accuracy can be improved by ensuring the presence of matching nodes at the interface. A model can have dissimilar meshes in regions shared in the Abaqus Standard and Abaqus Explicit model definitions. However, there are known limitations associated with dissimilar mesh in the co-simulation region. When the Abaqus Standard and Abaqus Explicit co-simulation region meshes differ, the solution accuracy may be affected.

In the co-simulation, the Abaqus Standard can be forced to use the same increment size as Abaqus Explicit, or use different increment sizes in Abaqus Standard from those in Abaqus Explicit. This is called sub-cycling. The chosen time incrementation scheme for coupling

affects the solution computational cost and accuracy but not the solution stability. The sub-cycling scheme is frequently the most cost effective since Abaqus Standard time increments are commonly much longer than Abaqus Explicit time increments.

The Implicit model of the brake included the same components compared to the CEA model and the Explicit model consisted of the brake disc, friction materials and hub. The side surfaces of the friction materials were chosen as the Implicit-Explicit common nodes. The anchor mount was constrained in all degrees of freedom. The brake hub was modelled as a rigid body tied to the disc rotating with it. The disc was constrained to the hub and limited to only rotation about its central axis resembling normal rotation of the brake disc. Rotational velocity was not supplied to the disc in this standard analysis. Figure 89 shows the FEA model of the co-simulation.
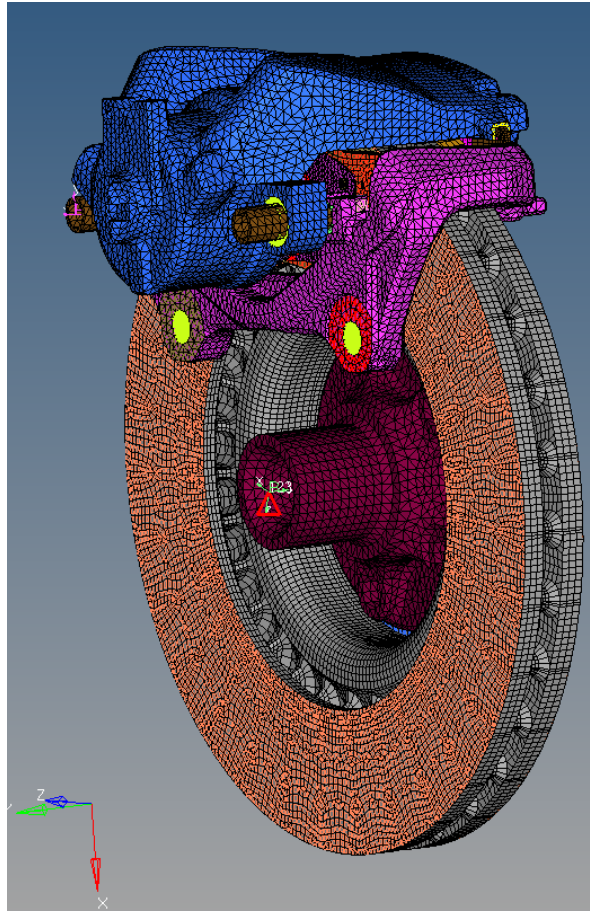
Figure 89, Co-simulation FEA model, inboard view

In this study, the Explicit model consisted of the brake disc, hub and friction materials where the assembly was subject to rotation applied to the disc through the rigid hub. An analytical rigid surface was created and tied to the disc. Angular velocity was applied to the rigid surface reference node, which will drive the disc. Application of angular velocity was simulated in Abaqus Explicit.

## 6.3.    Co-simulation FEA Model

The FEA model of the brake system consisted of all components of the corner unit, excluding the suspension links and connections of the brake unit to the chassis. Figure 90 represents this.
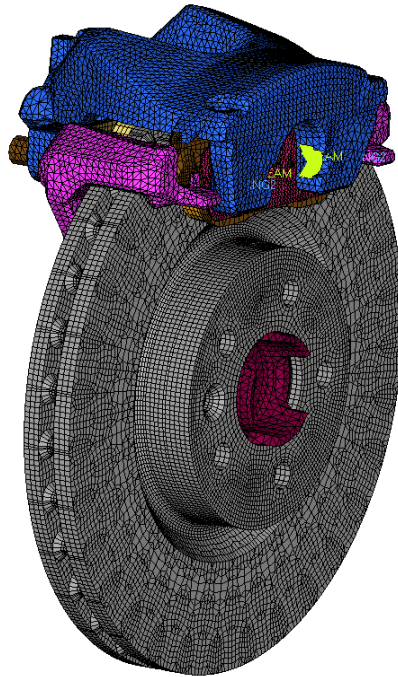
**Figure 90, FEA model of the brake unit, outboard view**

Major components included in the model were disc, hub, caliper (and anchor), pad assembly.

Brake fluid was also simulated to replicate the transfer of pressure which is more realistic than

application of force on the pistons. Each component was assigned its corresponding material

properties. The material properties of the FEA model are provided in Table 11.

Table 11, Material properties assigned to the brake FEA model

| Component | Material | Density (kg/m^3) | Young's Modulus (MPa) | Poisson's Ratio | Section Type | Element Type |
|---|---|---|---|---|---|---|
| Disc | Grey Iron | 7,100 | 107,000 | 0.26 | Solid | C3D8/C3D6 |
| Pads | Friction Material | 2,800 | - | - | Solid | C3D8/C3D6 |
| Anchor Body | SG Iron | 7,100 | 170,000 | 0.275 | Solid | C3D10 |
| Anchor Spring | - | - | - | - | Spring | SPRING2 |
| Caliper | SG Iron | 7,100 | 170,000 | 0.275 | Solid | C3D10 |
| Piston | Steel | 7,900 | 207,000 | 0.3 | Solid | C3D10 |
| Piston Spring | Steel | 7,900 | 207,000 | 0.3 | Solid | C3D10 |
| Hub | - | - | - | - | Rigid | R3D3 |
| Back-plate | Steel | 7,820 | 206,800 | 0.29 | Solid | C3D8/C3D6 |
| Shim | Aluminium | 2,750 | 71,000 | 0.33 | Solid | C3D8/C3D6 |
| Brake Fluid | - | - | - | - | Fluid | F3D3 |

Different iterations of CEA form a set of squeal analysis. Variables differentiating each iteration of the CEA in this study were the level of disc-pad contact interface COF and the brake pressure level. Different levels of COF were simulated and analysed as a safety margin for the analysis, to ensure every possible instability is captured. Although in reality there are slight variations on the level of COF from one stop to the next (due to the surface undergoing different temperatures), this is assumed to be minimal resulting in the overall COF not varying significantly. The piston pressure variations simulate different levels of application of the brake. This level of pressure takes the pressure increase of the booster into account. The

analysis procedure was repeated for different combinations of friction and pressure. The set of results obtained from all different iterations mentioned formed the squeal analysis results.

FEA model of the disc was constructed using first order hexahedral and pentahedral elements. The pad assembly consisted of the friction material (pad), back-plate and the shim. The back-plates and the shims were simulated as Steel and the pads were made of anisotropic friction material. The COF used for the friction material was in the range of [0.35, 0.7]. Different parts of the pad assembly are presented in Figure 91. All parts were modelled using the hexahedral and pentahedral elements; meshed individually and tied together.
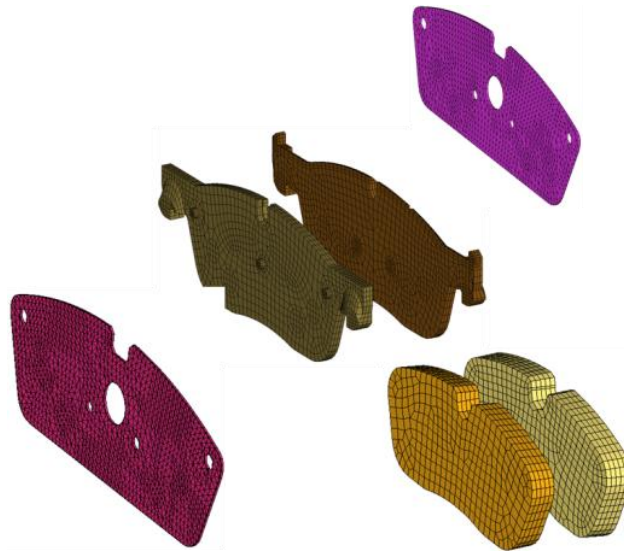


Figure 91, Brake pad assembly

The outer mesh of the piston was in contact with the inner surface of the bore of the caliper and the brake fluid there in between was modelled with fluid elements. Caliper body and anchor were modelled with second order tetrahedral elements. Anchor spring which holds the caliper and anchor together were modelled as 1D elements with a directional stiffness to replicate the spring. The hub was an independent component from the rest of the assembly spinning along with the disc. Consequently it was modelled as a rigid body. Figure 92 shows a cut-away view of the disc brake assembly showing the interaction of all components.
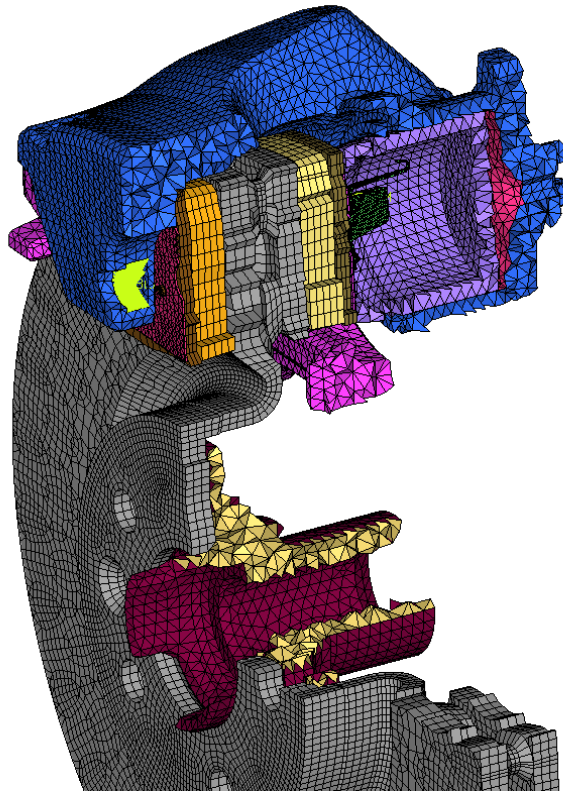
**Figure 92, Brake assembly cross section**

## 6.3.1. Modal Investigation

There are numerous experimental, analytical and numerical methods to investigate the brake noise problem. In order to investigate the capabilities of a specific numerical approach, it is a common practice to correlate the simulation results with the experimental data. Experimental methods are usually very useful for confirming results from other studies, as they demonstrate a complete presentation of the NVH performance of brakes.

The FEA model is required to be a very accurate representation of the individual components of the system. Geometry of the system components and their material properties are expected to significantly contribute to this. In order to validate the FEA model of the brake, individual components were tested using impact hammer test method or shaker test. Figure 93 shows the

points on the surface of the disc, where data was recorded while the disc was excited using a shaker.
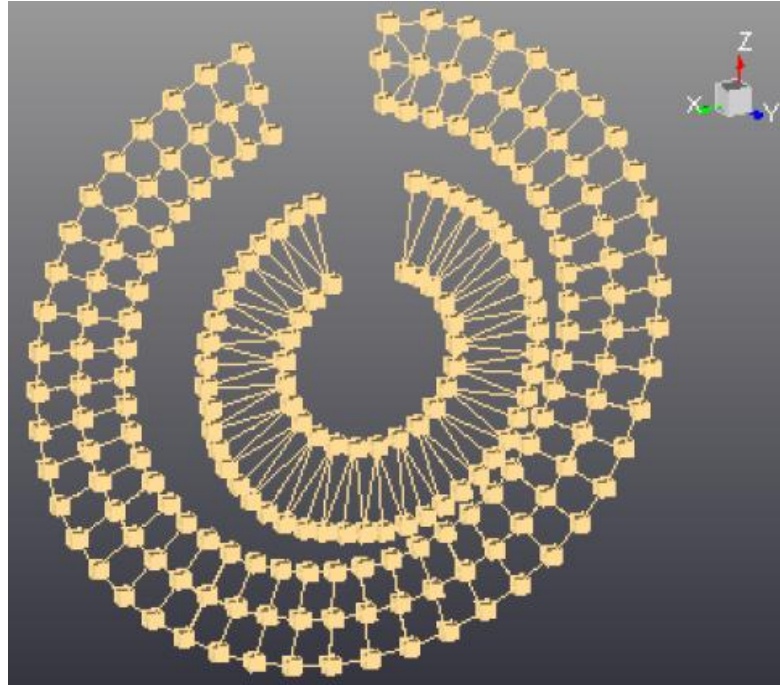


Figure 93, Shaker test response recording points - brake disc

Resonant frequencies of the component were correlated with the FEA model and the Relative Frequency Difference (RFD) [79] was obtained for each mode. An RFD of less than 5% was assumed to be acceptable in this study. Also, the Modal Assurance Criteria (MAC) [161] was evaluated for each mode, to confirm the modal behaviour of the part is matching that of the FEA model. As a representative, Table 12 presents the experimental and FEA frequencies of the disc, as well as the RFD and MAC percentages which show an acceptable correlation.

**Table 12, FEA model validation - disc modal correlation**

| Mode Number | Test Frequency (Hz) | FEA Frequency (Hz) | RFD (%) | MAC (%) |
|---|---|---|---|---|
| 1 | 711 | 737 | 3.6 | 98 |
| 2 | 920 | 944 | 2.7 | 85 |
| 3 | 1244 | 1270 | 2.1 | 73 |
| 4 | 1247 | 1270 | 1.8 | 79 |
| 5 | 1325 | 1365 | 3 | 42 |
| 6 | 1335 | 1367 | 2.4 | 71 |
| 7 | 1971 | 1993 | 1.1 | 84 |
| 8 | 1975 | 1991 | 0.8 | 86 |
| 9 | 2490 | 2508 | 0.7 | 88 |
| 10 | 2907 | 2933 | 0.9 | 91 |
| 11 | 2915 | 2933 | 0.6 | 88 |
| 12 | 3443 | 3513 | 2 | 72 |
| 13 | 4043 | 4071 | 0.7 | 65 |
| 14 | 4056 | 4071 | 0.4 | 51 |
| 15 | 4301 | 4355 | 1.3 | 31 |
| 16 | 4620 | 4740 | 2.6 | 82 |
| 17 | 4684 | 4655 | -0.6 | 88 |
| 18 | 5346 | 5383 | 0.7 | 86 |
| 19 | 5362 | 5383 | 0.4 | 63 |
| 20 | 5497 | 5505 | 0.2 | 80 |
| 21 | 6032 | 6083 | 0.8 | 97 |
| 22 | 6655 | 6825 | 2.5 | 66 |
| 23 | 6813 | 6851 | 0.6 | 71 |

Table 12 shows that RFD percentage for all modes of the disc are under the target of 5%. Also the MAC percentage confirmed that the right modes are excited in both simulation and experiment and the modal behaviour is correlating in both cases.

The FEA model of the brake corner unit was correlated using the mentioned method repeated for other components. Once the FEA model was validated in terms of being an acceptable representation of the actual parts, the NVH performance of the assembled unit was also subject to test. The brake unit was assembled to a vehicle and tested on the road. The results were correlated with the response from the assembled FEA model undergoing CEA.

### 6.3.2. Experimental NVH Investigation: Vehicle Test

The vehicle test is the most accurate representation of the NVH performance of the brake in real life since some brake noise initiation mechanisms only exist on the car and are dependent on the actual manoeuvre performed.

To validate the FEA simulation using co-simulation technique, initially a full vehicle test was conducted. This was aimed at replicating the SAE J2521 dynamometer noise search procedure. The vehicle test is performed by installing various sensors at different parts of the vehicle, to record the required data. In order to record the brake noise, microphones were installed inside the car, approximately near the driver or passenger's ear. To obtain a robust and reliable result from the vehicle noise search tests, the SAE J2521 test procedure manoeuvres were repeated to identify the recurrent noises. These manoeuvres are described in Table 1 (Chapter 3). Figure 4 previews the vehicle test results, based on the most frequent noise occurrences obtained from a set of tests.
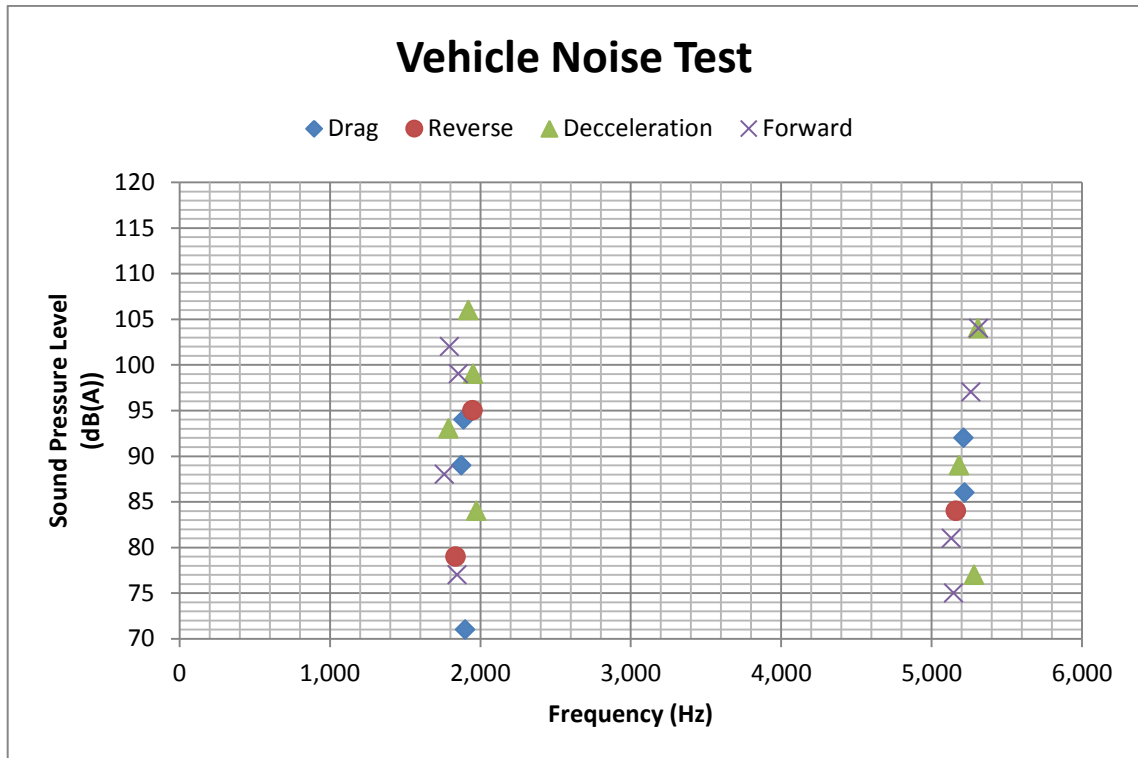
**Figure 94, Vehicle brake noise test result (JLR)**

As seen in Figure 4, there were occurrences of brake noise in the frequency ranges of 1.9 kHz and 5.2 kHz, which were repeated in different manoeuvres. Therefore, the numerical analysis of the same brake unit was expected to represent instabilities in these frequencies as an indication of likelihood of noise occurrence.

### 6.3.3. FEA Model Correlation: Implicit (CEA) Analysis

In order to validate the FEA model of the brake unit, and before performing the co-simulation analysis, the performance of the FEA model from instability viewpoint was assessed. The CEA was performed following the method described in Chapter 3.

Figure 27 illustrates squeal analysis results for pressure variations of 2, 5, 10 and 25 bars and COF of 0.35, 0.45, 0.55, 0.65 and 0.7. It is repeatedly mentioned in the literature that not all instabilities predicted by CEA may occur in reality as the CEA always overestimates the instabilities [162]. Analysing different COF levels helps repetition of instabilities to occur

from different combinations of friction, pressure and operating direction. This can highlight the actual unstable frequency compared to the other over-predicted instabilities by CEA.
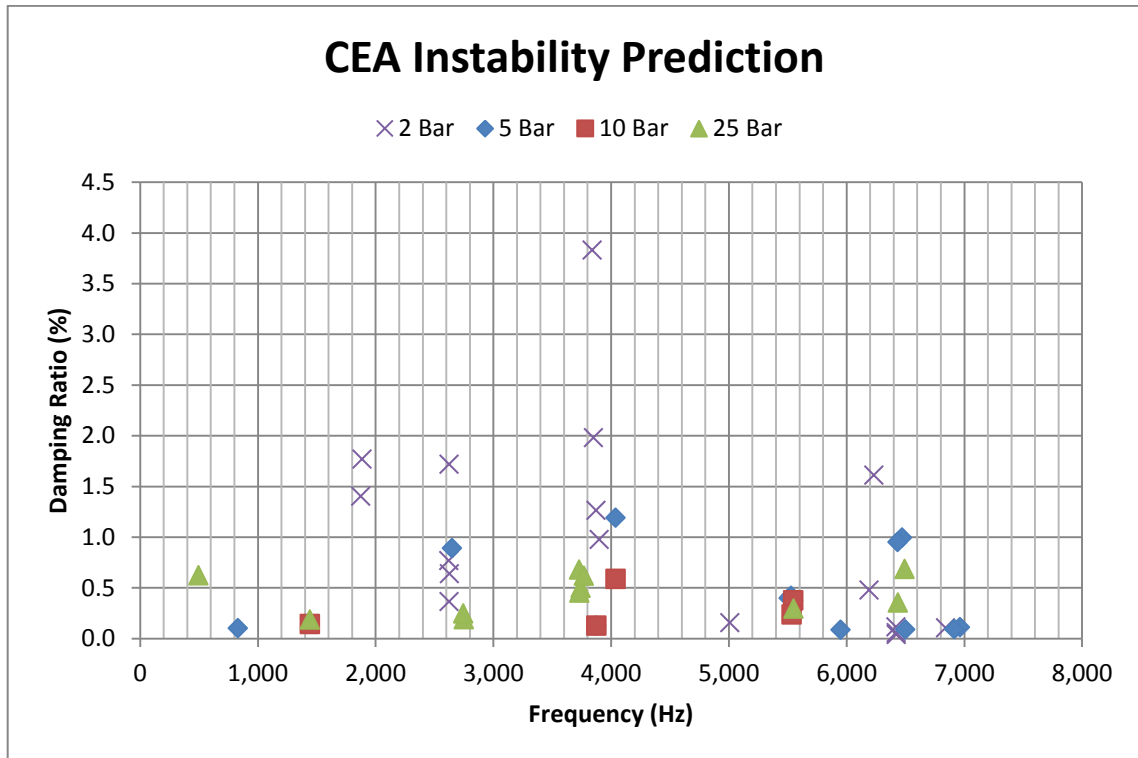


**Figure 95, CEA squeal analysis results - baseline model - Friction levels of 0.35, 0.45, 0.55, 0.65 and 0.7 and pressures of 2, 5, 10 and 25 bars**

The squeal analysis results show that instabilities occur potentially in the frequency ranges of 1.9, 2.6, 3.8 and 6.2 kHz. Comparison of the CEA results with the vehicle test results also reveal that among two noisy frequencies only 1.9 kHz is reported, although the number of instability occurrences (only two) is not significant. These frequencies are identified on the graph.

## 6.4. Co-simulation Squeal Analysis Model Set-up

In the co-simulation analysis, the Implicit section of the model performs similar to the CEA. The Implicit and Explicit sides of the model transfer data on predefined increments. The Implicit and Explicit sections of the model are not completely independent. The analysis

results in the Implicit section are transferred to the Explicit section. This happens in time increments and either sections of the model can transfer data in predefined time increments. Abaqus uses a timing logic of the data transfer called subcycle. Figure 96 shows the common nodes on the friction material, which are utilised to transfer the data on predefined increments (subcycles).
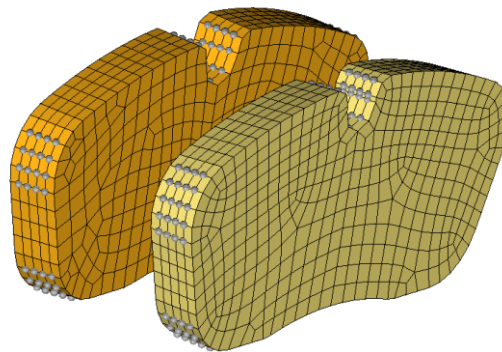


**Figure 96, Co-simulation common region on the friction materials**

The disc was rotated with the initial velocity of 2 km/h and by deceleration it reached a full stop. This replicates the brake system during drag and stopping in forward or reverse direction, based on the direction of the velocity. Simulation of deceleration is achieved by gradual increase in the level of applied pressure. Figure 97 presents this gradual application of pressure, reaching 10 bar in 0.1 sec and maintaining that level of pressure for another 0.1 sec.
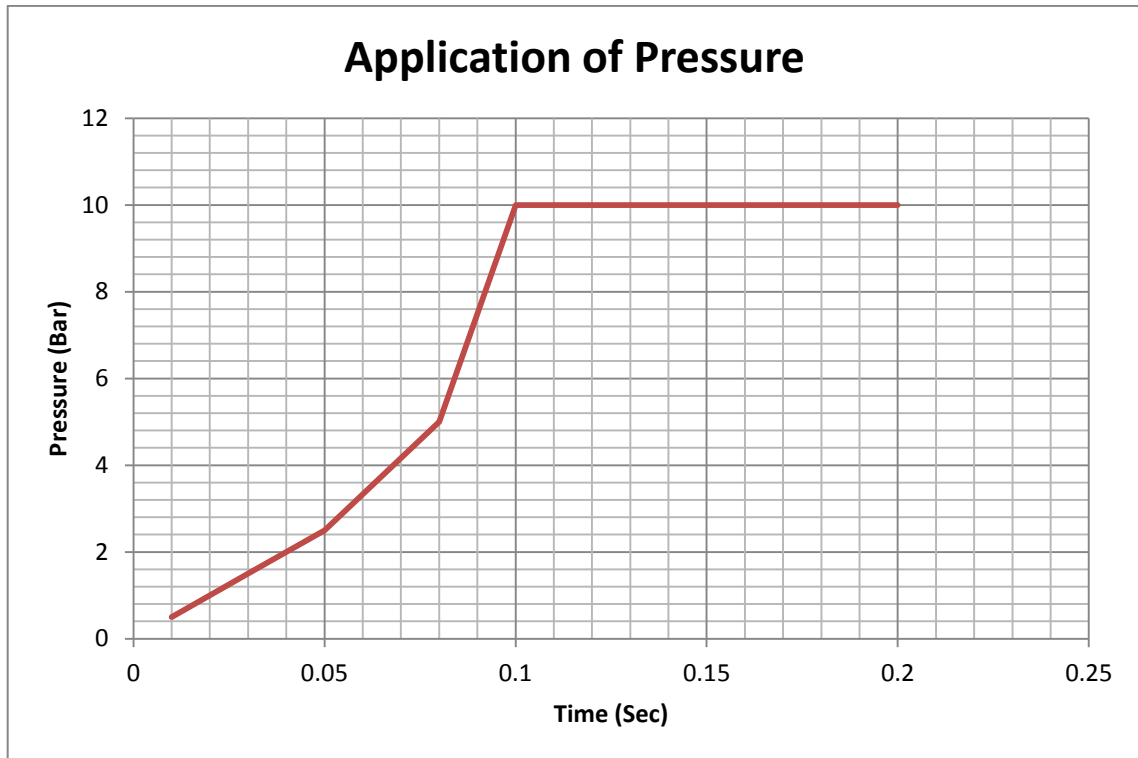
Figure 97, Application of pressure

In the co-simulation analysis, the analytical surface on the disc is assumed as the major output point. This is based on the hypothesis that for all major noise initiation mechanisms in the brake system, the brake disc acts as the amplifier to the noise and it is considered as the radiator of the noise. Therefore, the co-simulation analysis is based on the hypothesis that acceleration at the disc surface, where the maximum displacement takes place, is an indication of noise-related instabilities. This is commonly on the outer layer of the disc where the structural support from the hub connections and the swan neck of the disc are minimal. Figure 98 shows the Explicit model of the co-simulation analysis.
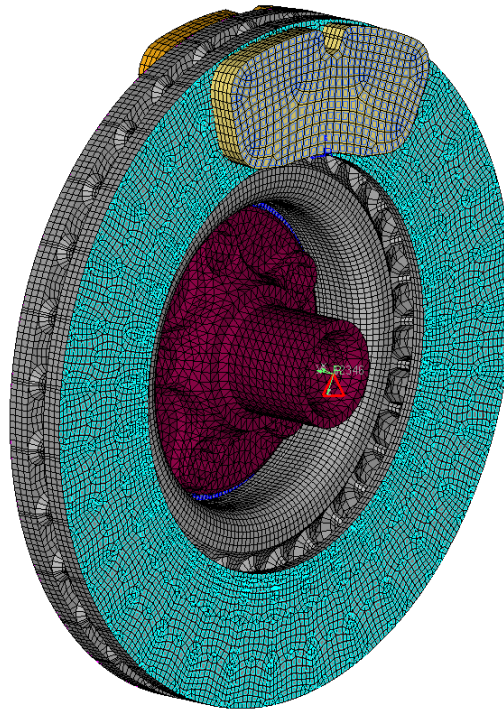
Figure 98, Co-simulation model - Explicit

## 6.5.    Co-simulations Analysis Results and Discussion

By performing the co-simulation analysis, the Explicit section of the model provides time domain results. The node with the maximum displacement is identified on the disc outer layer, and acceleration is obtained as the output. Once the acceleration versus time data is obtained in Abaqus Explicit, it is transformed into acceleration versus frequency. Peaks in the acceleration-frequency graph are assumed as an indication of squeal frequency.

Figure 99 and Figure 100 present two of the co-simulation analyses results. Figure 99 corresponds to the co-simulation analysis with COF of 0.55, and Figure 100 represents result of the co-simulation with COF of 0.70. In Figure 99, unstable frequencies are predicted at 1.9 kHz and 5.1 kHz which are in good correlation with the noisy frequencies of the vehicle test presented in Figure 94.
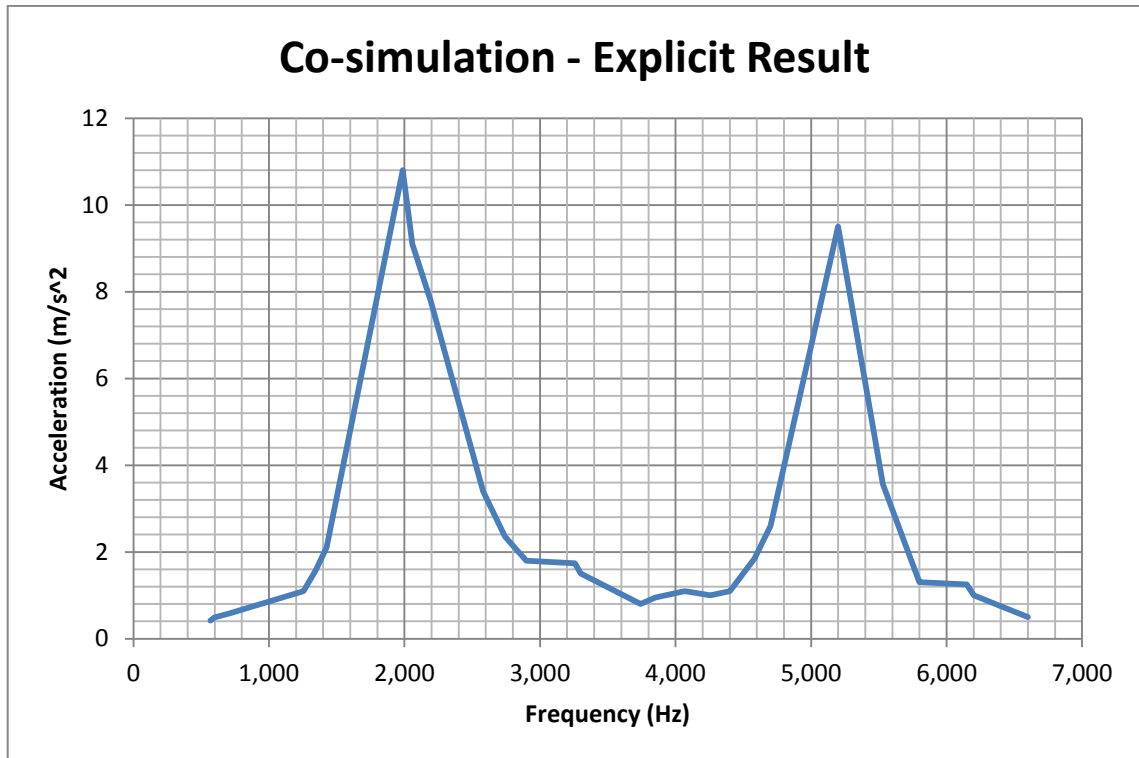
**Figure 99, Acceleration vs. frequency - co-simulation - COF: 0.55**

The Figure 100 indicates no modal coupling happening in this simulation as the acceleration response does not indicate any resonant frequency. Fluctuations refer to the normal vibrations of the system components.

**Figure 100, Acceleration vs. frequency - co-simulation - COF: 0.70**

The computing time for the co-simulation analysis is approximately 12 hours, which is 6 hours less than each CEA analysis, presented in Figure 95. Figure 101 is another example of the co-simulation where brake noise is not observed.
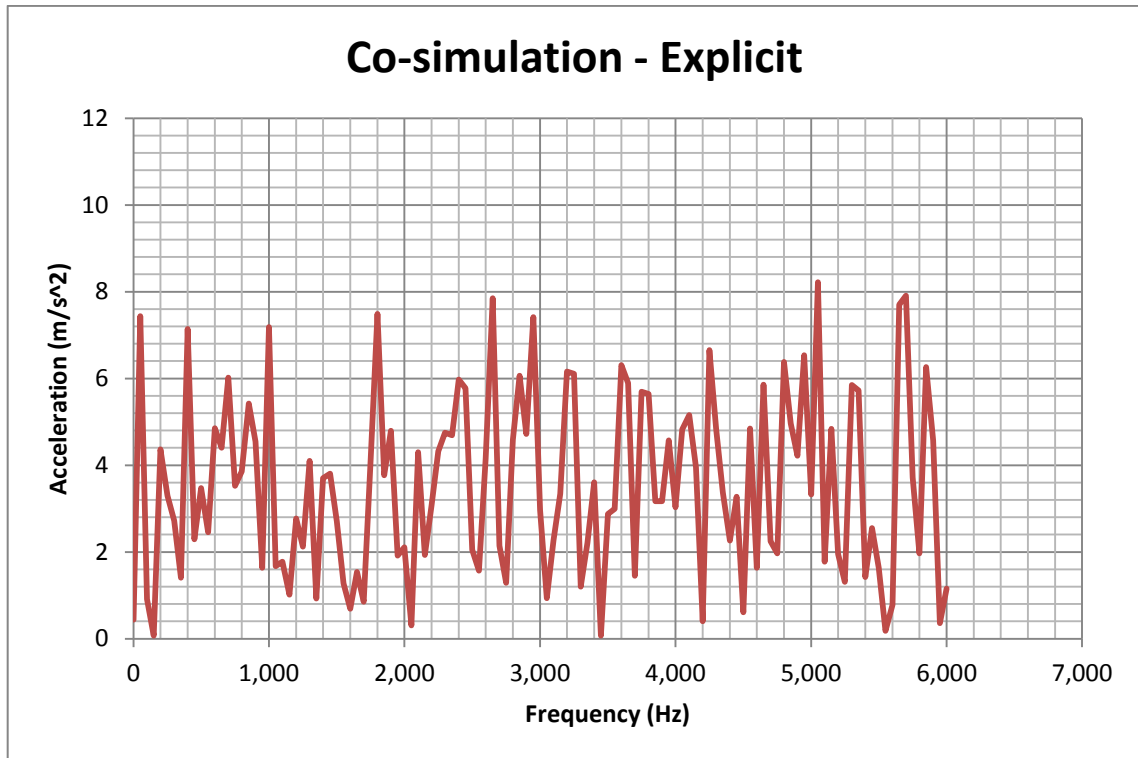
**Figure 101, Acceleration vs. frequency - co-simulation - COF: 0.35**

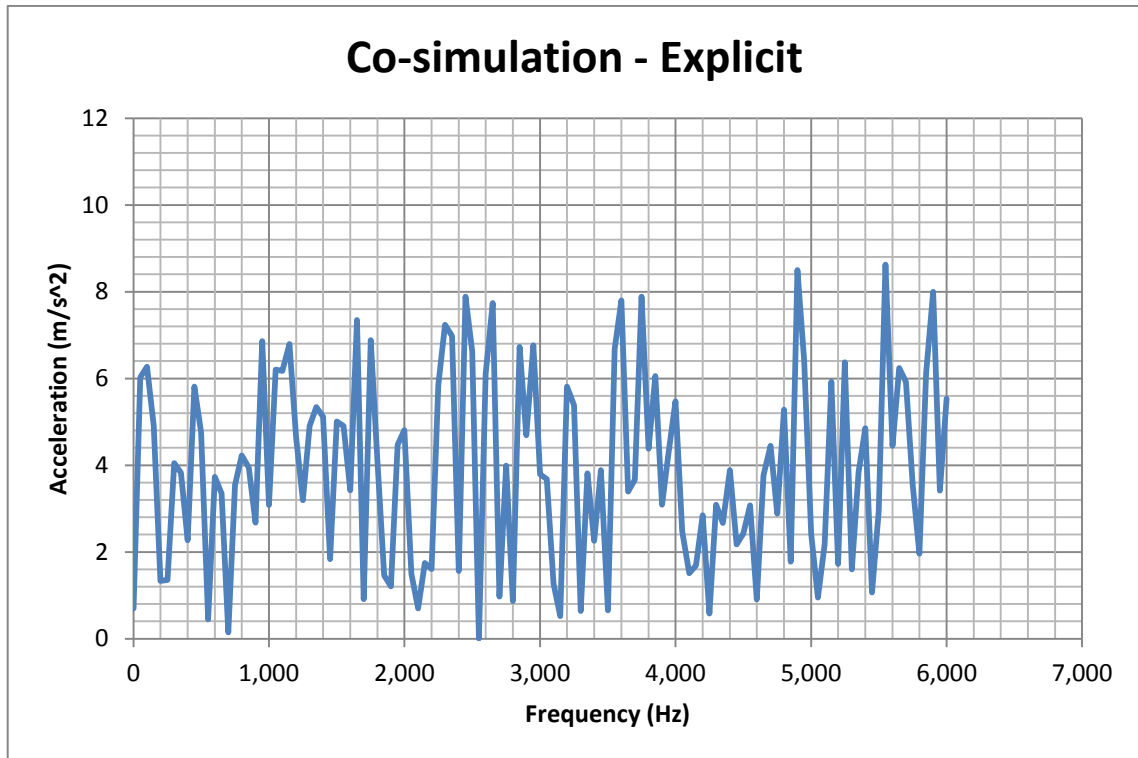## 6.6.     Summary and Conclusions

Addressing the debate on the efficiency and effectiveness of the time domain and the frequency domain analyses, a hybrid analysis method was introduced. The co-simulation analysis divides the model into two Implicit and Explicit sections and simulates each section using the allocated solver.

A co-simulation analysis for brake noise investigation was developed using Abaqus FEA software. The brake FEA co-simulation model comprised of the disc and pads. In Abaqus Standard to Abaqus Explicit co-simulation technique the two solvers are simultaneously running on the corresponding sections of the model. The co-simulation model is capable of accurately predicting the unstable frequency by providing time-domain results in a lower computing time.

The rotation of the disc was simulated in Explicit domain while the rest of the loadings were based in the frequency domain. The simulation results were correlated with the vehicle test results. The performance of the co-simulation solution scheme was evaluated and compared to the Implicit CEA analysis.

Co-simulation is a powerful tool to efficiently analyse the response of a full brake model. Co-simulation technique is capable of performing squeal analysis by simulating the rotation of the disc and the disc-pad contact interface in Abaqus Explicit and the rest of the loadings in Implicit domain using Abaqus Standard, saving on the computing time and cost.

# Chapter 7: Conclusions and Recommendations for Further Work

## 7.1. Conclusions

This thesis was aimed at obtaining a fundamental understanding of the attributes of the brake system's functionality and developing modelling and analysis methodologies to more accurately simulate the brake system. Significance of different aspects of the system damping were investigated and CAE damping tuning techniques were developed to tune the material damping of the system components of the FEA model using the Rayleigh damping method. Also, significance of the contact damping (as in the bolted joints) as well as the damping in the bushes were investigated. Contact damping was found to be less significant relative to the material damping, and application of the damping in the bushes were only visibly different in the lower frequencies below 1 kHz. A simplified model for the brake shim was developed. The three-layer model included two sections of rubber, on either side of a steel middle section, simulated using hyper-elastic rubber material properties. The rubber sections were tuned with the material damping using Rayleigh damping tuning method. Performing the squeal analysis using the CEA method on the model with the damping tunings showed a significantly higher level of correlation with the experimental brake noise tests in terms of the unstable frequency and the likelihood of brake noise occurrence.

A new time-frequency domain simulation technique for investigation of brake noise was developed. By developing the co-simulation model the nonlinear analysis was limited to the dynamic parts (brake disc and the friction materials), and the static parts were analysed using the CEA in the frequency domain. The hybrid frequency-time domain solution scheme

delivered time domain analysis results using less computing time and power associated with the frequency domain analysis (CEA). The analysis results were in agreement with the experimental brake noise test results.

A novel design for a brake pad was proposed based on the hypothesis that radially increasing level of COF in the brake pad can provide a more stable contact interface by limiting the stick-slip phenomenon. The concept was tested using FEA simulation and the analyses results suggested the new brake pad can potentially reduce brake noise. Different sets of prototypes were built and tested to investigate the brake noise as well as wear patterns and possible material integrity problems. The concept proved to pass all the expected performance criteria. Also the theoretical braking torque resulting from the new design were investigated using FEA models which indicated more than 30% higher braking torque compared to the original brake pad design.

## 7.2.     Suggestions for Future Work: Improvements of CAE Modelling & Analysis

This section provides a set of recommendations for the potential continuation of the studies conducted in this research.

- A better simulation technique for modelling the frictional interface, taking into account the material clusters formed in the manufacturing process, resulting in different local COF would enhance the simulation accuracy. This also results in more accurately simulating the burnishing effects on the disc. Also, an understanding of general variations of the COF relative to the local tangential velocity can be a major step forward in simulation of brake pads.

- Damping characteristics of the brake shim vary due to the functional temperature and this is an existing data available from the suppliers of the parts. Application of that data into the model can provide a better representation of the functionality of the damping characteristic of the brake shims.

- Simulation of the effect of deceleration in the CEA can provide a more realistic representation of the NVH attributes of the brake system.

- Simulation of the vehicle tyre in the CEA model can improve the accuracy of the analysis results due to the significant source of damping indirectly interacting with the brake contact interface.

## 7.3.    Summary of Contributions of This Thesis

Patents:

- Brake pad and Method of Forming Such

    o   UK Patent Publication: GB2506950

    o   International Patent Publication: WO2014/060430A1

Journal Publications:

- "CAE Prediction of Brake Noise: Modelling of Brake Shims" - Journal of Vibration of Control – Published Paper.

- "Implicit - Explicit Co-simulation of Brake Noise" – Journal of Finite Elements in Analysis and Design – Manuscript in Peer Review.

Conference Publications:

- "Frictional Coefficient Distribution Pattern on Brake Disk-Pad Contact Interface to Reduce Susceptibility of Brake Noise Instabilities Causing Brake Squeal" – Conference Paper – EuroBrake 2013
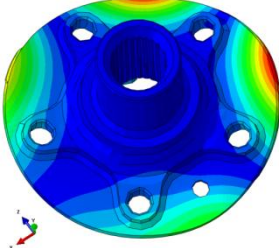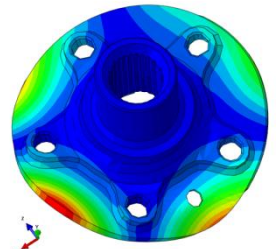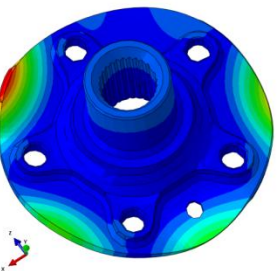
- "Effect of Damping in Complex Eigenvalue Analysis of Brake Noise to Control Over-Prediction of Instabilities: An Experimental Study" – SAE Brake Colloquium and Exhibition (31st annual) 2013
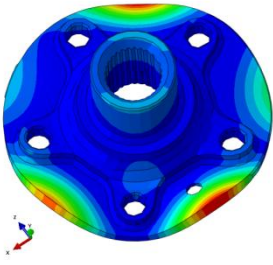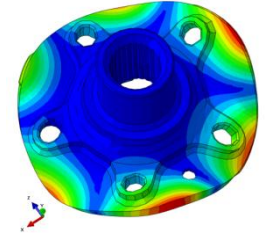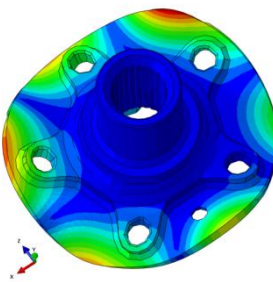
# Appendices

## A. Component Modal Correlation and Damping Estimation

### Hub

Table 13, Hub CAE and Hammer test modes correlation
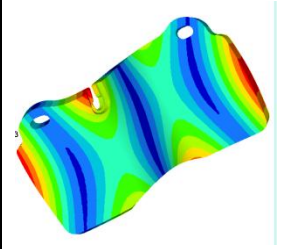
| CAE Frequency (Hz) | CAE Mode Shape | Hammer Test Frequency (Hz) | $F$ (%) |
|---|---|---|---|
| 3706.4 |  | 3698 | 0.23 |
| 3986.2 |  | | |
| 4763.6 | | 4776 | 0.26 |
| 5361.1 |  | | |

| | | | |
|---|---|---|---|
| 5438.8 |  | | |
| 5562.3 |  | | |
| 6542.6 |  | | |

## Pad Assembly
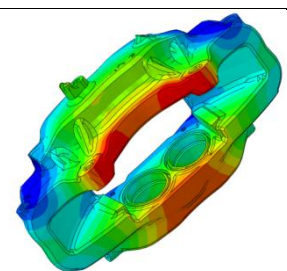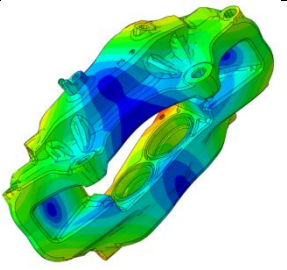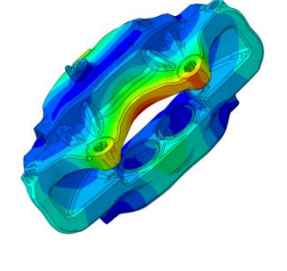
**Table 14, Back-plate CAE and Hammer test modes correlation**
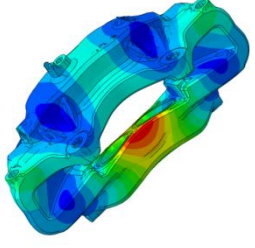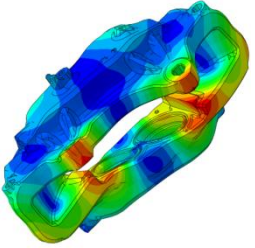
| CAE Frequency (Hz) | CAE Mode Shape | Hammer Test Frequency (Hz) | $F\,(\%)$ |
|---|---|---|---|
| 1,626.7 |  | 1,589 | 2.3 |

| 4445,6 |  | 4,736 | 6.5 |
|---|---|---|---|

## Caliper
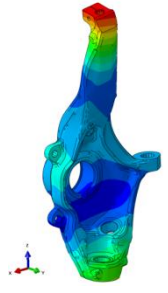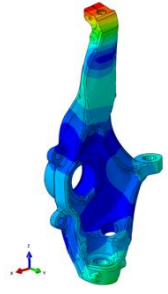
Table 15, Caliper CAE and hammer test mode shapes correlation

| CAE Frequency (Hz) | CAE Mode Shape | Hammer Test Frequency (Hz) | F (%) |
|---|---|---|---|
| 1,830.4 |  | 1,754 | 4.1 |
| 2800 |  | 2,748 | 1.8 |
| 3,948.1 |  | 3,924 | 0.6 |

| | | | |
|---|---|---|---|
| 4,863.3 |  | 4,834 | 0.6 |
| 6,080.3 |  | 5,683 | 6.5 |
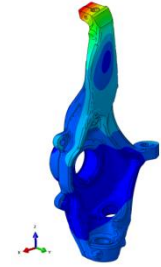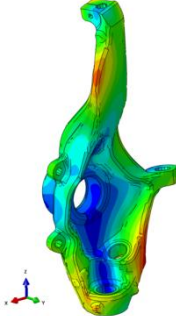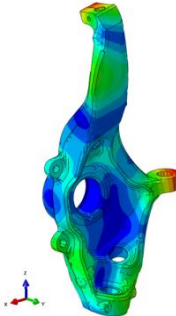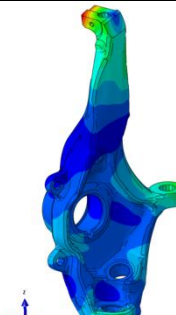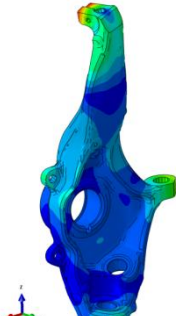
## Knuckle
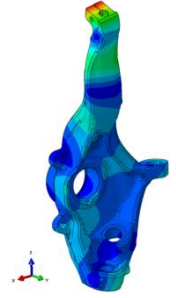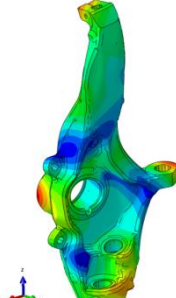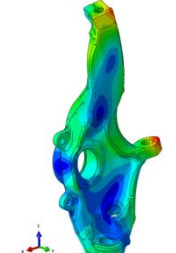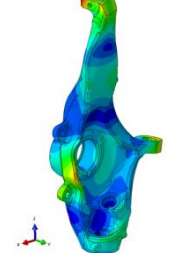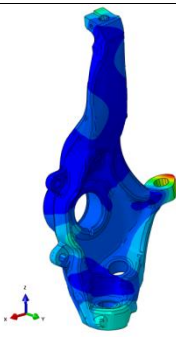
**Table 16, Knuckle CAE hammer test, and shaker test modes correlation**

| CAE Frequency (Hz) | CAE Mode Shape | Hammer Test Frequency (Hz) | $F(\%)$ | Shaker Test Frequency (Hz) | $F(\%)$ |
|---|---|---|---|---|---|
| 487,34 |  | 488.2 | 0.2 | 485 | 0.5 |
| 856,19 |  | 843.3 | 1.5 | 830 | 3 |

| | | | | | |
|---|---|---|---|---|---|
| 1053,2 |  | - | - | 1,015 | 3.6 |
| 1493 |  | 1,527 | 2.3 | 1,555 | 4.1 |
| 1849,7 |  | 1,770 | 4.3 | 1,770 | 4.3 |
| 2155 |  | - | - | 2,075 | 3.7 |
| 2655,2 |  | - | - | 2,510 | 5.4 |

| | | | | | |
|---|---|---|---|---|---|
| 3023,9 |  | 2,979 | 1.5 | 2,965 | 1.9 |
| 3255,9 |  | - | - | 3,220 | 1.1 |
| 3337,4 |  | - | - | - | - |
| 3531,6 |  | - | - | - | - |
| 4020 |  | 4,086 | 1.6 | 4,085 | 1.6 |

# List of References

1. Clark, C.S., *The Lanchester legacy: a trilogy of Lanchester Works*. 1995: Coventry University.
2. Harper, G.A., *Brakes and friction materials: the history and development of the technologies*. 1998: Mechanical Engineering Publications.
3. Newcomb, T.P., R. T. Spurr, *A technical history of the motor car*. 1989: A. Hilger.
4. Kinkaid, N., O. O'Reilly, and P. Papadopoulos, *Automotive disc brake squeal.* Journal of Sound and Vibration, 2003. **267**(1): p. 105-166.
5. Lamarque, P. and C. Williams, *Brake squeak: the experiences of manufacturers andoperators and some preliminary experiments*, 1938, The Institution of Automobile Engineers.
6. Mills, H.R., *Brake squeak*, 1939, The Institution of Automobile Engineers.
7. Ouyang, H., N. Wayne, Y. Yongbin, C. Frank, *Numerical analysis of automotive disc brake squeal: a review.* Int. J. Vehicle Noise and Vibration, 2005. **1**(3/4): p. 207-231.
8. Ouyang, H., Q. Cao, J. E. Mottershead, T. Treyde. *Vibration and squeal of a disc brake: modelling and experimental results*. in *The Institution of Mechanical Engineers, Part D: Journal of Automobile Engineering*. 2003.
9. Coudeyrasa, N., J. J. Sinoua, S. Nacivet, *A New Treatment for Predicting the Self-Excited Vibrations of Nonlinear Systems with Frictional Interfaces: The Constrained Harmonic Balance Method, with Application to Disc Brake Squeal.* Journal of Sound and Vibration, 2008. **319**(3-5): p. 1175-1199.
10. Rhee, S.K., P. H. S. Tsang, Y. S. Wang, *Friction-induced noise and vibration of disc brakes.* Wear, 1989. **133**(1): p. 39-45.
11. Kinkaid, N., O. M. O'Reilly, P. Papadopoulos, *Automotive disc brake squeal.* Journal of Sound and Vibration, 2003. **267**(1): p. 105-166.
12. Papinniemi, A., J. Lai, J. Zhao, L. Loader, *Brake squeal: a literature review.* Applied acoustics, 2002. **63**(4): p. 391-400.
13. Oden, J.T., J. A. C. Martins, *Models and computational methods for dynamic friction phenomena.* Computer Methods in Applied Mechanics and Engineering, 1985. **52**(1–3): p. 527-634.
14. Crolla, D.A., A. M. Lang. *Brake noise and vibration-the state of the art*. 1991. Elsevier Science Ltd.
15. Ibrahim, R.A., *Friction-Induced Vibration, Chatter, Squeal, and Chaos - Part II: Dynamics and Modeling.* American Society of Mechanical Engineers, Applied Mechanics Reviews, 1994. **47**(7): p. 227-254.
16. Ibrahim, R.A., *Friction-Induced Vibration, Chatter, Squeal and Chaos - Part I: Mechanics of Contact and Friction.* American Society of Mechanical Engineers, Applied Mechanics Reviews, 1994. **47**(7): p. 17.
17. Sinclair, D., *Frictional vibrations, v. 22, June 1955, p. 207–213.* Journal of applied mechanics, 1955: p. 207-214.
18. Shin, K., *Analysis of Disc Brake Noise Using a Two-Degree-of-Freedom Model.* Journal of Sound and Vibration, 2002. **254**(5): p. 837-848.
19. Hochlenert, D., P. Hagedorn, *Control of disc brake squeal − modelling and experiments.* Structural Control and Health Monitoring, 2006. **13**(1): p. 260-276.
20. Vonwagner, U., D. Hochlenert, P. and Hagedorn, *Minimal models for disk brake squeal.* Journal of Sound and Vibration, 2007. **302**(3): p. 527-539.
21. Ibrahim, R.A., *Friction-Induced Vibration, Chatter, Squeal, and Chaos---Part II: Dynamics and Modeling.* Applied Mechanics Reviews, 1994. **47**(7): p. 227-253.

22. Mottershead, J.E., H. Ouyang, M. P. Cartmell, M. I. Friswell, *Parametric resonances in an annular disc, with a rotating system of distributed mass and elasticity; and the effects of friction and damping* Royal Society Publishing, 1997. **453**(1956): p. 1-19.
23. Millner, N., *An analysis of disc brake squeal*. 1978: Society of Automotive Engineers.
24. Felske, A., G. Hoppe, H. Matth, *Oscillations in Squealing Disc Brakes - Analysis of Vibration Modes by Holographic Interferometry.* Society of Automotive Engineers, 1978.
25. Fosberry, R.A.C., Z. Holubecki, *An investigation of the cause and nature of brake squeal*. 1955: Motor Industry Research Association.
26. Fosberry, R.A.C., Z. Holubecki, *Disc brake squeal: its mechanism and suppression*. 1961: Motor Industry Research Association.
27. Behrendt, J., C. Weiss, N. P. Hoffmann, *A numerical study on stick–slip motion of a brake pad in steady sliding.* Journal of Sound and Vibration, 2011. **330**(4): p. 636-651.
28. Jearsiripongkul, T., *A Simplified Model of The Floating Caliper Disk Brake With Respect o High Frequency Noise.* ThammasatI nt. J. Sc. Tech, 2006. **11**(2): p. 61-68.
29. Spurr, R.T., *A theory of brake squeal.* Institution of Mechanical Engineers Automotive Division, 1961/62(Proc No. 1): p. 30-40.
30. Abubakar, A., *Ph.D Thesis: Modelling and Simulation of Disc Brake Contact Analysis and Squeal*, in *Department of Mechanical Engineering, Faculty of Engineering*2005, Liverpool, United Kingdom: University of Liverpool, Liverpool, United Kingdom.
31. Earles, S.W.E., G. B. Soar, *Squeal Noise in Disc Brakes, Symp. on Vibration and Noise in Motor Vehicles.* Institution of Mechanical Engineers, 1971.
32. Sinou, J., F. Thouverez, L. Jezequel, *Analysis of friction and instability by the centre manifold theory for a non-linear sprag-slip model.* Journal of Sound and Vibration, 2003. **265**(3): p. 527-559.
33. Fieldhouse, J.D., N. Ashraf, C. Talbot, *The Measurement and Analysis of the Disc/Pad Interface Dynamic Centre of Pressure and Its Influence on Brake Noise.* Society of Automotive Engineers International Journal of Passenger Cars - Mech. Syst., 2008. **1**(1): p. 736-745.
34. Fieldhouse, J.D., D. Bryant, C. J. Talbot, *The Influence of Pad Abutment on Brake Noise Generation*, 2011, SAE International.
35. Jarvis, R.P., B. Mills, *Vibrations induced by dry friction.* Proceedings of Institution of Mechanical Engineers, Conference 178 (32), 1963/1964: p. 847-866.
36. North, M.R., *A mechanism of disc brake squeal.* 14th FISITA Congress, 1972.
37. North, M.R., *Disc brake squeal in: Braking of Road Vehicles.* Automobile Division of the Institution of Mechanical Engineers, 1976.
38. Millner, N., *An analysis of disc brake squeal.* SAE Paper, 1978. **780332**.
39. D'Souza, A.F., A. H. Dweib, *Self-excited vibrations induced by dry friction, part 2: Stability and limit-cycle analysis.* Journal of Sound and Vibration, 1990. **137**(2): p. 177-190.
40. Kung, S.W., K. B. Dunlap,R. S. Ballinger, *Complex eigenvalue analysis for reducing low frequency brake squeal.* Society of Automotive Engineers, 2000. **109**(6): p. 559-565.
41. Flint, J., *Lining-Deformation-Induced Modal Coupling as Squeal Generator in a Distributed Parameter Disc Brake Model.* Journal of Sound and Vibration, 2002. **254**(1): p. 1-21.
42. Giannini, O., A. Sestieri, *Predictive model of squeal noise occurring on a laboratory brake.* Journal of Sound and Vibration, 2006. **296**(3): p. 583-601.
43. Giannini, O., A. Akay, F. Massi, *Experimental analysis of brake squeal noise on a laboratory brake setup.* Journal of Sound and Vibration, 2006. **292**(1-2): p. 1-20.
44. Khan, M., K. Johnson, T. Lichtensteiger, C. Lockrem, *Evaluation and Countermeasure Development of Brake Noise on a Motorcycle Platform.* 2010.
45. Park, J.S., J. C. Lee, S. Cho, K. Yoon, *Reduction of Brake Squeal Analyzed in Terms of Coupling Between In-Plane and Out-of-Plane Modes.* SAE Int. J. Passeng. Cars - Mech. Syst., 2012. **5**(4): p. 1230-1243.

46. Lamarque, P.V., C. G. Williams, *Brake squeak: the experiences of manufacturers and operators and some preliminary experiments.* Institution of Automobile Engineers, 1938.

47. Tarter, J.H., *Disc brake squeal*, 1983.

48. Ichiba, Y., Y. Nagasawa, *Experimental study on brake squeal.* SAE paper, 1993. **930802**.

49. James, S., *An experimental study of disc brake squeal*, 2003, University of Liverpool.

50. Kumamoto, F., O. Doi, *A Study on Relationship between Pad Restraint Condition and Brake Squeal Generation.* 2004.

51. Nishiwaki, M., H. Harada, H. Okamura, T. Ikeuchi, *Study on disc brake squeal.* SAE, 1989.

52. Fieldhouse, J.D., T. P. Newcomb. *An investigation into disc brake noise using holographic interferometry*. in *3rd International Conference on Vehicle Dynamics and Powertrain Engineering*. 1991. Strasbourg, France: (Unpublished).

53. Fieldhouse, J.D., T. P. Newcomb, *Double pulsed holography used to investigate noisy brakes.* Optics and Lasers in Engineering, 1996. **25**(6): p. 455-494.

54. Steel, W.P., J. D. Fieldhouse, C. J. Talbot, A. Crampton. *In-plane vibration investigations of a noise brake*. in *IMechE International Conference- Braking 2004*. 2004. Professional Engineering Publishing Ltd.

55. Matsuzaki, M., T. Izumihara, *Brake noise caused by longitudinal vibration of the disc rotor*, 1993, Society of Automotive Engineers, 400 Commonwealth Dr, Warrendale, PA, 15096, USA.

56. McDaniel, J.G., X. Li, J. Moore, S. Chen, *Analysis of Instabilities and Power Flow in Brake Systems with Coupled Rotor Modes.* 2001.

57. Vadari, V., *An Experimental Investigation of Disk Brake Creep-Groan in Vehicles and Brake Dynamometer Correlation.* 1999.

58. Nishiwaki, M., K. Sorimachi, R. Misumi, *An Experimental Set Up Development for Brake Squeal Basic Research*, 2013, SAE International.

59. Nishiwaki, M., *Generalized theory of brake noise.* Institution of Mechanical Engineers Journal of Automobile Engineering, 1993. **207**.

60. Ouyang, H., J. E. Mottershead, M. P. Cartmell, D. J. Brookfield, *Friction-induced vibration of an elastic slider on a vibrating disc.* International journal of mechanical sciences, 1999. **41**(3): p. 325-336.

61. Ouyang, H., J. E. Mottershead, D. J. Brookfield, S. James, M. P. Cartmell, *A methodology for the determination of dynamic instabilities in a car disc brake.* International Journal of Vehicle Design, 2000. **23**(3): p. 241-262.

62. Chowdhary H. V., A.K.B., C.M. Krousgrill. *An analytical approach to model disc brake system for squeal prediction*. in *DETC '01 ASME 2001 Design Engineering Technical Conference and Computers and Information in Engineering Conference*. 2001. Pittsburgh, PA: American Society of Mechanical Engineers.

63. Hoffmann, N., M. Fischer, R. Allgaier, L. Gaul, *A minimal model for studying properties of the mode-coupling type instability in friction induced oscillations.* Mechanics Research Communications, 2002. **29**(4): p. 197-205.

64. Yang, M.M., A. H. Afaneh, *A study of disc brake high frequency squeals and disc in-plane/out-of-plane modes.* 2003.

65. Brooks, P.C., D.A. Crolla, A.M. Lang, D.R. Schafer. *Eigenvalue sensitivity analysis applied to disc brake squeal*. in *PROCEEDINGS OF THE INSTITUTION OF MECHANICAL ENGINEERS. BRAKING OF ROAD VEHICLES. INTERNATIONAL CONFERENCE HELD 23-24 MARCH 1993 AT BIRDCAGE WALK, LONDON (PAPER NUMBER C444/004/93)*. 1993.

66. Hany, S., *Effect of contact stiffness on the establishment of self-excited vibrations.* Wear, 1991. **141**(2): p. 227-234.

67. Nossier, T.A., M. Said, N. S. El Nahas, G. Abu El Fetouh, *Significance of squeal in disc brake design.* International Journal of Vehicle Design, 1998. **19**(1): p. 124–133.

68. Watany, M., S. Abouel-Seoud, A. Saad, I. Abdel-Gawad, *Brake squeal generation.* SAE transactions, 1999. **108**(6): p. 2730-2739.

69. El-Butch, A.M., *Modeling and analysis of geometrically induced vibration in disc brakes considering contact parameters.* 1999.

70. Ahmed, I., *Analysis of Ventilated Disc Brake Squeal Using a 10 DOF Model*, 2012, SAE International.

71. Hu, Y., S. Mahajan, K. Zhang, *Brake Squeal DOE Using Nonlinear Transient Analysis*, 1999, SAE International.

72. Cao Q., M.F., H. Ouyang, J. E. Mottershead, S. James, *Car Disc Brake Squeal - Theoretical and Experimental Study.* Trans Tech Publications, Switzerland, 2003. **440-441**: p. 269-276.

73. Yang, S., R. F. Gibson, *Brake vibration and noise: reviews, comments, and proposals.* International Journal of Materials and Product Technology, 1997(12): p. 496–513.

74. Nagy, L.I., J. Cheng, Y. Hu, *A New Method Development to Predict Brake Squeal Occurrence*, 1994, SAE International.

75. Chargin, M.L., L. W. Dunne, D. N. Herting, *Nonlinear dynamics of brake squeal.* Finite Elements in Analysis and Design, 1997. **28**(1): p. 69-82.

76. Hu, Y., L. I. Nagy, *Brake squeal analysis using nonlinear transient finite element method.* Society of Automotive Engineers, 1997.

77. Hamzeh, O.N., W. W. Tworzydlo, H. J. Chang, S. T. Fryska, *Analysis of friction-induced instabilities in a simplified aircraft brake.* SAE transactions, 2000. **108**(6; PART 2): p. 3404-3418.

78. Auweraer, H.D., *Experimental and Numerical Modelling of Friction-Induced Noise in Disc Brakes.* 2002.

79. Massi, F., L. Baillet, O. Giannini, A. Sestieri, *Brake squeal: Linear and nonlinear numerical approaches.* Mechanical Systems and Signal Processing, 2007. **21**(6): p. 2374-2393.

80. Liles, G.D., *Analysis of disc brake squeal using finite element methods.* Society of Automotive Engineers, 1989. **891150**: p. 1138-1146.

81. Ghesquiere, H., L. Castel, *High frequency vibrational coupling between an automobile brake-disc and pads.* Proceedings of I. Mech. E, 1991.

82. Spelsberg-Korspeter, G., P. Hagedorn, *Complex Eigenvalue Analysis and Brake Squeal: Traps, Shortcomings and their Removal.* SAE Int. J. Passeng. Cars - Mech. Syst., 2012. **5**(4): p. 1211-1216.

83. Ouyang, H., A. AbuBakar, *Complex eigenvalue analysis and dynamic transient analysis in predicting disc brake squeal.* International Journal of Vehicle Noise and Vibration, 2006. **2**(2): p. 143-155.

84. Nouby, M., K. Srinivasan, *Parametric Studies of Disk Brake Squeal Using Finite Element Approach.* Jurnal Mekanikal, 2009. **29**: p. 52-66.

85. Wallner, D., S. Bernsteiner, W. Hirschberg, A. Rabofsky, *Numerical and Experimental Parameter Studies on Brake Squeal.* SAE Technical Paper, 2010.

86. Dom, S., M. Riefe, T. S. Shi, ed. *Brake squeal noise testing and analysis correlation*. 2003-01-1616 ed. SAE Brake Colloquium & Exhibition. 2003, SAE International.

87. Goto, Y., T. Amago, K. Chiku, T. Matshushima, Y. Ishihara, *Experimental identification method for interface contact stiffness of FE model for brake squeal.* Proceedings of Braking 2004 on Vehicle Braking and Chassis Control, 2004: p. 143-155.

88. Nack, W.V., *Brake squeal analysis by finite elements.* International Journal of Vehicle Design, 2000. **23**(3): p. 263-275.

89. Kung, S.W., G. Stelzer, V. Belsky, A. Bajer. *2003-01-3343 Brake Squeal Analysis Incorporating Contact Conditions and Other Nonlinear Effects*. in *SAE CONFERENCE PROCEEDINGS*. 2003. SAE; 1999.

90. Bajer, A., V. Belsky, L. J. Zeng, *Combining a Nonlinear Static Analysis and Complex Eigenvalue Extraction in Brake Squeal Simulation*, 2003, SAE International.

91. Yuan, Y. *A study of the effects of negative friction-speed slope on brake squeal*. in *ASME Design Engineering Technical Conferences*. 1995.

92. Blaschke, P., M. Tan, *On the analysis of brake squeal propensity using finite element method.* 2000.

93. Chung, C.-H.J., M. Donley, *Mode coupling phenomenon of brake squeal dynamics*, 2003, SAE Technical Paper.

94. Guan, D., J. Huang, *The method of feed-in energy on disc brake squeal.* Journal of Sound and Vibration, 2003. **261**(2): p. 297-307.

95. Sinou, J., F. Thouverez, L. Jezequel, *Application of a nonlinear modal instability approach to brake systems.* Journal of vibration and acoustics, 2004. **126**(1): p. 101-107.

96. Hornig, S.A., U. Von Wagner, *Improvement of Brake Squeal Simulation Reliability by Measurement and Identification of Friction Material Properties*, 2012, SAE International.

97. Cao Q., M.F., H. Ouyang, J. E. Mottershead, S. James, *Linear eigenvalue analysis of the disc-brake squeal problem.* International Journal for Numerical Methods in Engineering, 2004. **61**(9): p. 1546-1563.

98. Giannini, O., F. Massi. *An experimental study on the brake squeal noise*. in *International Conference on Noise and Vibration Engineering*. 2004. Leuven, Belgium: ISMA.

99. Berger, E.J., *Friction modeling for dynamic system simulation.* Applied Mechanics Reviews, 2002. **55**(6): p. 535-577.

100. Gao, J., W. D. Luedtke, D. Gourdon, M. Ruths, J. N. Israelachvili, U. Landman, *Frictional forces and Amontons' law: from the molecular to the macroscopic scale.* The Journal of Physical Chemistry B, 2004. **108**(11): p. 3410-3425.

101. Dweib, A.H., A. F. D'souza, *Self-excited vibrations induced by dry friction, Part 1: Experimental study.* Journal of Sound and Vibration, 1990. **137**(2): p. 163-175.

102. Tworzydlo, W.W., E. B. Becker, J. T. Oden, *Numerical modeling of friction-induced vibrations and dynamic instabilities.* Applied Mechanics Reviews, 1994. **47**: p. 255.

103. Tworzydlo, W.W., O. N. Hamzeh, W. Zaton, T. J. Judek, *Friction-induced oscillations of a pin-on-disk slider: analytical and experimental studies.* Wear, 1999. **236**(1): p. 9-23.

104. Ibrahim, R.A., S. Madhavan, S. L. Qiao, W. K. Chang, *Experimental investigation of friction-induced noise in disc brake systems.* International Journal of Vehicle Design, 2000. **23**(3): p. 218-240.

105. Jacobson, S., M. Eriksson. *Friction behaviour and squeal generation of disc brakes at low speeds*. in *The Institution of Mechanical Engineers, Part D: Journal of Automobile Engineering*. 2001.

106. Kim, S.W., S. J. Lee,B. K. Park, S. K. Rhee, *A Comprehensive Study of Humidity Effects on Friction, Pad Wear, Disc Wear, DTV, Brake Noise and Physical Properties of Pads*, 2011, SAE International.

107. Hohmann, C.H., K. Schiffner, J. Brecht, *Pad wear simulation model.* SAE transactions, 1999. **108**(6): p. 3389-3397.

108. Bajer, A., V. Belsky, S. Kung, *The influence of friction-induced damping and nonlinear effects on brake squeal analysis.* SAE paper, 2004: p. 01-2794.

109. Kim, N.H., D. Won, D. Burris, B. Holtkamp, G. R. Gessel, P. Swanson, W. G. Sawyer, *Finite element analysis and experiments of metal/metal wear in oscillatory contacts.* Wear, 2005. **258**(11): p. 1787-1793.

110. Yuhas, D.E., C. L. Vorres, J. Remiasz, T. Klosowiak, J. A. Lloyd, *Ultrasonic Methods for Characterizing the Non-Linear Elastic Properties of Friction Materials*, in *EuroBrake 2013*2013, FISITA: Germany.

111. Chen, F., *On automotive disc brake squeal-Part IV: Reduction and prevention.* 2003.

112. Ishihara, N., M. Nishiwaki, H. Shimizu, *Experimental analysis of low-frequency brake squeal noise.* JSAE Review, 1996. **17**(4): p. 440-440.

113. Dunlap, K.B., M. A. Riehle, R. E. Longhouse, *An investigative overview of automotive disc brake noise.* SAE transactions, 1999. **108**(6; PART 1): p. 515-522.

114. Nakajima, T., Y. Okada, *Study on reduction method of brake squeal*, 1997, SAE Technical Paper.

115. Dessouki, O., G. Drake, B. Lowe, W. K. Chang, *Disc brake squeal: diagnosis and prevention*, 2003, SAE Technical Paper.

116. Kido, I., T. Kurahachi, M. Asai, *A study on low-frequency brake squeal noise*, 1996, SAE Technical Paper.

117. Baba, H., T. Wada, T. Takagi, *Study on reduction of brake squeal caused by in-plane vibration on rotor*, 2001, SAE Technical Paper.

118. Bergman, F., M. Eriksson, S. Jacobson, *Influence of disc topography on generation of brake squeal.* Wear, 1999. **225-229, Part 1**(0): p. 621-628.

119. Liu, W., J. Pfeifer, *Reducing high frequency disc brake squeal by pad shape optimization*, 2000, SAE Technical Paper.

120. Hoffman, C.T., *Damper design and development for use on disc brake shoe and lining assemblies*, in *Society of Automotive Engineers*1988.

121. Lewis, T.M., P. Shah, *Analysis and Control of Brake Noise.* Society of Automotive Engineers, 1987.

122. Flint, J., *Instabilities in brake systems.* Society of Automotive Engineers, 1992.

123. Matsuzaki, M. and T. Izumihara, *Brake noise caused by the longitudinal vibration of the disc rotor.* SAE, 1993.

124. Dihua, G. and J. Dongying, *A Study on Disc Brake Squeal Using Finite Element Methods.* SAE, 1998.

125. Baba, H., M. Okade, and T. Takeuchi, *Study on Reducing Low Frequency Brake Squeal - From Modal Analysis of Mounting Bracket.* SAE, 1995: p. 307.

126. Matsui, H., H. Murakami, H. Nakanishi, Y. Tsunda, *Analysis of disc brake squeal.* Society of Automotive Engineers, 1992.

127. Murakami, H., N. Tsunada, T. Kitamura, *A Study Concerned with a Mechanism of Disc-Brake Squeal.* Society of Automotive Engineers, 1984.

128. Fieldhouse, J. and T. Newcomb, *An investigation into disc brake noise using holographic interferometry.* IMechE, 1991.

129. Instruments, N., *LabVIEW (Laboratory Virtual Instrument Engineering Workbench)*, 2013. p. Data acquisition, instrument control, and industrial automation.

130. Olatunbosun, O.A., *Modal Experiments Modal Behaviour Visualisation*, 2013, Dr Olatunbosun: Birmingham, UK.

131. Olmos, B.A., J. M. Roesset, *Evaluation of the half-power bandwidth method to estimate damping in systems without real modes.* Earthquake Engineering & Structural Dynamics, 2010. **39**(14): p. 1671-1686.

132. Liu, P., H. Zheng, C. Cai, Y. Wang, C. Lu, K. Ang, G. Liu, *Analysis of disc brake squeal using the complex eigenvalue method.* Applied Acoustics, 2007. **68**(6): p. 603-615.

133. Bathe, K.J., E. L. Wilson, *Large Eigenvalue Problems in Dynamic Analysis.* Journal of the Engineering Mechanics Division, 1972. **98**(6): p. 14.

134. Ericsson, T.a.A.R., *The Spectral Transformation Lanczos Method for the Numerical Solution of Large Sparse Generalized Symmetric Eigenvalue Problems.* Mathematics of Computation, 1980. **35**(152): p. 18.

135. Murthy, D.V., R. T. Haftka, *Derivatives of eigenvalues and eigenvectors of a general complex matrix.* International Journal for Numerical Methods in Engineering, 1988. **26**(2): p. 293-311.

136. Parlett, B.N., *The Symmetric Eigenvalue Problem*, in *The Symmetric Eigenvalue Problem*. 1998, Prentice-Hall: New Jersey. p. i-xxvi.

137. Shaw, J., S. Jayasuriya, *Modal sensitivities for repeated eigenvalues and eigenvalue derivatives.* AIAA Journal, 1992. **30**(3): p. 850-852.

138. Goto, Y., H. Saomoto, N. Sugiura, T. Matsushima, S. Ito, A. Fukui, *Structural Design Technology for Brake Squeal Reduction Using Sensitivity Analysis.* 2010.

139. Dassault-Systemes, *Abaqus FEA*, in *Abaqus/CAE, Computer-Aided Engineering. Abaqus/Standard, General-purpose Finite-Element analyzer.*2010, ABAQUS Inc.

140. Liu, M., D. G. Gorman, *Formulation of Rayleigh damping and its extensions.* Computers & Structures, 1995. **57**(2): p. 277-285.

141. Meerbergen, K., *Fast frequency response computation for Rayleigh damping.* International Journal for Numerical Methods in Engineering, 2008. **73**(1): p. 96-106.

142. Flint, J., J. G. McDaniel, X. Li, A. Elvenkemper, A. Wang, S. Chen, *Measurement and Simulation of the Complex Shear Modulus of Insulators*, 2004, SAE International: Warrendale, PA.

143. Nishizawa, Y., S. Wakamatsu, H. Yanagida, Y. Takahara, *Study of Dynamic Pad Stiffness Influencing Brake Squeal*, 2007, SAE International.

144. McDaniel, J.G., X. Li, A. Elvenkemper, E. Wegmann, A. Wang, S. Chen, J. Flint, *Simulating the Effect of Insulators in Reducing Disc Brake Squeele*, 2005, SAE International.

145. Esgandari, M., O. A. Olatunbosun, *Computer aided engineering prediction of brake noise: modeling of brake shims.* Journal of Vibration and Control, 2014.

146. Siemens, *LMS Testing Solutions*, 2014, Siemens Industry Software Limited: United Kingdom.

147. International, S., *SAE International Standards J 2694: Anti-Noise Brake Pads Shims: T-pull Test*, 2009, SAE Intenrational: Warrandale, PA.

148. Saw, C.L., A. R. Abu Bakar, W. M. M. W. Harujan, B. Abd Ghani, M. R. Jamaluddin, *SUPPRESSING DISC BRAKE SQUEAL THROUGH STRUCTURAL MODIFICATIONS.* Jurnal Mekanikal, 2009. **29**: p. 67-83.

149. al., J.G.M.e., *Simulating the Effect of Insulators in Reducing Disc Brake Squeal*, in *Brake Colloquium & Exhibition, 23rd Annual*2005, SAE International: Orlando, Florida.

150. Day, A.J., *Friction and Friction Materials*, in *Braking of Road Vehicles 2009*, J.K. A. J. Day, Editor. 2009, University of Bradford: UK.

151. Wallner, D., M. Meister, *Elaborate Measuring System for Sensitivity Analyses and In-Depth Investigations of a Squealing Brake System.* SAE Int. J. Passeng. Cars - Mech. Syst., 2012. **5**(3): p. 1107-1115.

152. Dezi, M., P. Forte, F. Frendo, *Motorcycle brake squeal: experimental and numerical investigation on a case study.* Meccanica, 2014. **49**(4): p. 1011-1021.

153. Nishizawa, Y., K. Kosaka, Y. Kurita, Y. Oura, *Influence of Pad Thickness and Surface Roughness on Pad Stiffness*, 2012, SAE International.

154. Trcka, M., J. L. M. Hensen, M. Wetter, *Co-simulation of Innovative Integrated HVAC Systems in Buildings.* Journal of Building Performance Simulation, 2009. **2**(3): p. 21.

155. Duni, E., G. Toniato, R. Saponaro, P. Smeriglio, *Vehicle Dynamic Solution Based on Finite Element Tire/Road Interaction Implemented through Implicit/Explicit Sequential and Co-Simulation Approach.* Training, 2010. **2013**: p. 11-18.

156. Gravouil, A., A. Combescure, *Multi-time-step explicit-implicit method for non-linear structural dynamics.* International Journal for Numerical Methods in Engineering, 2001. **50**(1): p. 199-225.

157. Harewood, F.J., P. E. McHugh, *Comparison of the implicit and explicit finite element methods using crystal plasticity.* Computational Materials Science, 2007. **39**(2): p. 481-494.

158. Ypma, T., *Historical Development of the Newton–Raphson Method.* SIAM Review, 1995. **37**(4): p. 531-551.

159. Yang, D.Y., D. W. Jung, I. S. Song, D. J. Yoo, J. H. Lee, *Comparative investigation into implicit, explicit, and iterative implicit/explicit schemes for the simulation of sheet-metal forming processes.* Journal of Materials Processing Technology, 1995. **50**(1): p. 39-53.

160. Wang, N.M., B. Budiansky, *Analysis of sheet metal stamping by a finite-element method.* Journal of Applied Mechanics, 1978. **45**(1): p. 73-82.

161. Massi, F., O. Giannini, L. Baillet, *Brake squeal as dynamic instability: An experimental investigation.* The Journal of the Acoustical Society of America, 2006. **120**(3): p. 1388.

162. Esgandari, M., O. A. Olatunbosun, R. Taulbut, *Frictional Coefficient Distribution Pattern On Brake Disk-pad Contact Interface To Reduce Susceptibility Of Brake Noise Instabilities Causing Brake Squeal*, in *EuroBrake*2013, FISITA: Dresden, Germany.